

**Aggregation-Induced Scaffolding of Helical Polysilanes:  
Instantaneous Generation of Optically Active Polyfluorenes**

(光分解性らせんポリシランを足場材料とする光学活性  
ポリフルオレンの発生に関する研究)

**NOR AZURA BINTI ABDUL RAHIM**

(ノル アズラ ビンティ アブドル ラヒム)

**Nara Institute of Science and Technology**

**Graduate School of Materials Science**

**Advanced Polymer Science Laboratory**

**(Prof. Fujiki Michiya)**

**October 2016**

## Chapter 1. General Introduction

### 1.1 Supramolecular and polymer chiral formation

The origin of biomolecular handedness on Earth is one of the greatest mysteries investigated by geochemists and chiral scientists.<sup>1,2</sup> To convey these specific shapes in synthetic macromolecules and supramolecules<sup>3-9</sup>, a chiral center with nonsuperimposed dissymmetry in its mirror image must be present in the chemical structure. As a result, two distinct hands of right and left helices can be obtained.<sup>10-18</sup> Detection of chiral units can be performed in nuclear resonance (NMR) experiments or by means of circularly polarized light using optical rotation dispersion (ORD), circular dichroism (CD) in the ground state or circular polarized luminescence (CPL) in the excited state.<sup>15-21</sup>

In 1997, Palmans' group demonstrated the first chirality amplification in supramolecular self-assemblies comprising helical columns of  $C_3$ -symmetrical discotic 'propeller'-like bipyridine in a stack achieved by intermolecular hydrogen bonding (Figure 1.1).<sup>22</sup> It was confirmed that the chiral unit serves as a driving force for amplification of a mixed stack of large achiral bipyridine propeller chromophores. The basic principle was adopted from the sergeants-and-soldiers principle proposed by Green.

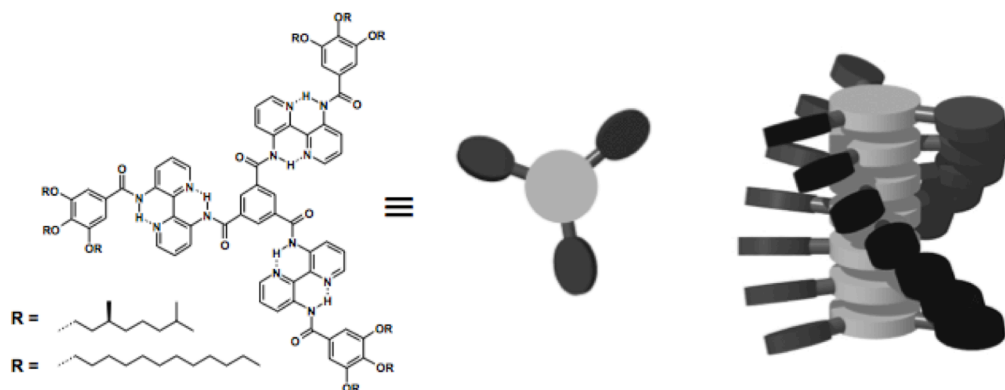


Figure 1.1. The first bipyridine based  $C_3$ -symmetrical disks and a cartoon representing their helical supramolecular stacking. Reprinted from *Angewandte Chemie International Edition*, Vol. 66, A. R. A. Palmans, J. A. J. M. Vekemans, E. E. Havinga, E. W. Meijer. "Sergeant-and-soldiers principles in chiral columnar stacks of disc-shaped molecules with  $C_3$ -symmetry", pp. 2648-2651, Copyright (1997), with permission from Wiley InterScience.

The principle allows control of dynamic poly(alkyl-isocyanate) helicity by the incorporation of small amounts of sergeant chiral vinyl monomer to control a large number of cooperative achiral monomers at the solution level. The helix sense was reported to be strongly influenced by the temperature and solvent dependency.<sup>23, 24</sup> Recently, Suginome *et al.* observed "abnormal" phenomena in poly(quinoxaline-2,3-diyl) copolymers containing chiral and achiral propoxymethyl side chain units. Instead of obeying the simple sergeant-soldier principle, the polymer exhibited backbone chirality switching in aromatic solvents.<sup>25</sup>

Green also coined the expression 'majority-rule' to describe the generation of CD spectra caused by the slight excess of either one of the helical enantiomers of 2,6-dimethylheptyl isocyanates in rigid polyisocyanates. This surprising discovery was achieved by the incorporation of only a 2 % enantiomeric excess, which produced a strong bias toward the helicity of the major

enantiomer. The overall results exhibit non-linear behavior, which makes it difficult to predict the actual sequence. Ignoring the generating pattern, the majority-rule principle has become a powerful method to amplify chiral superstructures either in covalent or non-covalent supramolecular polymer systems.<sup>26-28</sup>

Based on these two principles, new information on molecules, polymers, organic nanoparticles and organogel self-assembled systems, including transfer, amplification, the memory effect and helicity control, has been reviewed to establish understanding in the field of supramolecular chirality over the past 20 years. However, studies of supramolecular helical formation based on synthetic  $\pi$ - and  $\sigma$ -conjugating polymers and the polymer stereocomplex construction, mechanism and structure of the helical conformation still remain a great challenge due to the dynamic nature of the long-chain polymer system when subjected to certain environmental factors.<sup>29-32</sup>

## 1.2 Stereocomplex helix association

Right-handed DNA natural homoduplex nucleic acids chains spiraling along the same axis with contrasting direction were identified by X-ray diffraction in 1953 by Watson and Crick<sup>33</sup>; subsequently, a series of folded ribbon associations in protein, RNA and collagen were observed in biological systems.<sup>34-36</sup> These biopolymers contain selective and active binding sites to convey specific structures to accommodate certain functions. Fundamentally, the helical strands are joined by the non-covalent weak bonding of intermolecular forces and hydrogen bonding through a self-assembly process to form twisted ribbons, wires, fibers and tubes.<sup>37-39</sup>

Owing to its unique chiral helical sense, which provides impressive chiroptical properties, work has been extended to synthetic  $\pi$ - and  $\sigma$ -conjugating polymers. A common way to

produce these artificial architectures with right- or left- handed helices is through synthesis procedures. Subjected to macromolecular helicity, either the static helical polymer or dynamic ones may be more stable; both can be controlled by their helix inversion barrier.<sup>32,40</sup> Recently, instead of focusing on the polymerization technique to control the single-strand polymer helical pitch, molar mass and polydispersity, research has shifted to evaluating the structure, mechanism and properties of the stereocomplex.

The first synthetic stereocomplexation was performed by Fox *et al.* in 1958 in poly(methyl methacrylate) (PMMA) with the association of isotactic and syndiotactic parts. The formation was maintained by the stereoselective van der Waals force. In 2007, Yashima *et al.* clearly visualized the PMMA structure consisting a double-strand helical polymer of isotactic (*it*) and syndiotactic (*st*) character with a stoichiometry of 1:2 using high-resolution atomic force microscopy (AFM) with further confirmation by IR measurement. The detailed structure is shown in Figure 1.2. The two-dimensional (2D) helix bundles have an average height of 1.4-1.6 nm with chain-chain lateral spacing of  $(2.4 \pm 0.1)$  nm. The obtained bundle structure with measured helical pitch of 0.92 nm represented a major correction to previous claims suggesting that the PMMA stereocomplex helical pitch was 1.84 nm.<sup>41-45</sup>

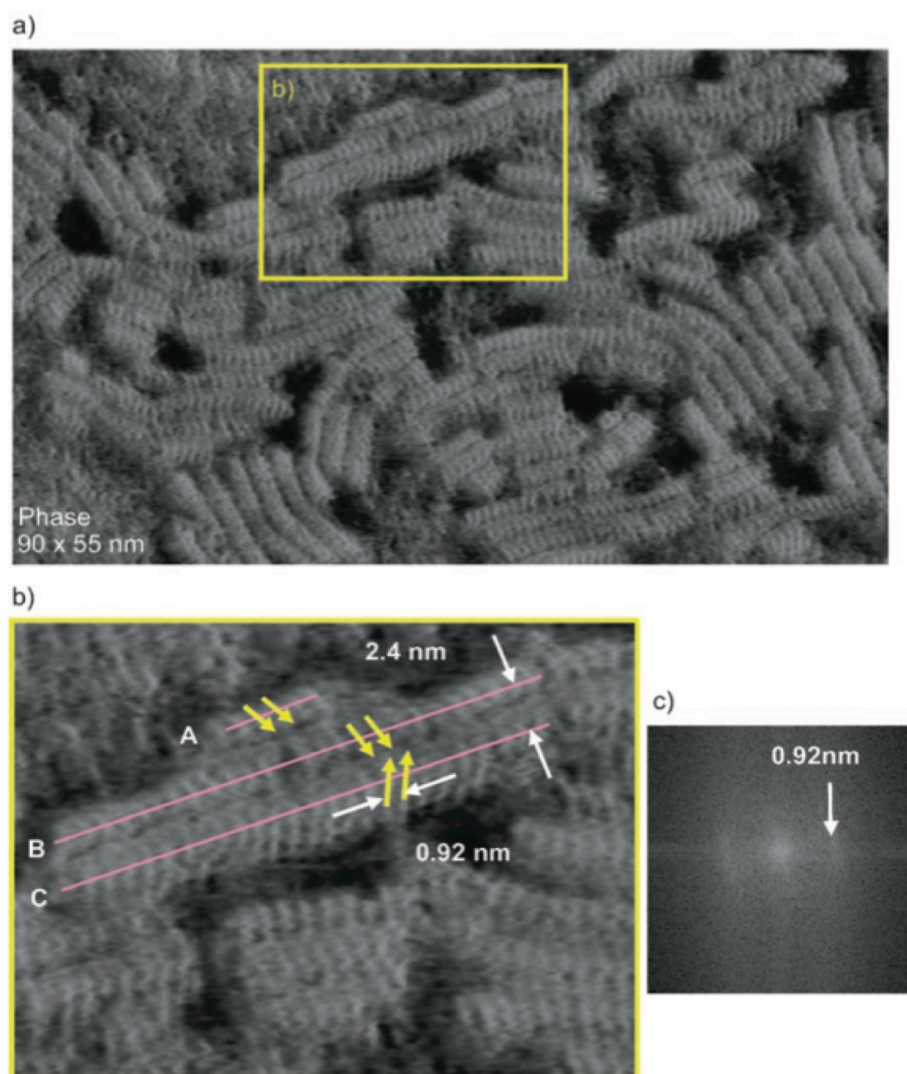


Figure 1.2. AFM phase image of a monolayer of an *it*- and *st*-PMMA mixture ( $it/st = 1:2$ ) deposited on mica at  $10\text{mNm}^{-1}$ . b) Magnified image of the area indicated by the yellow square in (a); the pink lines represent the main-main axes of the stereocomplex; the yellow arrows indicate the antipodal oblique pendant helical arrangement with respect to the main axes. c) Typical Fourier transform of a section of (a) Reprinted from *Angewandte Chemie International Edition*, Vol. 66, J. Kumaki, T. Kawauchi, K. Okoshi, H. Kusanagi, and E. Yashima. "Supramolecular Helical Structure of the Stereocomplex Composed of Complementary Isotactic and Syndiotactic Poly(methyl methacrylate)s as Revealed by Atomic Force Microscope", pp. 5348-5351, Copyright (2007), with permission from Wiley InterScience.

Another example of a stereocomplex is enantiomeric PLA biomaterial, which has been widely used in biomedical applications. The polymer was constructed from *R*- and *S*-configured polymers with the ideal combination being a 1-to-1 ratio of poly(L-lactide) and poly(D-lactide). Individual components of fiber-like PLA aggregates displayed enhanced circular dichroism (CD) in various solvents, indicating the existence of a helical structure. The formed complementary helices were stably attached by intermolecular hydrogen bonding. The most stable formation of the PLA stereocomplex was reported when both *R*- and *S*-handed helical components were present in equal concentrations. This conclusion applies to the combination of a 1-to-2 ratio of *it/st* PMMA. However, no optical activity was observed for the stereocomplex due to racemization.<sup>41-43</sup>

Shinkai et al. conducted several helicity transfer experiments in water-DMSO cosolvent from non-charged helical polysaccharide (schizophyllan and curdlan) to CD-/CPL-silent cationic charge polythiophene with a stoichiometric 1-to-1 ratio and CD-/CPL-silent anionic charge poly(fluorene-*alt-m*-phenylene) with a non-stoichiometric 13-to-8 ratio as repeating units. This macromolecule-to-macromolecule complexation can instantly form the corresponding CD- and CPL-active  $\pi$ -conjugated polymers. Alternatively, cationic charge curdlan forms a complex with non-charged permethyloligosilane and single-walled carbon nanotubes.<sup>44,45</sup>

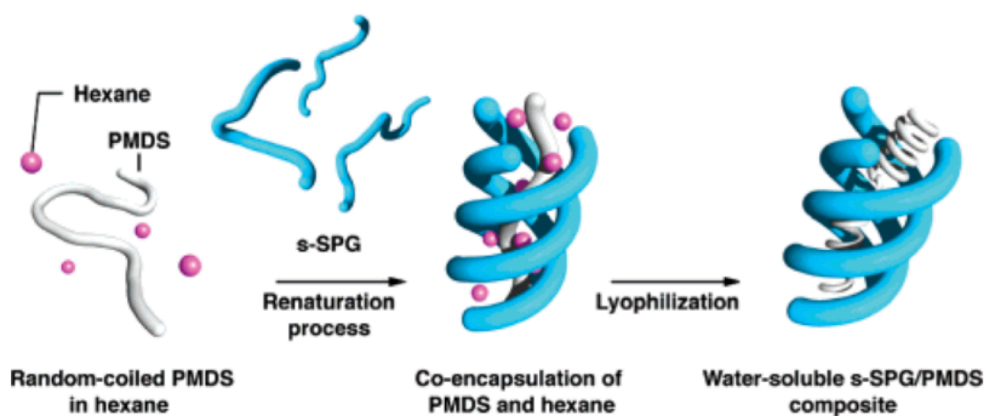


Figure 1.3. Schematic illustration of the composite formation of s-SPG with PMDS. Reprinted from *Organic Letters*, Vol. 7, S. Haraguchi, T. Hasegawa, M. Numata, M. Fujiki, K. Uezu, K. Sakurai and S. Shinkai. " Oligosilane-Nanofibers Can Be Prepared through Fabrication of Permethyldecasilane within a Helical Superstructure of Schizophyllan", pp. 5605-5608, Copyright (2005), with permission from American Chemical Society.

### 1.3 Aggregation in $\pi$ - and $\sigma$ -conjugated polymers

There are two fundamental types of aggregation systems depending on the chromophore producing spectroscopic properties of intermolecular excitonic interactions. *J* aggregation or Scheibe aggregates result in significant red-shifted and narrow band absorption compared to the monomer absorption band at low energy states. This effect can be recognized by the minimal Stokes shift with high quantum yield.<sup>46-51</sup> In contrast to *J* aggregation, *H* aggregation indicates the reverse characteristic, in which the absorption spectrum is shifted to the blue region. The aggregations are distinguished by the geometrical arrangement of the molecules' different slip angles, where a small angle slippage is associated with *J* aggregation and one larger than  $R < 32^\circ$  is categorized as *H* aggregation.<sup>47,51,52</sup> In aggregate-induced emission of a composite chiral supramolecular structure, *J* aggregation is preferable to *H* aggregation.

The discoveries by the Tang group of non-emissive silole molecules, which appear to be strongly luminescent under UV illumination upon aggregation regardless of the solution, has prompted others to extend their work to a polymer system.<sup>53</sup> In line with this finding, Zahn and Swager provided a detailed report of the electronic spectra of poly(phenylene ethynylene) (PPE) with chiral alkyloxy groups with significant chirality enhancement during aggregation. Considering that polymer backbones twist, the aggregations are easily achieved by the addition of a poor solvent of methanol to a solution to generate relatively small fluorescence-quenching nonscattering particles with an interlocking structure and transparent CD bands.<sup>54</sup> The other interesting feature is that the system confirms generation of a second chromophore at higher energy that has the same CD sign, indicating the presence of exciton coupling as illustrated in Figure 1.4.<sup>54,55</sup>

Fujiki presented a series of chirality transfers to achiral  $\sigma$ -conjugated and  $\pi$ -conjugated polymers via acid/base or host/guest interactions in an aggregated system based on the sergeant-soldier and the majority-rule principles. Using relatively weak intermolecular interactions of hydrogen bonding and  $\pi$ - $\pi$  interactions through the presence of non-solvent units that facilitate the formation of exciton coupling, significant enhancements in CD spectra in comparison to the solution state were obtained. Moreover, the generated chiral polyfluorenes, poly(diphenylacetylene)s (PDPA)s, polythiophene and poly(*p*-phenylene-vinylene) (PPV) also demonstrated a highly circularly polarized light (CPL) signal in the excited state ranging from  $10^{-4}$  to  $10^{-2}$  in the aggregated system.<sup>30,40,54-57</sup>

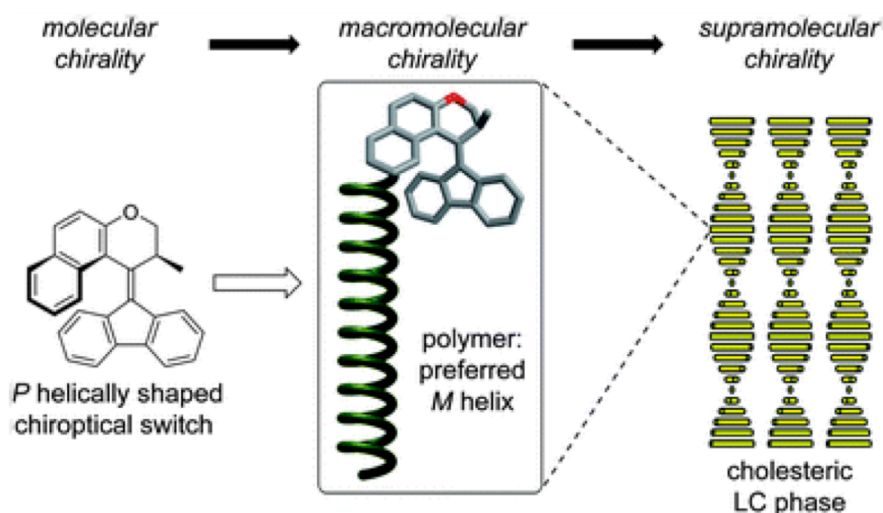


Figure 1.4. Schematic representing of the hierachiral transmission of chiral information from the molecular level of a single chiroptical switch molecule, via the macromolecular level of a polyisocyanates, to the supramolecular level of a cholesteric LC phase. Reprinted from Journal of Americam Chemical Society, Vol. 130, D. Pijper, M. G. M. Jongejan, A. Meetsma and B. L. Feringa. "Light-Controlled Supramolecular Helicity of a Liquid Crystalline Phase Using a Helical Polymer Functionalized with a Single Chiroptical Molecular Switch", pp. 4541-4552, Copyright (2008), with permission from American Chemical Society.

#### 1.4 Templating and scaffolding in supramolecular assembly

A scaffold is defined as a removable substance that induces a construction material to take its shape. It is a frequently used term in the context of biological tissue regrowth and regeneration. Scaffolds provides a sufficient support before they are removed through degradation.<sup>58</sup> In some cases, scaffolds remain stable and stay intact with the biological system. Previous researchers used helical DNA, peptides, aromatic foldamers and non-helical rigid linkers as scaffolds for cofacial positioning of plural chromophores.<sup>59-63</sup> However, these scaffolds cannot be removed from the original molecular skeletons because they are chemically, physically, and thermally stable in the operational environment.

As an extension to macromolecular scaffolding using synthetic polymers, the Nolte group designed and synthesized a rigid chiral poly(isocyanide) with pendent alanine side chains that point away from the polymer backbone.<sup>64</sup> The side chains enable proper positioning of the self-assembled chromophoric small molecules to form a highly ordered supramolecular architecture around the poly(isocyanide). A successful helical scaffolding process was achieved owing to non-covalent intermolecular forces of hydrogen bonding and  $\pi$ - $\pi$  interaction, backbone rigidity and the solubility of the scaffold (which depends on the length of the alkyl side chain). In the report, the scaffold remained stable and stayed intact to bind to and position the templating chromophore.<sup>59-64</sup>

More recently, Liu et al. demonstrated scaffold removal from co-gelation helical nanoassemblies after their co-assembly with an amphiphilic L- or D-glutamide gelator. Interestingly, the fabricated chiral assembly polymer gels, including PCz8 and PSi8, could still be produced after the gelator molecules were removed via washing with methanol. Both the gelator-containing and gelator-free chiral polymer assemblies exhibited circularly polarized luminescence (CPL), which is usually inherent to intrinsic chiral polymers.<sup>65</sup>

## **1.5 Photochemical decomposition and photobleaching**

Degradation is a decomposition process employing specific types of chemical transformation in organic or non-organic materials. In polymers, a light source can thermodynamically change the electronic structure of the molecular orbital. The photochemical reaction starts from the absorption of light to induce a transition to higher energy states. Higher quantum yield elements make it easier to form metastable states that are prone to photodegradation. The quantum yield strongly depends on wavelength; a shorter wavelength band is more photoactive than a longer one. Depending on the element, sufficient energy sources are required to create a

photoexcited state.<sup>66-70</sup>

Takeda *et al.* has conducted the light-induced electron spin-resonance technique using a 500 W high-pressure Xe arc lamp and 150 W low-pressure Xe arc lamp as light sources to observe photogenerated metastable centers in solid-state polysilane (**PSi**). It was found that tuning the photon energy to irradiate **PSi** could facilitate different types of metastable states. Lower excitation was related to the  $\sigma\text{-}\sigma^*$  transition to induce Si-Si bond stretching to form weak bonds (WBs). When the excitation rate was intense, the dissociating forces acting on the pendant bond (side group) activated and formed dangling bonds (DBs).

Photobleaching manifests itself in a process referred to as “photofatigue”. Photobleaching is attributed to reactions involving oxygen. In conjugated polymers, the photobleaching technique has become the technique of choice to increase emissions, shift wavelengths and provide greater stability.<sup>72</sup> In poly(para-phenylene-vinylene) (PPV), it has been predicted that a singlet oxygen with an alkenyl group causes a defect in the carbonyl group that eventually leads to chain scission. Although the specific mechanism is not clear, the mechanism is irreversible photodestruction of a chromophore.<sup>72-74</sup>

Swager and his colleagues have studied the photobleaching mechanism of conjugated polymers (CPs) under irradiation in film and solutions. CPs possesses great photostability when irradiated under anaerobic conditions in the presence of oxygen. Thioether-containing poly(para-phenylene-ethynylene) (PPE) copolymers exhibit strong fluorescence turn-on emission when exposed to oxidants in solution, as illustrated in Figure 1.4. It was also noted that oxidation does not cause a decrease in emission to the polyfluorene unit with or without the attachment of an oxide comonomer.<sup>75</sup>

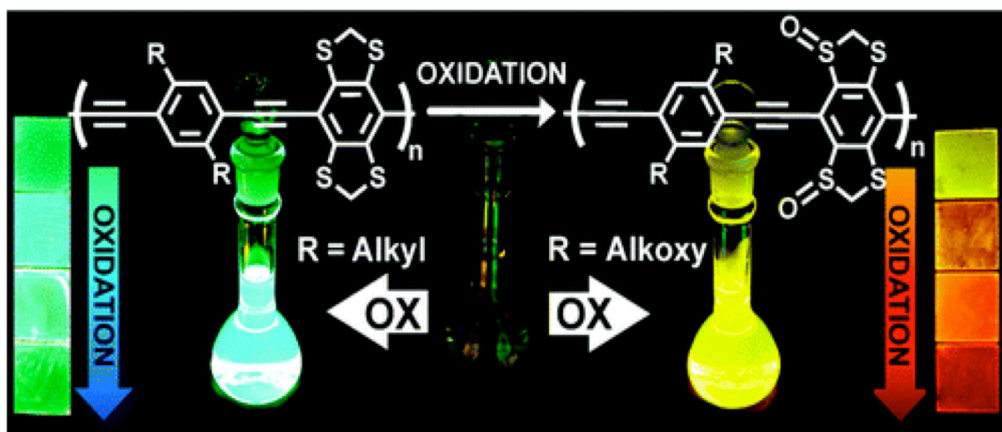


Figure 1.4. Thioether-containing poly(para-phenylene-ethynylene)(PPE) copolymer show a strong fluorescence turn-on response when exposed to oxidation in solution as a results of a selective conversion of thioether substituents into sulfoxides and sulfones . Reprinted from Journal of American Chemical Society, Vol. 132, E. L. Dane, S. B. King and T. M. Swager. "Conjugated Polymers That Respond to Oxidation with Increased Emission", pp. 7758-7768, Copyright (2010), with permission from American Chemical Society.

## 1.6 Purpose of this research

The study reports on the first photochemically controlled scaffolding of hetero-aggregates consisting of **PSi** and **PF8** via a **PSi**-selective photoscissoring reaction. This protocol allows for the successful production of a CPL- and CD-active **PF8** aggregate by complete removal of **PSi**. This work is divided into 3 main sections, from Chapter 3 to Chapter 5.

In Chapter 3, chirality amplification and removal of the **PSi** scaffold from **PF8** will be discussed. The **PF8-PSi-S** hetero-aggregate CD spectra are measured to configure the formation of helical **PF8** either at the  $\alpha$ -phase and  $\beta$ -phase or both of the chiral **PF8** structures to confirm that macromolecular helicity transfer from non-charged **PSi** to non-charged non-helical **PF8** is possible.

**PSi-S** decomposes rapidly after 60 s; thus, the author investigates whether the chirality of **PF8** is retained or disappears after the photoscissoring reaction of the Si-Si bond at 313 nm. The results indicate that **PSi** acts efficiently as a photochemically removable scaffold that enables the generation of chiral **PF8** when non-helical **PF8** is employed as a starting material.

Chapter 4 provides detail on the possible scaffold structures transferred from **PSi** to **PF8** and the formation mechanisms. Due to the high sensitivity of **PSi** during TEM and SEM measurements, the structures of **PF8**, **PSi-S**, and **PSi-S-and-PF8** hetero-aggregates are visualized using DFM-AFM. From several height profiles of DFM-AFM images, the height profiles of **PSi-S** and **PF8** aggregates on HOPG are obtained for further evaluation.

Lastly, Chapter 5 discusses factors affecting the ability of helix scaffold control by **PSi** to **PF8**. The cosolvent effect (in which a mixture of good and poor solvents, namely, toluene and methanol, is varied) is investigated. Additionally, the stoichiometry ratio dependency between **PSi-S** and **PF8** mixtures and the molecular weight of the polymers and alkyl side chain for both **PSi-S** and **PF8** are measured. Furthermore, majority-rule of **PSi** (**PSi-R-ran-PSi-S**) and sergeant-soldier action of **PSi** (**PSi-R(S)-ran-PSi-tBu**) are also characterized to determine if either is applicable to the current **PSi** scaffolding systems. Tests are also conducted by replacing **PF8** with non-helical **PF8T2** to characterize the take-up trend in a co-aggregate system of **PSi** by analyzing the CD and CPL spectra.

## 1.7 References

- (1) Pauling, L.; Corey, R. B.; Branson, H. R. *Proc. Natl. Acad. Sci.* **1951**, *37*, 205.
- (2) Watson, J. D.; Crick, F. H. *Nature* **1953**, *171*, 737.
- (3) van Beijnen, A. J. M.; Nolte, R. J. M.; Zwikker, J. W.; Drenth, W. *J. Mol. Catal.* **1978**, *4*, 427.
- (4) Rowan, A. E.; Nolte, R. J. M. *Angew. Chem. Int. Ed.* **1998**, *37*, 63.
- (5) Okamoto, Y.; Suzuki, K.; Ohta, K.; Hatada, K.; Yuki, H. *J. Am. Chem. Soc.* **1979**, *101*, 4763.
- (6) Green, M. M.; Peterson, N. C.; Sato, T.; Teramoto, A.; Cook, R.; Lifson, S. *Science* **1995**, *268*, 1860.
- (7) Yashima, E.; Maeda, Y.; Matsushima, T.; Okamoto, Y. *Chirality* **1997**, *9*, 593.
- (8) Inouye, M.; Waki, M.; Abe, H. *J. Am. Chem. Soc.* **2004**, *126*, 2022.
- (9) Schlitzer, D. S.; Novak, B. M. *J. Am. Chem. Soc.* **1998**, *120*, 2196.
- (10) Katagiri, H.; Miyagawa, T.; Furusho, Y.; Yashima, E. *Angew. Chem. Int. Ed.* **2006**, *45*, 1741.
- (11) Lehn, J. M. *Proc. Natl. Acad. Sci.* **2002**, *99*, 4763.
- (12) Lehn, J. M.; Rigault, A.; Siegel, J.; Harrowfield, J.; Chevrier, B.; Moras, D. *Proc. Natl. Acad. Sci. U.S.A.* **1987**, *84*, 2565.
- (13) Piguet, C.; Bernardinelli, G.; Hopfgartner, G. *Chem. Rev.* **1997**, *97*, 2005.
- (14) Prince, R. B.; Barnes, S. A.; Moore, J. S. *J. Am. Chem. Soc.* **2000**, *122*, 2758.
- (15) Yan, N.; He, G.; Zhang, H.; Ding, L.; Fang, Y. *Langmuir* **2010**, *26*, 5909.
- (16) Langeveld-Voss, B. M. W.; Christiaans, M. P. T.; Janssen, R. A. J.; Meijer, E. W. *Macromolecules* **1998**, *31*, 6702.
- (17) Palmans, A. R. A.; Meijer, E. W. *Angew. Chem. Int. Ed.* **2007**, *46*, 8948.
- (18) Barton, J. K. *Science*, **1986**, *233*, 727.
- (19) Liu, M.; Zhang, L.; Wang, T. *Chem. Rev.* **2015**, *115*, 7304.
- (20) Bonner, W. A. *Orig. Life Evol. Biosph.* **1992**, *21*, 407.
- (21) Inoue, Y. *Chem. Rev.* **1992**, *92*, 741.
- (22) Palmans, A. R. A.; Vekemans, J. A. J. M.; Havinga, E. E.; Meijer, E. W. *Angew. Chem. Int. Ed. Engl.* **1997**, *36*, 2648.
- (23) Green, M. M. and Reidy, M. P. *J. Am. Chem. Soc.* **1989**, *111*, 6452.
- (24) Gestel van, J.; Schoot van der, P.; Michels, M. A. J. *Macromolecules* **2003**, *36*, 6668.
- (25) Nagata, Y.; Nishikawa, T.; Suginome, M. *ACS Macro Lett.* **2016**, *5*, 519.
- (26) Green, M. M.; Garetz, B. A.; Munoz, B.; Chang, H. P. *J. Am. Chem. Soc.* **1995**, *117*, 4181.
- (27) Green, M. M.; Peterson, N. C.; Sato, C.; Teramoto, A.; Cook, R.; Lifson, S. *Science* **1995**,

- 268, 1860.
- (28) Jha, S. K.; Cheon, K.-S.; Green, M. M.; Selinger, J. V. *J. Am. Chem. Soc.* **1999**, *121*, 1665.
- (29) Tang, Z. L.; Lida, H.; Hu, H. Y.; Yashima, E. *ACS Macro Lett.* **2012**, *1*, 261.
- (30) Kawagoe, Y.; Fujiki, M.; Nakano, Y. *New J. Chem.* **2010**, *34*, 637.
- (31) Hayasaka, H.; Miyashita, T.; Tamura, K.; Akagi, K. *Adv. Funct. Mater.* **2010**, *20*, 1243.
- (32) Liu, Y.; Chen, C.; Wang, T.; Liu, M. *Langmuir* **2016**, *32*, 322.
- (33) Watson, J. D. and Crick, F. H. C. *Nature* **1953**, *171*, 737.
- (34) Hasenknopf, B.; Lehn, J. M.; Baum, G.; Fenske, D. *Proc. Natl. Acad. Sci.* **1996**, *93*, 1397.
- (35) Aida, T.; Meijer, E. W.; Stupp, S. I. *Science* **2012**, *335*, 813.
- (37) Jeong, S.-H.; Lee, J. W.; Ge, D.; Sun, K.; Nakashima, T.; Seong, I. Y.; Agarwai, A.; Li, Y.; Kotov, N. A. *J. Mater. Chem.* **2011**, *21*, 11639.
- (38) Habaue, S.; Seko, Y.; Okamoto, Y. *Macromolecules* **2003**, *36*, 2604.
- (39) Nakashima, H.; Koe, J.; Torimitsu, K.; Fujiki, M. *J. Am. Chem. Soc.* **2001**, *123*, 4847.
- (40) Fujiki, M.; Yoshida, K.; Suzuki, N.; Zhang, J.; Zhang, W.; Zhu, X. *RSC Adv.* **2013**, *3*, 5213.
- (41) Kumaki, J.; Kawauchi, T.; Okoshi, K.; Kusanagi, H.; Yashima, E. *Angew. Chem. Int. Ed.* **2007**, *46*, 5348.
- (42) Kawauchi, T.; Kitaura, A.; Kumaki, J.; Kusanagi, H.; Yashima, E. *J. Am. Chem. Soc.* **2007**, *129*, 11889.
- (43) Tsuji, H. *Macromol. Biosci.* **2005**, *5*, 569.
- (44) Ikeda, M.; Hasegawa, T.; Numata, M.; Sugikawa, K.; Sakurai, K.; Fujiki, M.; Shinkai, S. *J. Am. Chem. Soc.* **2007**, *129*, 3979.
- (45) Shiraki, T.; Dawn, A.; Tsuchiya, Y.; Shinkai, S. *J. Am. Chem. Soc.* **2010**, *132*, 13928.
- (46) Yao, H.; Domoto, K.; Isohashi, T.; Kimura, K. *Langmuir* **2005**, *21*, 1067.
- (48) Israelachvili, J. N. *Intermolecular and Surface Forces*, 2<sup>nd</sup> ed.; *Academic Press: London*, **1991**.
- (49) Metelitsa, A. V.; Coudret, C.; Micheau, J. C.; Voloshin, N. A. *RSC Adv.* **2014**, *4*, 20974.
- (50) Kobayashi, T. *J-Aggregates*, *World Scientific: Singapore*, **1996**.
- (51) Owens, R. W.; Smith, D. A. *Langmuir* **2000**, *16*, 562.
- (52) Meinardi, F.; Cerminara, M.; Sasella, A.; Bonifacio, R.; Tubino, R. *Phys. Rev. Lett.* **2003**, *91*, 247401
- (53) Luo, J.; Xie, Z.; Lam, J. W. Y.; Cheng, L.; Chen, H.; Qiu, C.; Kwok, H. S.; Zhan, X.; Liu, Y.; Zhu, D.; Tang, B. Z. *Chem. Commun.* **2001**, 1740.
- (53) Zahn, S.; Swager, T. M. *Angew. Chem. Int. Ed.* **2002**, *41*, 4226.
- (54) Nakano, Y.; Fujiki, M. *Macromolecules* **2011**, *44*, 7511.
- (55) Lee, D.; Jin, Y.-J.; Kim, H.; Suzuki, N.; Fujiki, M.; Sakaguchi, T.; Kim, S. K.; Lee, W.-E.; Kwak, G. *Macromolecules* **2012**, *45*, 5379.

- (56) Nakano, Y.; Liu, Y.; Fujiki, M. *Polym. Chem.* **2010**, *1*, 460.
- (57) Wang, L.; Suzuki, N.; Liu, J.; Matsuda, T.; Rahim, N. A. A.; Zhang, W.; Fujiki, M.; Zhang, Z.; Zhou, N.; Zhu, X. *Polym. Chem.* **2014**, *5*, 5920.
- (58) Griffin, D. R.; Weaver, W. M.; Scumpia, P. O.; Carlo, D. D.; Segura, T. *Nat. Mater.* **2015**, *14*, 737.
- (59) Glowacki, J.; Mizuno, S. *Biopolymers* **2008**, *89*, 338.
- (60) Le Gac, S.; Schwartz, E.; Koeph, M.; Cornelissen, J. J. L. M.; Rowan, A. E.; Nolte, R. J. M. *Chem. Eur. J.* **2010**, *16*, 6176.
- (61) Pinto, J. D.; Le, Y. N.; Seeman, C.; Musier-Forsyth, K.; Taton, T. A.; Kiehl, R. A. *Nano Lett.* **2004**, *4*, 2343.
- (62) Guo, Y.-M.; Oike, H.; Aida, T. *J. Am. Chem. Soc.* **2004**, *126*, 716.
- (63) Hill, D. J.; Mio, M. J.; Prince, R. B.; Hughes, T. S.; Moore, J. S. *Chem. Rev.* **2001**, *101*, 3893.
- (64) Schwartz, E.; Stephane, L. G.; Cornelissen, J. J. L. M.; Nolte, R. J. M.; Rowan, A. E. *Chem. Soc. Rev.* **2010**, *39*, 1576.
- (65) Yang, D.; Zhao, Y.; Lv, K.; Wang, X.; Zhang, W.; Zhang, L.; Liu, M. *Soft Matter* **2016**, *12*, 1170.
- (66) Feringa, B. L.; van Delden, R. A.; Koumura, N.; Geertsema, E. M. *Chem. Rev.* **2000**, *100*, 1789.
- (67) Nakai, H.; Ohmori, Y.; Nakatsuji, H. *J. Phys. Chem.* **1995**, *99*, 8550.
- (68) Nakatsuji, H.; Saito, S. *J. Chem. Phys.* **1990**, *93*, 1865.
- (69) Romaner, L.; Pogantsch, A.; de Freitas, P. S.; Scherf, U.; Gall, M.; Zojer, E.; List, E. J. W. *Adv. Funct. Mater.* **2003**, *13*, 597.
- (70) Yamazaki, S. *Bull. Chem. Soc. Jpn.* **1996**, *69*, 2955.
- (71) Takeda, K.; Shiraishi, K.; Fujiki, M.; Kondo, M.; Morigaki, K. *Phys. Rev. B* **1994**, *50*, 5171.
- (72) Duan, C.; Adam, V.; Byrdin, M.; Ridard, J.; Kieffer-Jaquinod, S.; Morlot, C.; Arcizet, D.; Demachy, I.; Bourgeois, D. *J. Am. Chem. Soc.* **2013**, *135*, 15841.
- (73) Ci, X.; Matthew, A.; Whitten, D. G. *J. Am. Chem. Soc.* **1991**, *113*, 3893.
- (74) Dane, E. L.; King, S. B.; Swager, T. M. *J. Am. Chem. Soc.* **2010**, *132*, 7758.
- (75) McQuade, D. T.; Pullen, A. E.; Swager, T. M. *Chem. Rev.* **2000**, *100*, 2537.

## Chapter 2. Experimental procedures

### 2.1 Polymeric materials

The  $\pi$ -conjugated polymer of **PF8** was mainly used in these studies as an achiral substituent to chiral **Psi**. In Chapter 5, on the studies of helicity transfer capability to other  $\pi$ -conjugated polymers, **PF8** was replaced with **PF8T2**. **PF8** and **PF8T2** were purchased from Sigma-Aldrich Japan (Tokyo, Japan) with a PDI of 3.6 and 1.58. The **PF8T2** was used as is; the **PF8** was fractionated according to the fractionation procedure due to its broad dispersion range. **PF6**, **PF7** and **PF12** were prepared according to previous reports<sup>1-3</sup> based on the Yamamoto coupling method. The polymers' chemical structures are illustrated in Figure 2.1.

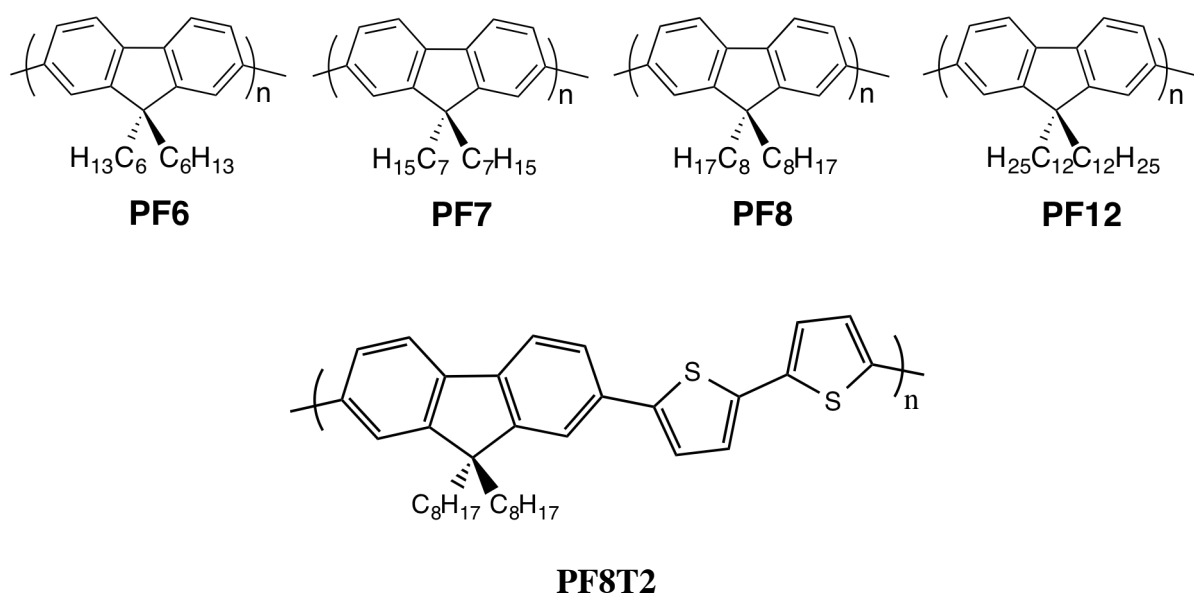


Figure 2.1. Chemical structures of poly(9,9-di-*n*-hexylfluorene) (**PF6**), poly(9,9-di-*n*-heptylfluorene) (**PF7**), poly(9,9-di-*n*-octylfluorene) (**PF8**), poly(9,9-di-*n*-dodecylfluorene) (**PF12**) and poly[(9,9-di-*n*-octylfluorene-2,7-diyl)-*alt*-bithiophene] (**PF8T2**).

## 2.2. Preparation of polysilane

The main scaffolds used in this research were poly(*n*-hexyl-(*S*)-2-methylbutylsilane) (**PSi-S**) and poly(*n*-hexyl-(*R*)-2-methylbutylsilane) (**PSi-R**); an unfractionated rigid rod-like helical **PSi-S** and **PSi-R** pair was prepared according to a previously reported protocol.<sup>4-7</sup>

### 2.2.1. Poly(*n*-hexyl-(*S*)-2-methylbutylsilane) (**PSi-S**)

To a mixture containing 50 mL of dry toluene (Wako), 1.0 g (43 mmol) of sodium (Wako), and 0.05 g (0.19 mmol) of 18-crown-6 (Wako) at 120 °C, 5.1 g (20 mmol) of **1S** was added dropwise under an N<sub>2</sub> atmosphere. The mixture was slowly stirred at 120 °C for 2 h. The reaction mixture became highly viscous. Additionally, 500 mL of dry toluene was added to reduce the solution viscosity; the resulting mixture was stirred overnight. The hot reaction slurry was passed immediately through 40 μm and 2 μm PTFE filters (Fluoropore F-40 and Fp-200, Sumitomo Electric Co. (Tokyo, Japan)) using the pressure of the N<sub>2</sub> gas. To the clear filtrate, ethanol and methanol were carefully added. White precipitates were collected by centrifugation with a Kubota model 5420 centrifuge at 3,000 rpm (Kubota Corporation (Tokyo, Japan)), followed by drying overnight at 120 °C under vacuum. The masses of the first (higher-*M<sub>w</sub>*) and second (middle-*M<sub>w</sub>*) fractions were 0.16 g (4.3 %) and 0.50 g (13.6 %), respectively. In addition, several fractionations from the second fraction were made based on the choice of toluene and poor solvents (IPA, ethanol, methanol and water). For the second fraction, <sup>29</sup>Si-NMR (CDCl<sub>3</sub>, 30 °C, ppm) exhibited peaks at –22.2, –22.4 and –23.0, and <sup>13</sup>C-NMR (CDCl<sub>3</sub>, 30 °C, ppm) exhibited peaks at 34.1, 31.4 and 23.0 as indicated in Figure 2.2 and Figure 2.3, respectively.

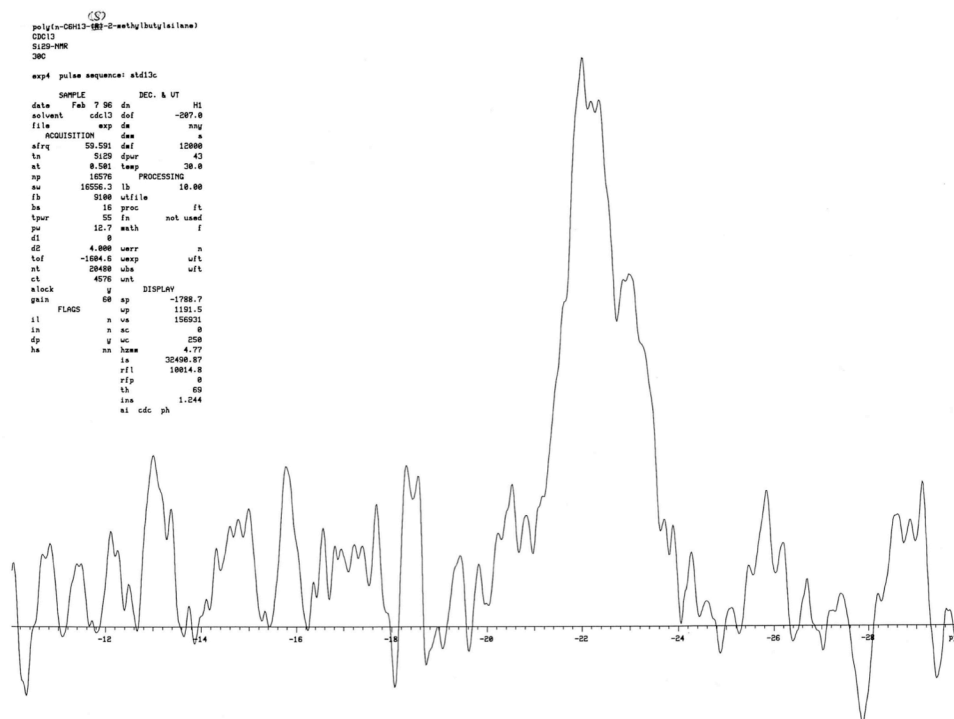


Figure 2.2.  $^{29}\text{Si}$ -NMR spectra of **PSi-S** in  $\text{CDCl}_3$  at  $30\text{ }^\circ\text{C}$ .  $^{29}\text{Si}$ -NMR signals exhibit broad resonances at  $-22.0$ ,  $-22.2$  and  $-22.7$  ppm relative to the  $\text{Me}_4\text{Si}$   $^{29}\text{Si}$  reference peak (0.000 ppm).

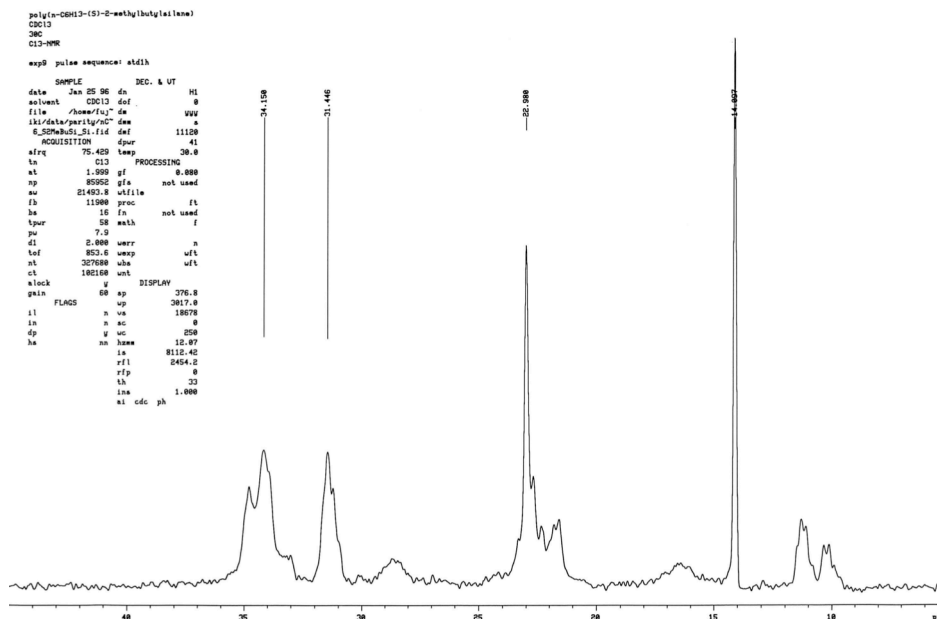


Figure 2.3.  $^{13}\text{C}$ -NMR spectra of **PSi-S** in  $\text{CDCl}_3$  at  $30\text{ }^\circ\text{C}$ .  $^{13}\text{C}$ -NMR signals exhibit broad resonances at  $34.1$ ,  $31.4$  and  $23.0$  ppm relative to the  $\text{Me}_4\text{Si}$   $^{29}\text{Si}$  reference peak (0.000 ppm).

### 2.2.2. Poly(n-hexyl-(*R*)-2-methylbutylsilane) (PSi-*R*)

Similarly, 2.55 g (10 mmol) of *IR* was added dropwise under an N<sub>2</sub> atmosphere to a mixture of 25 mL of dry toluene (Wako), 0.80 g (35 mmol) of sodium (Wako) and 0.03 g (0.11 mmol) of 18-crown-6 (Wako) at 120 °C. The mixture was stirred at 120 °C for 2 h. The reaction mixture became highly viscous. Additionally, 500 mL of dry toluene were added to reduce the solution viscosity, followed by stirring overnight. The hot reaction slurry was passed immediately through 40 μm and 2 μm PTFE filters (Fluoropore F-40 and Fp-200, Sumitomo Electric Co.) using the pressure of the N<sub>2</sub> gas flow. To the clear filtrate, ethanol and methanol were carefully added. The white precipitates were collected by centrifugation using a Kubota 5420 at 3,000 rpm and were subsequently dried overnight at 120 °C under vacuum. The masses of the first (higher-Mw) and second (middle-Mw) fractions were 0.17 g (9.2 %) and 0.37 g (20.1 %), respectively. Further fractionations from the second fraction were conducted based on the choice of toluene and poor solvents (IPA, ethanol, methanol and water). Three broad <sup>29</sup>Si-NMR resonance peaks were observed for the second fraction (100 MHz, CDCl<sub>3</sub>) at -22.0, -22.2 and -22.7. For the second fraction, the <sup>29</sup>Si-NMR spectrum (CDCl<sub>3</sub>, 30 °C, ppm) contained peaks at -22.0, -22.2 and -22.7 (Figure 2.4).

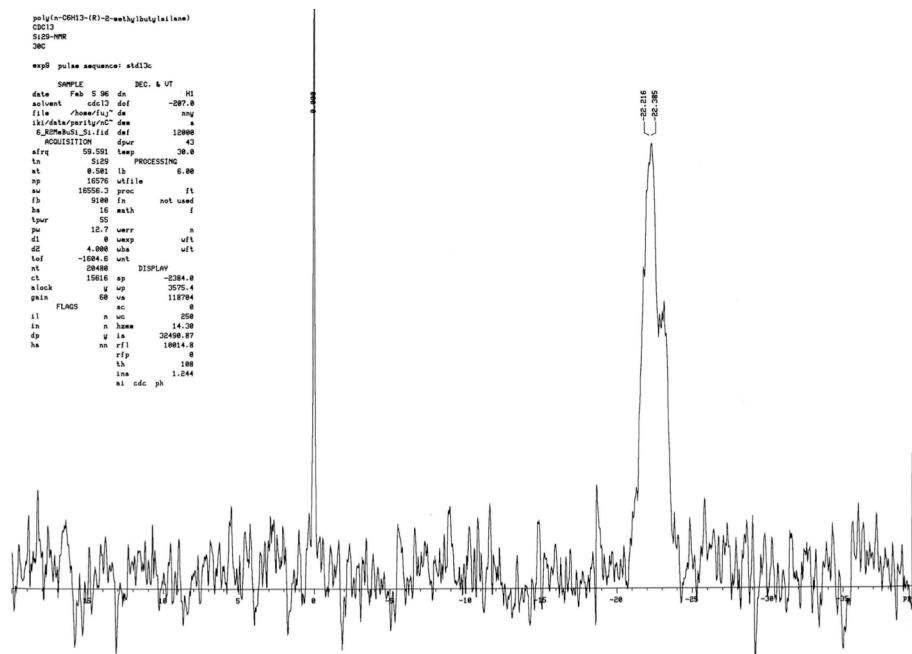


Figure 2.4.  $^{29}\text{Si}$ -NMR spectra of **PSi-R** in  $\text{CDCl}_3$  at  $30\text{ }^\circ\text{C}$ .  $^{29}\text{Si}$ -NMR signals exhibit broad resonances at  $-22.2$ ,  $-22.4$  and  $-23.0$  ppm relative to the  $\text{Me}_4\text{Si}$   $^{29}\text{Si}$  reference peak ( $0.000$  ppm).

### 2.2.3. Chain rigidity of **PSi-S** and **PSi-R**

The degree of polysilane stiffness was confirmed by the high viscosity index observed in the viscometric data ( $\alpha$ ) in Kuhn-Mark-Houwink-Sakurada plots ( $[\eta] = \kappa \cdot M^\alpha$ , where  $[\eta]$  is the intrinsic viscosity,  $M$  is the molecular mass,  $\kappa$  is a constant, and  $\alpha$  is the viscosity index) in toluene at  $70\text{ }^\circ\text{C}$ . This viscometric measurement has been well established as a physico-chemical method for the characterization of floppy chain-like polymers in dilute solution. The  $\alpha$  values of **PSi-S** and **PSi-R** were  $1.24$  and  $1.52$ , respectively.

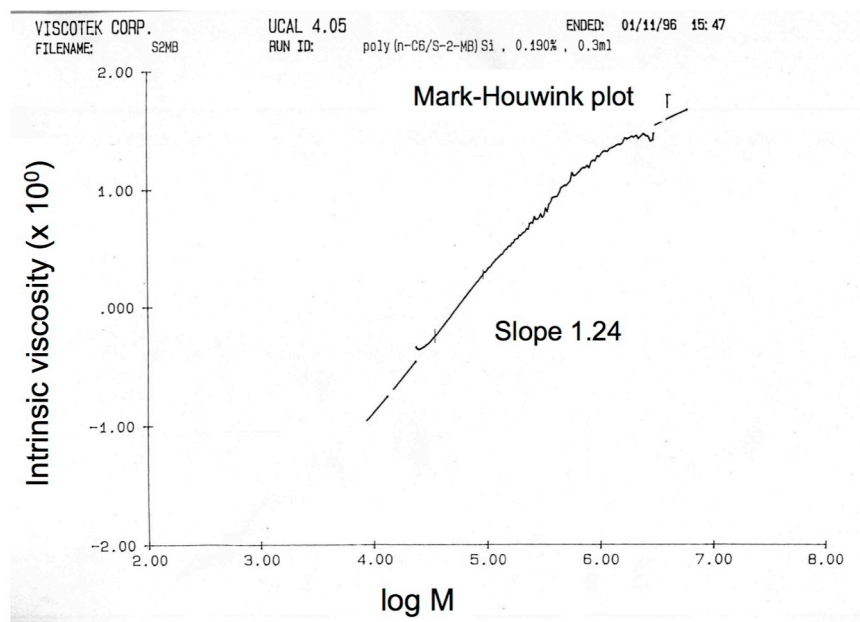


Figure 2.5. Raw data of  $\log[\eta]$  as a function of  $\log M$  for **PSi-S** in toluene at 70 °C using a Waters model 150C GPC system (three GMHXL columns (30 cm  $\times$  8 mm ID, Tosoh (Tokyo, Japan) equipped with a Viscotek H502a detector) at a flow rate of 0.97 mL min<sup>-1</sup>.

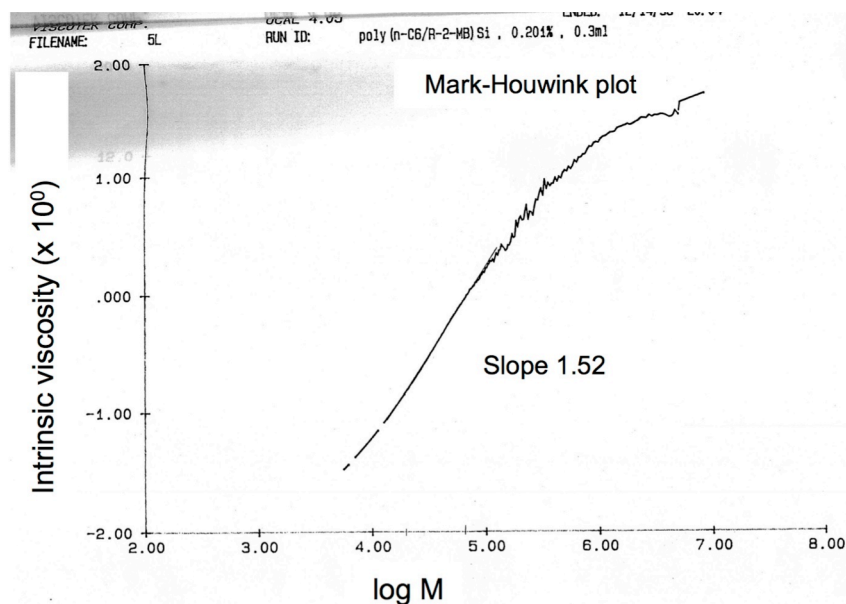


Figure 2.5. Raw data of  $\log[\eta]$  as a function of  $\log M$  for **PSi-R** in toluene at 70 °C using a Waters model 150C GPC system (three GMHXL columns (30 cm  $\times$  8 mm ID, Tosoh (Tokyo, Japan) equipped with a Viscotek H502a detector) at a flow rate of 0.97 mL min<sup>-1</sup>.

The **PSi-S** was fractionated according to the fractionation procedure. In addition to **PSi-R** and **PSi-S** other types of polysilanes with different alkyl side chain lengths were tested in this study. The polysilane chemical structures are illustrated in Figure 2.6.

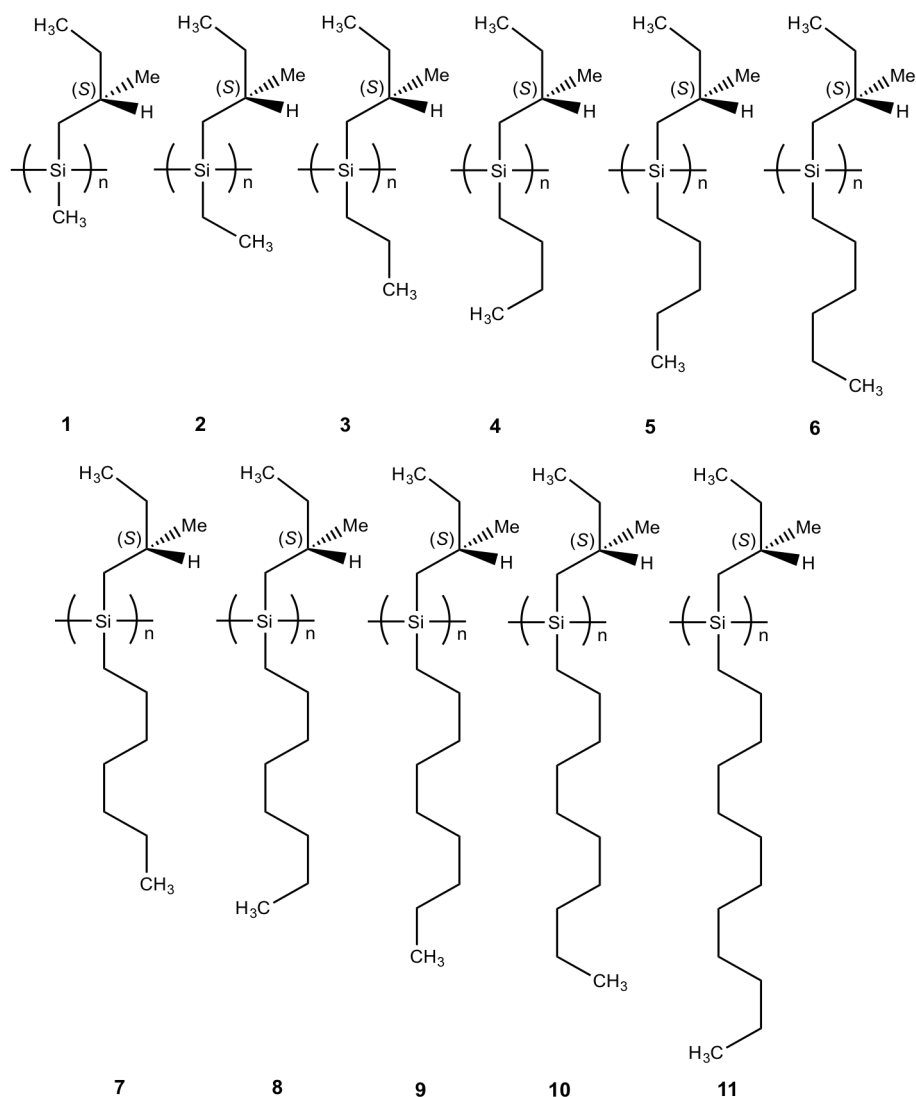


Figure 2.6. Chemical structures of optically active polysilane of poly[*n*-methyl-(*S*)-2-methylbutylsilane] (**1**), poly[*n*-ethyl-(*S*)-2-methylbutylsilane] (**2**), poly[*n*-propyl-(*S*)-2-methylbutylsilane] (**3**), poly[*n*-butyl-(*S*)-2-methylbutylsilane] (**4**), poly[*n*-pentyl-(*S*)-2-methylbutylsilane] (**5**), poly[*n*-hexyl-(*S*)-2-methylbutylsilane] (**6**), poly[*n*-heptyl-(*S*)-2-methylbutylsilane] (**7**), poly[*n*-octyl-(*S*)-2-methylbutylsilane] (**8**), poly[*n*-nonyl-(*S*)-2-methylbutylsilane] (**9**), poly[*n*-decyl-(*S*)-2-methylbutylsilane] (**10**),

### 2.3. Fractionation of PF8 and PSi

The **PSi** and **PF8** were fractionated by the addition of a poor solvent to a chloroform solution containing the **PF8**. In the fractionation process, the polymers were first dissolved in chloroform (Wako, special grade) followed by the gradual addition of isopropanol (IPA) and stirring until the aggregate precipitated in the stock solution. The polymer was then filtered with a Whatman® PTFE 1.0 mm membrane filter. The remaining polymer on the filler was collected and dried in a vacuum oven overnight. Similar fractionation processes were repeated with higher-polarity solvents (i.e., ethanol and methanol) and finally distilled water. **PF8** with  $M_n$  of 78,400 with 1.8 PDI was selected for the studies in Chapter 3 and 4. The other fractionate, **PF8**, was used in Chapter 5 for the studies on the molecular weight dependency of the achiral unit.

### 2.4 Hetero-aggregation of fractionated PF8, PSi-R (or PSi-S), and PF8T2

Spectroscopic-grade toluene and chloroform (Dojindo, Kumamoto, Japan) as good solvents and methanol (Dojindo) as a poor solvent were added to produce an optically active hetero-aggregate in a 10 mm synthetic quartz (SQ)-grade quartz cuvette. The optimized volume ratio was 1:1, with the total volume content of mixed toluene and methanol being fixed at 3.0 mL. The molar ratio of the polymers in dissolved toluene was tuned according to the experimental requirements. The dissolved **PF8** was added to the cuvette, followed by the rapid addition of fractionated **PSi-S** or **PSi-R** to produce a well-mixed complex, and methanol was slowly added. Simultaneously, CD-UV-Vis and CPL-PL spectroscopic data were collected within several minutes after completion of the hetero-aggregation process. Figure 2.7 illustrates the production of the optically active polymer hetero-aggregate.

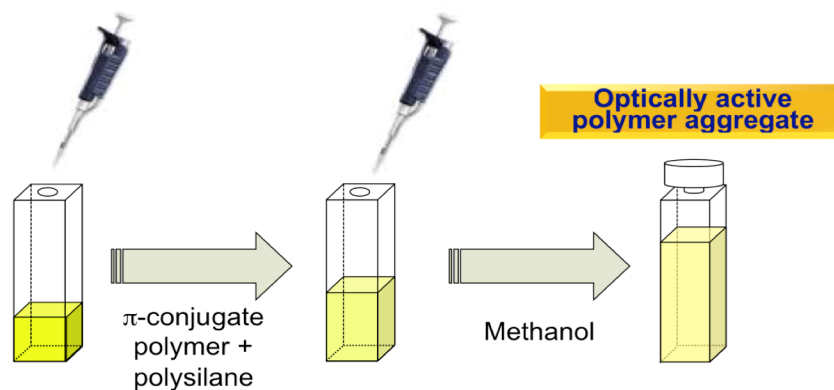


Figure 2.7. The production of the optically active polymer hetero-aggregate.

## 2.5 Characterization

### 2.5.1 Chiroptical analysis

The magnitude of CD in the ground state was calculated as  $g_{CD} = 2 \times (\epsilon_L - \epsilon_R) / (\epsilon_L + \epsilon_R)$ , where  $\epsilon_L$  and  $\epsilon_R$  are the extinction coefficients for left- and right-handed circularly polarized light, respectively. The parameter  $g_{CD}$  was obtained as  $\Delta\epsilon/\epsilon = [\text{ellipticity}/32,980]/\text{absorbance}$  at the CD extremum of the hetero-aggregates. The degree of circular polarization in the photoexcited state was defined as  $g_{CPL} = 2 \times (I_L - I_R) / (I_L + I_R)$  at the CPL extremum of the hetero-aggregates, where  $I_L$  and  $I_R$  are the output signals for left- and right-handed circularly polarized emission, respectively.

### 2.5.2 Refractive index of cosolvents

The refractive index ( $n_D$ ) value was evaluated by the equation  $n_{D,\text{ave}} = x n_{D(\text{MeOH})} + (1 - x) n_{D(\text{Toluene})}$ , where  $x$  is the volume fraction of MeOH in the cosolvent. The  $n_D$  values of pure MeOH and toluene were used for this evaluation.

### 2.5.3 Number-average degree of polymerization

The main chain lengths of **PF8**, **PSi-S** and **PSi-R** were evaluated by the product of their monomer unit lengths and number-average degree of polymerization  $DP_n = M_n/M_0$ , where  $M_n$  and  $M_0$  are the number-average of the molecular weight and the molecular weight of the monomer unit, respectively.

## 2.6 Instrumentation

### 2.6.1 CD /UV and CPL/PL measurement

The CD/UV-Vis spectra of the aggregate were recorded using a JASCO (Tokyo, Japan) J-820 spectropolarimeter with Peltier-controlled equipment to control the solution temperature. A scanning rate of  $100 \text{ nm min}^{-1}$ , a bandwidth of 2 nm and a response time of 1 s at 20 °C were used to simultaneously obtain the CD and UV-Vis spectra. The CPL/PL spectra were recorded at 20 °C on a JASCO CPL-200 spectrofluoropolarimeter with Peltier-controlled equipment. A path length of 10 mm, scanning rate of  $100 \text{ nm min}^{-1}$ , bandwidth for excitation of 10 nm, bandwidth for monitoring of 10 nm, response time of photomultiplier tube of 2 s and single accumulation were applied during the measurements.

### 2.6.2 NMR measurement

The  $^{13}\text{C}$ -NMR spectra were measured for solid **PF8**, **PSi-S** and a combination of 2-to-1 **PSi-PF8** ratio using a JOEL JNM-ECX 400 (400 MHz). The dichlorosilane monomers and their starting source materials were characterized by  $^{13}\text{C}$ (75.43 MHz) and  $^{29}\text{Si}$ (59.59 MHz) NMR spectra in  $\text{CDCl}_3$  at 30 °C with a Varian Unity 300 MHz NMR spectrometer.

### 2.6.3 Optical rotation

The optical rotation at the Na-D line was measured with a JASCO DIP-370 polarimeter using a SQ cuvette with a path length of 10 mm at room temperature (24 °C).

### 2.6.4 Gel permeation chromatography (GPC)

The weight-average molecular weight ( $M_w$ ),  $M_n$  and polydispersity index ( $PDI = M_w/M_n$ ) were evaluated by GPC (Shimadzu (Kyoto, Japan) A10 chromatograph, Shodex KF-806M column and HPLC-grade tetrahydrofuran as eluent at 30 °C) based on calibration with polystyrene standards (Tosoh, Tokyo, Japan) using a PLGel mixed B column (25 cm in length, 4.6 mm ID, Varian-Agilent). HPLC-grade THF (Wako Chemical, Osaka, Japan) was used as the eluent, and the data were calibrated based on the polystyrene standards (Varian-Agilent).

### 2.6.5 Dynamic force mode images of atomic force microscopy (DFM-AFM)

DFM-AFM images were captured using an SPA 400 SPM unit with an SII SPI 3800 probe station (Seiko Instruments, Inc.) Hitachi High-Tech Science Corporation (Tokyo, Japan). The sample was deposited onto an HOPG substrate (IBS-MikroMasch, Sofia, Bulgaria; the Japanese vendor is Tomoe Engineering Co. (Tokyo, Japan)) by dropping the aggregate suspension in a mixed solvent of methanol (0.05–0.10 (v/v)) and chloroform (0.95–0.90 (v/v)) and by casting dilute chloroform solutions of **PF8** ( $0.5 \times 10^{-5}$  M), **PSi-S** ( $1 \times 10^{-5}$  M) and their mixed solution. The deposited specimens were observed after the solvents were removed. Herein, we chose chloroform with a low bp ( $\approx 61$  °C) in place of toluene with a high bp ( $\approx 110$  °C) to obtain satisfactory AFM images of these aggregates on HOPG.

### 2.6.6 Wide-angle X-ray diffraction (WAXD)

WAXD data were collected by a Rigaku RINT-TTR III/NM instrument (Tokyo, Japan) using an X-ray wavelength of 1.5418 Å, CuK $\alpha$  radiation with Ni filter,  $2\theta = 0.05^\circ$  interval scan and scanning speed of 2 deg min<sup>-1</sup>. The instrument was operated at 40 kV and 25 mA. Specimens on a crystalline Si substrate were prepared by mixing **PF8** solid ( $M_n = 78,400$ ), **PSi-S** solid ( $M_n = 75,800$ ) and **PSi-S-PF8** (=2:1 molar ratio) hetero-aggregate from chloroform-methanol (1/1 (v/v)) and from toluene-methanol (1/1 (v/v)). These specimens were dispersed in high-vacuum silicone grease (Dow-Corning-Toray).

### 2.6.7 Dynamic light scattering (DLS)

The aggregate sizes were analyzed by a DLS apparatus (DLS-6000, Otsuka Electronics, Hirakata-Osaka, Japan) with a detector angle of 90° and 30 accumulations using the solution viscosity obtained with a Sekonic viscometer (VM-100, Tokyo, Japan) at 25 °C, along with the  $n_D$  value of methanol-toluene (1:1 (v/v)) at 589 nm at 25 °C using an Atago thermo-controlled DR-M2 refractometer (Tokyo, Japan) at 589 nm at 20 °C.

### 2.6.8 Cryo-transmission electron microscopy (TEM)

For cryo-TEM analysis, the aggregate suspension in methanol-toluene (1:1 (v/v)) was drop-cast onto a carbon-coated copper grid of 200 mesh (JEOL, Akishima-Tokyo, Japan) and then directly exposed to liquid nitrogen. High-resolution HR-TEM images were obtained on a Philips Tecnai G2 F20 S-TWINN TEM operated at an accelerating voltage of 200 kV.

## 2.6.9 Computer-generated structural modeling

Computer-generated pentamer models of **PSi-S** with  $P-7_3$  helix (dihedral angle  $\approx 155^\circ$ ) and a trimer model of **PF8** (dihedral angle  $\approx 150^\circ$ ) were optimized with PM3 MM (Gaussian 09 rev. D.01, Gaussian, Inc., Wallingford CT, 2013) running on an Apple PowerMac (2.67 GHz clock, 8 cores and 32 GB memory).

## 2.6.10 Fluorescence lifetime (PL)

To measure the PL lifetime of **PF8**, we performed time-correlated single-photon counting (TCSPC). The second harmonic (SHG = 420 nm) of a tunable Ti:sapphire laser (Mira 900, Coherent) with  $\approx 150$  fs pulse width and 76 MHz repetition rate was used as an excitation source. The PL emission was spectrally resolved using a collection of optics and a monochromator (SP-2150i, Acton). A TCSPC module (PicoHarp, PicoQuant) with an MCP-PMT (C4780, Hamamatsu) was used for ultrafast detection. The total instrument response function (IRF) for PL decay was less than 100 ps, which provided a temporal resolution of less than 10 ps. The deconvolution of the actual fluorescence decay and IRF was performed using fitting software (FlouFit, PicoQuant) to deduce the time constant associated with each exponential decay.

## 2.7 Polysilane removal via photodegradable scaffolding

To photochemically decompose **PSi-S** (and **PSi-R**) in the **PSi-PF8** hetero-aggregate suspension in a cuvette at room temperature, an ultra-high-pressure 500 W Hg lamp (Optiplex BA-H501 and USH-500SC2 Ushio (Tokyo, Japan) with a narrow band-pass filter of 313 nm (Asahi Spectra, Tokyo, Japan) was used. The photon flux at 313 nm was  $14 \text{ mW cm}^{-2}$  using a Si photodetector system (Nova and PD300-UV, Ophir-Japan (Tokyo, Japan)).<sup>8,9</sup>

## 2.8 References

- (1) Yamamoto, T.; Morita, A.; Miyazaki, Y.; Maruyama, T.; Wakayama, H.; Zhou, Z.; Nakamura, Y.; Kanbara, T. *Macromolecules* **1992**, *25*, 1214.
- (2) Simas, E. R.; Gahlen, M. H.; Pinto, M. F. S.; Siqueira, J.; Misoguti, L. *J. Phys. Chem. A* **2010**, *114*, 12384.
- (3) Liu, Y.; Murao, T.; Nakano, Y.; Naito, M.; Fujiki, M. *Soft. Matter* **2008**, *4*, 2396.
- (4) Nakashima, H.; Fujiki, M.; Koe, J. R. *Macromolecules* **1999**, *32*, 7707.
- (5) Fujiki, M. *J. Am. Chem. Soc.* **2000**, *122*, 3336.
- (6) Fujiki, M. *Jpn. Kokai Tokyo Koho* **1993**, JP 05-202528.
- (7) Fujiki, M. *Symmetry*. **2010**, *2*, 1625.
- (8) Fujiki, M.; Yoshida, K.; Suzuki, N.; Zhang, J.; Zhang, W.; Zhu, X. *RSC Adv.* **2013**, *3*, 5213.
- (9) Fujiki, M.; Donguri, Y.; Zhao, A.; Nakao, A.; Suzuki, N.; Yoshida, K.; Zhang, W. *Polym. Chem.* **2015**, *6*, 1627.

## Chapter 3. Helical scaffolding of polysilane to polyfluorene

### 3.1 Chirality amplification from CD-active PSi to CD-silent PF8

Figure 3.1 shows the CD signals and broader UV-Vis spectra at approximately 399 nm that arise from  $\alpha$ -phase **PF8**. The longest CD band and a sharper visible band at 435 nm were assigned to  $\beta$ -phase **PF8**.<sup>1-3</sup> An intense bisignate CD band at 305 and 322 nm was characteristic of the exciton couplet arising from the helically assorted **PSi** aggregate<sup>4,6</sup>.

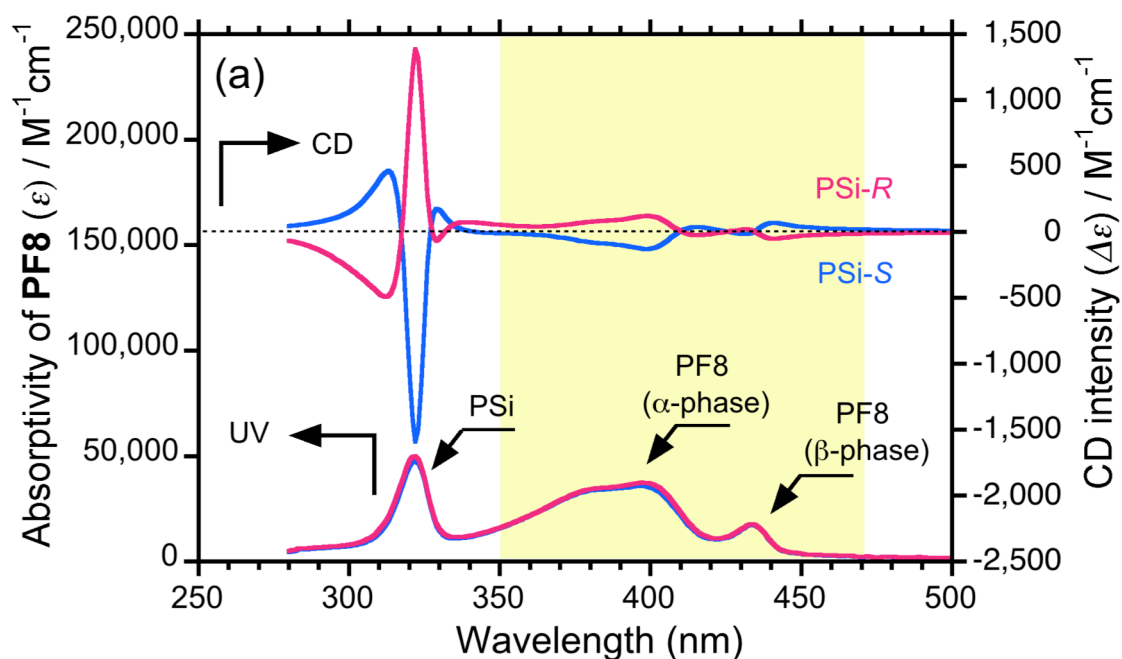


Figure 3.1. CD and UV-Vis spectra of hetero-aggregates including **PSi-S** (**PSi-R**) and **PF8** with a 2-to-1 ratio produced in a toluene-methanol cosolvent (1.5/1.5 (v/v)) with  $[\text{PF8}] = 2.5 \times 10^{-5} \text{ M}$  and  $[\text{PSi-S}] = 5.0 \times 10^{-5} \text{ M}$  as their repeating units. The  $M_w$  of **PSi-S**, **PSi-R** and **PF8** is 75,800, 73,900 and 78,800.

Our results indicate that macromolecular helicity transfer is possible between helical non-charged **PSi** and non-helical non-charged **PF8** during the course of hetero-aggregation using a toluene-methanol cosolvent. For comparison, chloroform-methanol cosolvents with several ratios make it possible to generate CD/CPL active PSi-S-PF8 hetero-aggregates, although the absolute  $g_{CD}$  values of **PF8** decreases to almost one-third of the initial value. The helix scaffolds of **PSi-S** and **PSi-R** have a similar  $M_n$  of  $\approx 70,000$ . They exhibit nearly ideal mirror-image CD spectral characteristics with optically active **PF8**, consistent with the characteristics previously reported for analogous chiral polymer systems<sup>1,7-9</sup>.

The coexistence of highly emissive  $\alpha$  and  $\beta$ -phase **PF8** in the aggregates led to the detection of clear CPL signals and PL spectra arising from the  $\beta$ -phase<sup>1,3</sup>, obeying a photoexcited energy migration scheme (Figure 3.2). The CPL- and PL-bands are assigned to vibronic 0–0' (438 nm), 0-1' (464 nm) and 0-2' (498 nm) bands with 1470–1490  $\text{cm}^{-1}$  spacing due to aromatic ring stretching vibration of chiral b-phase as a result of spontaneous relaxation from the lowest  $S_1$ -state with  $v = 0'$  to the  $S_0$ -state with  $v = 0,1,2$  by Kasha's rule.

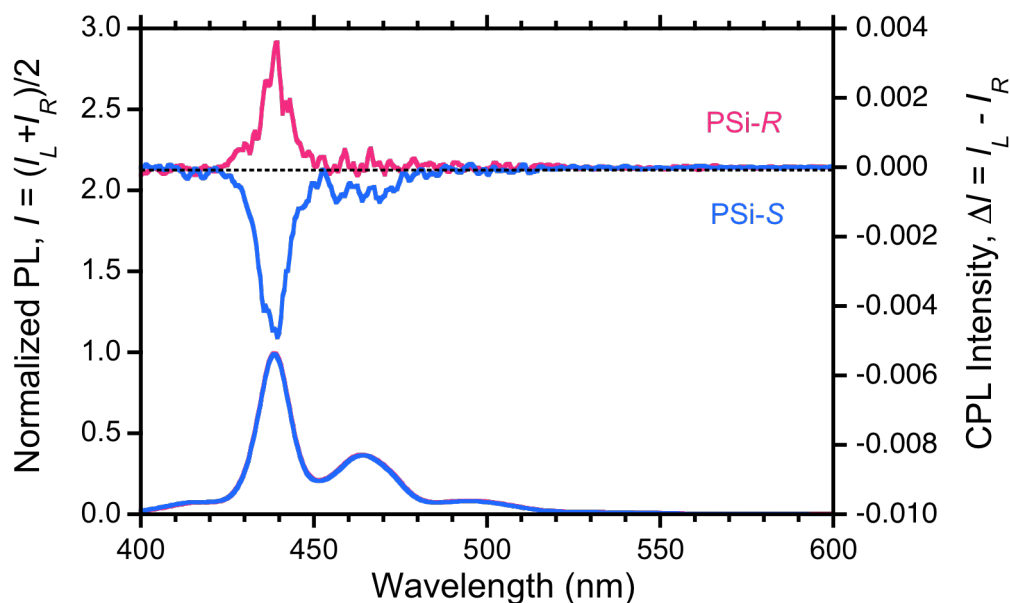


Figure 3.2. CPL and PL spectra of the as-prepared **PSi** and **PF8** (= 2:1 ratio) hetero-aggregate in toluene-methanol (1.5/1.5 (v/v)).

### 3.2 Removal of **PSi-S** and **PSi-R** scaffolds

To spectroscopically elucidate the scaffolding capability of **PSi-S** and **PSi-R** toward **PF8**, the  $g_{CD}$  value of the hetero-aggregate suspension in a methanol-toluene cosolvent (1.5/1.5 (v/v)) was plotted as a function of the photoirradiation time at 313 nm, which is the optimal wavelength for excitation of the  $\text{Si}\sigma\text{-Si}\sigma^*$  transition, as shown in Figure 3.3. To perform the polymer-selective photoscissoring experiment of the metastable **PSi**, we confirmed no oxidization of **PF8** aggregates by prolonged irradiation at 313 nm, as evident from the lack of the green PL band due to the **PF8** keto form<sup>10-14</sup> (Figure 3.4).

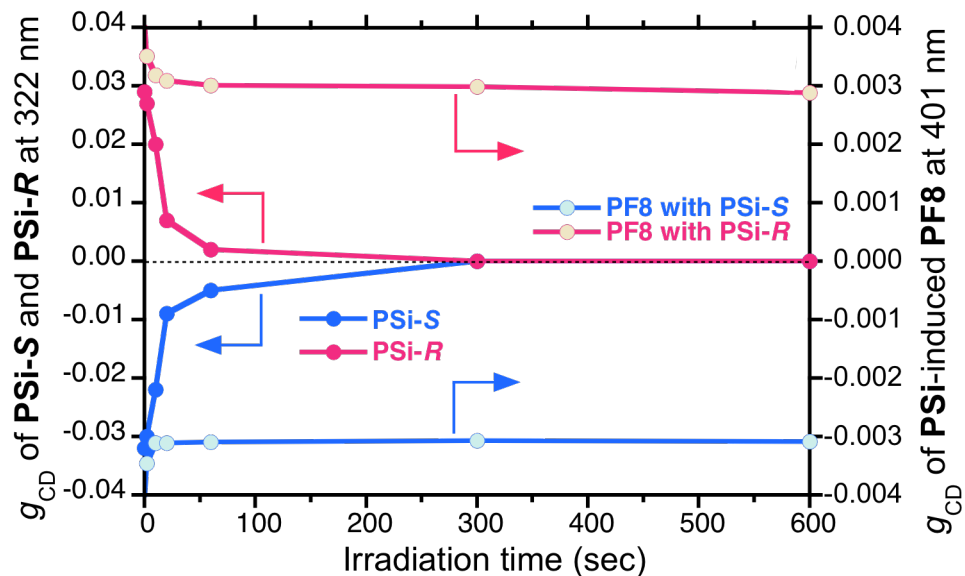


Figure 3.3. Hetero-aggregates  $g_{CD}$  values of **PF8** ( $2.5 \times 10^{-5}$  M) and **PSi-S** ( $5.0 \times 10^{-5}$  M) as a function of irradiation time at 313 nm ( $14 \mu\text{W cm}^{-2}$ ).

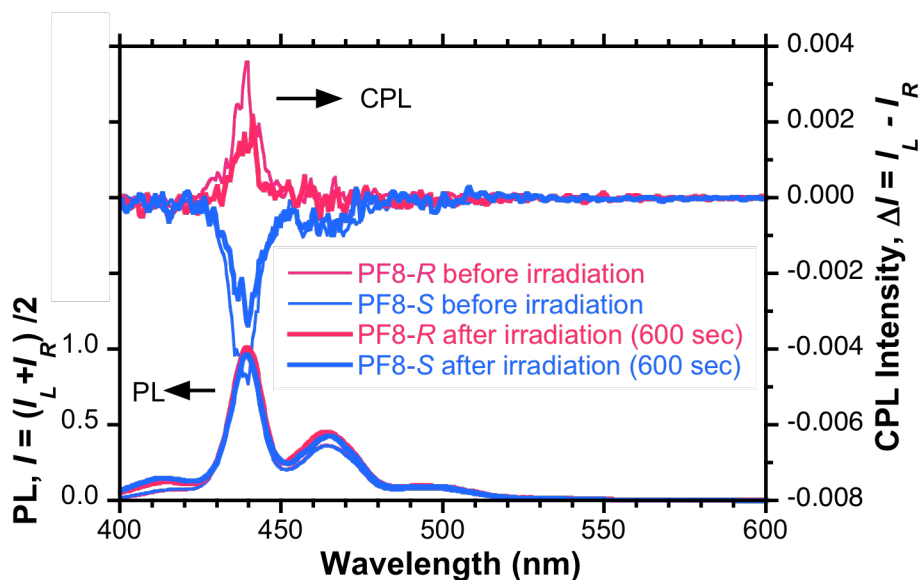


Figure 3.4. CPL and PL spectra excited at 370 nm for the **PSi-S-PF8** and **PSi-R-PF8** aggregates before and after 313 nm irradiation for 600 s. The  $M_n$  values of **PSi-S**, **PSi-R** and **PF8** are 75,800, 73,900 and 78,800, respectively.

As shown in Figure 3.3, **PSi-S** decomposed rapidly within 60 s and completely disappeared within 300 s. The CD and CPL (Figure 3.4) amplitudes for **PF8** in **PSi-S-PF8**, which was photoirradiated for 600 s, nearly retained their initial  $g_{\text{CD}}$  (approximately  $\pm 0.005$  at 401 nm) and  $g_{\text{CPL}}$  (approximately  $\pm 0.004$  at 438 nm) magnitudes along with the chiroptical signs of **PF8** in the non-irradiated **PSi-PF8** (=2:1) aggregates. An approximate 10–20 % decrease in the  $g_{\text{CD}}$  magnitudes of **PF8** was observed after complete removal of **PSi-R** and **PSi-S**. The **PSi**-selective photoscissoring reaction of the **PSi-PF8** hetero-aggregates was demonstrated.

### 3.3 Confirming the elimination of **PSi-S** and **PSi-R** scaffolds in **PF8**

For further verification, a PL decay experiment of the **PSi-S-PF8** hetero-aggregate before and after photoscission was employed (Figure 3.5). The PL decay curve due to  $\beta$ -phase **PF8** and its PL lifetime ( $\tau_{1/2}$ , detected at 460–480 nm) were nearly unchanged before and after **PSi-S** selective photoscissoring at 313 nm for 600 s. The  $\tau_{1/2}$  value of **PF8** was 2.35 ns. The hetero-aggregate  $\tau_{1/2}$  value of **PF8** was slightly delayed from 2.37 to 2.46 ns after prolonged UV irradiation. This result indicates that **PF8** maintained its original main chain structures, which resulted in photochemical removal of **PSi-S** as scaffolding. However, the helically assorted higher-order structure of **PF8** remained unchanged and was stable during the photochemical reaction.

The small-molecule fragments of the **Si-Si** chiral radical originating from photodegradation can provide active sites for other interactions. Since no pronounced effect was observed in the **PSi-S-PF8** hetero-aggregate results, it was assumed that any effect was minimal. The generated accessible small molecule aggregates after the irradiation could be easily removed by the addition of polar solvents.

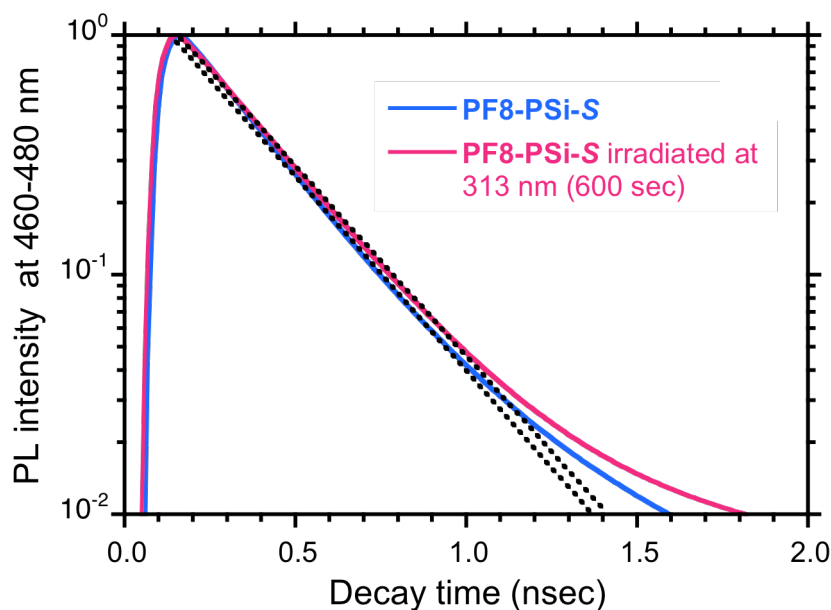


Figure 3.5. PL lifetime at 420 nm (excited by 150-fs pulse laser) of hetero-aggregates made of **PF8** ( $2.5 \times 10^{-5}$  M) and **PSi-S** ( $5.0 \times 10^{-5}$  M).

The results of the DLS study strongly supported this conclusion (Figure 3.6). The hetero-aggregates caused division into two particles that were  $\approx 2,000$  nm ( $\approx 40$  % by volume relative to the original) and  $\approx 300$  nm in diameter. This feature is similar to a cell division process, even though the original material consisted of a single aggregate with a diameter of  $\approx 2,730$  nm. The 40 % reduction by volume was nearly equal to 49 % **PF8** by weight in the original **PSi-S-and-PF8** with a 2-to-1 ratio of repeating units.

The scissoring product of **PSi-S** was assumed to be mostly concentrated in the 300 nm particles, whereas **PF8** mostly remained in the 2,000 nm particles. This result indicates that certain chiral species exist as sacrificial scaffolds in the chemical evolution process of life and catalyze the L-D preferences of biopolymers in *mm*-sized aggregates surrounded by aqueous medium;<sup>15</sup> this is the model of coacervate proposed by Oparlin and Haldane.

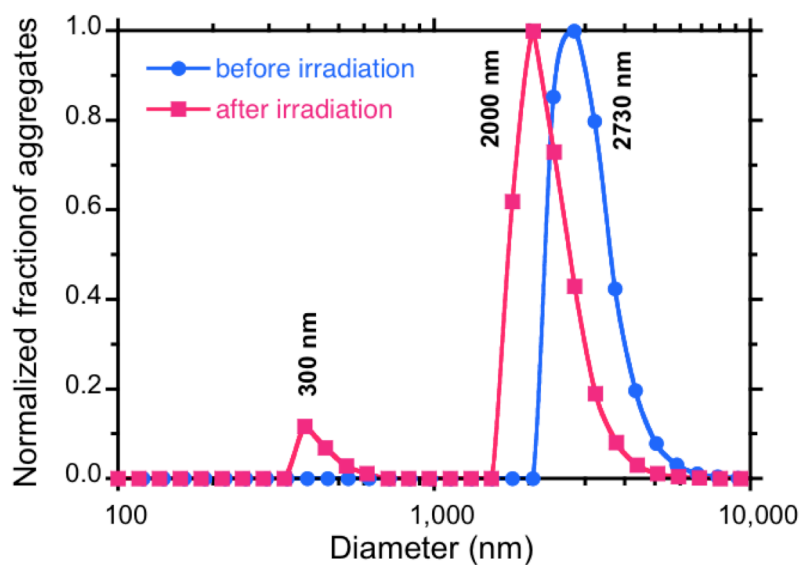


Figure 3.6. DLS data of the photobleached aggregates of **PF8** ( $2.5 \times 10^{-5}$  M) and **PSi-S** ( $5.0 \times 10^{-5}$  M) in a toluene-methanol cosolvent (1.5/1.5 (v/v)) before and after irradiation at 313 nm ( $14 \text{ mW cm}^{-2}$ ) for 600 s.

### 3.4 References

- (1) Nakano, Y.; Liu, Y.; Fujiki, M. *Polym. Chem.* **2010**, *1*, 460
- (2) Zhao, Y.; Rahim, N. A. A.; Xia, Y.; Fujiki, M.; Song, B.; Zhang, Z.; Zhang, W.; Zhu, X. *Macromolecules* **1999**, *32*, 7707
- (3) Scherf, U.; List, E. J. W. *Adv. Mater.* **2002**, *14*, 477
- (4) Nakano, Y.; Ichiyanagi, F.; Naito, M.; Y.-G. Yang.; Fujiki, M. *Chem. Commun.* **2012**, *48*, 6636
- (5) Eliel, E. L.; Wilen, S. H.; Mander, L. N. *Stereochemistry of Organic Compounds, Chapter 13. Chiroptical Properties*, Wiley-Interscience, New York (NY), **1994**.
- (6) Nakano, Y.; Fujiki, M. *Macromolecules* **2011**, *48*, 7511
- (7) Le Gac, S.; Schwartz, E.; Koepf, M.; Cornelissen, J. J. L. M.; Rowan, A. E.; Nolte, R. J. M. *Chem. Eur. J.* **2010**, *16*, 6176
- (8) Le, J. D.; Pinto, Y.; Seeman, N. C.; Musier, K.; Taton, T. A.; Kiehl, R. A. *Nano Lett.* **2004**, *4*, 2343
- (9) Guo, Y. M.; Oike, H.; Aida, T. *J. Am. Chem. Soc.* **2004**, *126*, 716
- (10) List, E. J. W.; Guentner, R.; De Freitas, P. S.; Scherf, U. *Adv. Mater.* **2002**, *14*, 374
- (11) Shiraki, T.; Shindome, S.; Toshimitsu, F.; Fujigaya, T.; Nakashima, T. *Polym. Chem.* **2015**, *6*, 5103
- (12) Zaikowski, L.; Kaur, P.; Gefind, C.; Selvaggio, E.; Asaoka, S.; Wu, Q.; Chen, H. C.; Takeda, N.; Cook, A. R.; Yang, A.; Rosanelli, J.; Miller, J. R. *J. Am. Chem. Soc.* **2012**, *134*, 10852
- (13) Knaapila, M.; Konopkova, Z.; Torkkeli, M.; Haase, D.; Liermann, H.-P.; Scherf, U. *Phys. Rev. E*, **2013**, *87*, 022602.
- (14) Feringa, B. L.; van Delden, R. A.; Koumura, N.; Geertsema, E. M. *Chem. Rev.* **2000**, *100*, 1789.
- (15) Fujiki, M.; Yoshida, K.; Suzuki, N.; Rahim, N. A. A.; Jalil, J. A. *Photochem. Photobiol. A. Chem.* **2016**, *331*, 120.

## Chapter 4. PSi to PF8 scaffolding structure and its possible mechanism

### 4.1 WAXD study of PSi-S, PF8 and PSi-S-PF8 with 2:1 ratio

We compare the WAXD profiles between **PSi-S-PF8** (2:1) hetero-aggregates and the corresponding **PF8** and **PSi-S** homo-aggregates in Figure 4.1 (a). The WAXD profile of **PSi-S-PF8** hetero-aggregates has three characteristic  $d$ -spacings at 4.4 Å, 7.5 Å and 12.4 Å. The 12.4 Å spacing is ascribed to the interchain distance of **PSi-S**. However, the origins of the 4.4 Å and 7.5 Å spacings are obscure because these are commonly seen among three aggregates. The WAXD profile of **PSi-S-PF8** hetero-aggregate was sensitive to sample preparation conditions, specifically whether the aggregate was cast from toluene-methanol (1/1 (v/v)) or chloroform-methanol (1/1 (v/v)) (Figure 4.1 (b)). The 12.4 Å spacing changed to 12.2 Å when chloroform was employed, and the 7.5 Å spacing shortened by  $\approx 0.8$  Å to  $\approx 6.7$  Å. The 4.4 Å spacing was unchanged, as shown in Figure 4.2 and 4.3.

The reductions of 0.2 Å and 0.8 Å in the hetero-aggregates imply certain interactions between **PF8** and **PSi-S** that depend on the solvent condition. However, no more useful information about these aggregates could be obtained due to the limited availability of clear X-ray scattering peaks. The helical pitch of polymers is susceptible to external physical and chemical biases. Recently, Knaapila *et al.* reported that high hydrostatic pressure strongly affects the helical pitch of poly[9,9-bis(2-ethylhexyl)fluorene].<sup>1</sup>

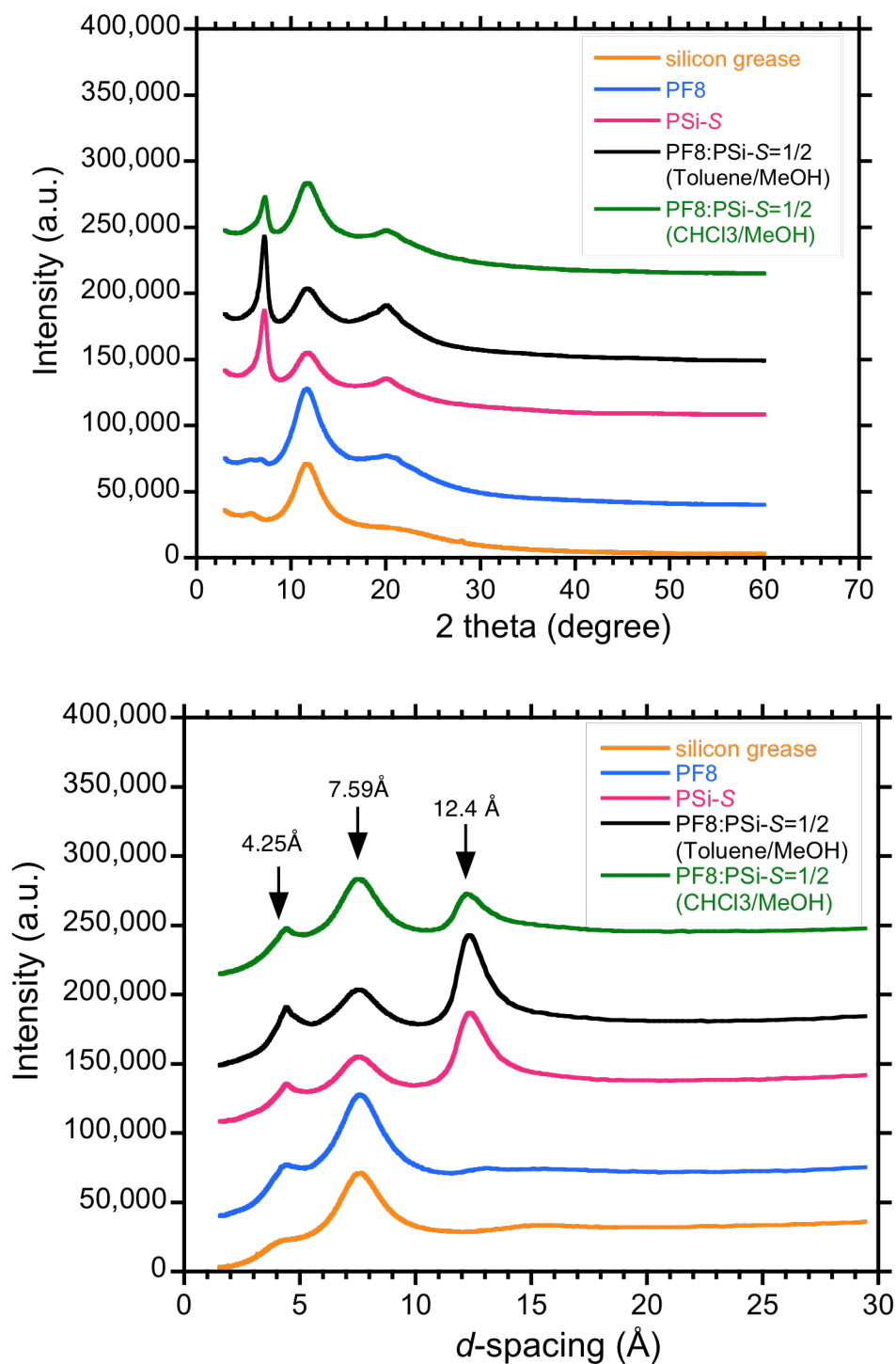


Figure 4.1. WAXD data of high-vacuum silicone grease (Dow-Corning-Toray), **PF8** ( $M_n = 78,800$ ), **PSi-S** ( $M_n = 75,800$ ) and their **PSi-S-PF8** (= 2:1) aggregate from chloroform and methanol (1/1 (v/v)) and from toluene and methanol (1/1 (v/v)) embedded to silicone grease onto an Si-crystal substrate as functions of (a) diffraction angle ( $2\theta$ ) and (b)  $d$ -spacing

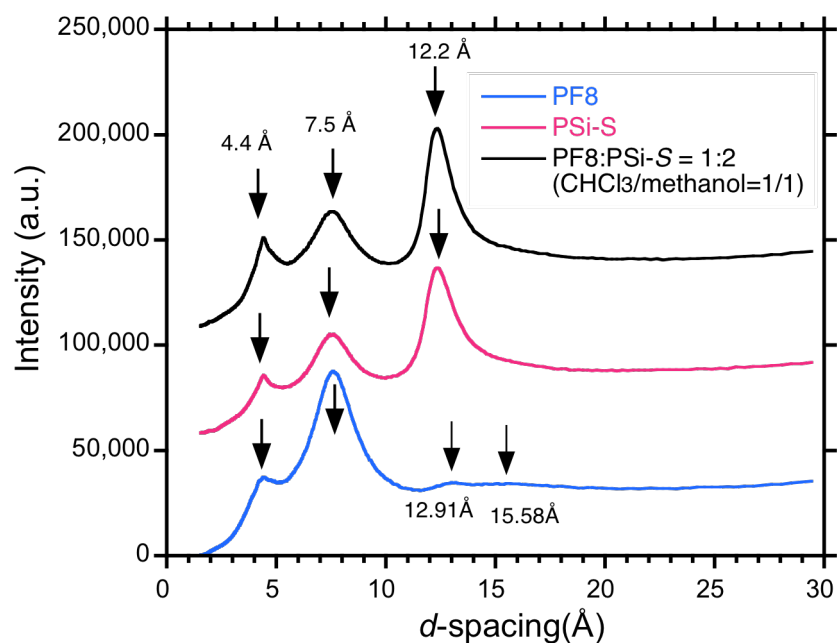


Figure 4.2. WAXD of **PF8** ( $M_n = 78,800$ ), **PSi-S** ( $M_n = 75,800$ ) and **PSi-S-PF8** (= 2:1) aggregate from chloroform and methanol (1/1 (v/v)) subtracted with WAXD data of the silicone grease.

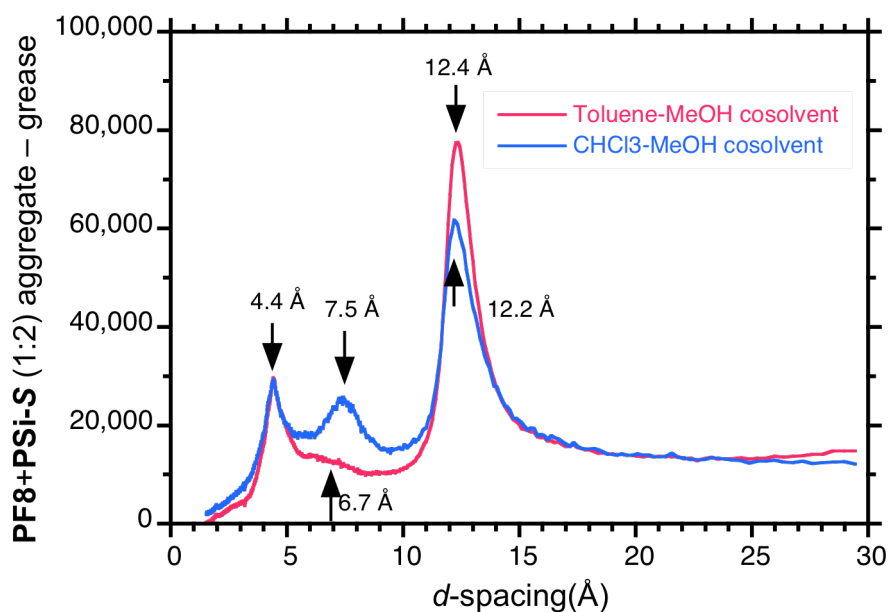


Figure 4.3. Comparison of WAXD between **PSi-S-PF8** (= 2:1) aggregates from chloroform and methanol (1/1 (v/v)) and from toluene and methanol (1/1 (v/v)) subtracted with WAXD data of the silicone grease.

## 4.2 Observation of **PSi-S**, **PF8** and **PSi-S-and-PF8** structure

We attempted to view the detailed structures of **PF8** and **PSi-S** homo-aggregates and **PSi-S-and-PF8** hetero-aggregates using cryogenic transmission electron microscopy (cryo-TEM) (Figure 4.4). Because of the rapid scissoring reaction of the Si-Si backbone over the TEM observation time, clear visualization was impossible even at liquid-nitrogen temperatures. For this reason, we employed DFM-AFM to avoid sample damage.

The first approach was applied to view DFM-AFM images of **PSi-S** and **PF8** homo-aggregates and **PSi-S-and-PF8** hetero-aggregates. These specimens were directly deposited onto HOPG by drop casting the aggregates suspension in  $10^{-4}$  M toluene-methanol (1/1 (v/v)). However, we did not obtain a clearer assortment of images (Figure 4.5).

The second approach was to use chloroform as a good solvent including a small volume fraction of methanol. We obtained improved AFM images of **PSi-S** and **PF8** homo-aggregates on HOPG by drop casting of their dilute chloroform solutions ( $10^{-5}$  M). As shown in the height profiles of Figure 4.6, the diameters of **PSi-S** cast from pure chloroform solution ranged from  $\approx 0.5$  to  $\approx 1.1$  nm on HOPG. These heights are nearly consistent with the diameters of individual **PSi-S** chains that were laterally aligned on HOPG surface. Two representative molecular diameters of  $7_3$ -helical **PSi-S** are given in Figure 4.7. One motif consists of elongated *n*-hexyl side groups with *all-trans* geometry; the other is a contracted shape with *gauche* form.

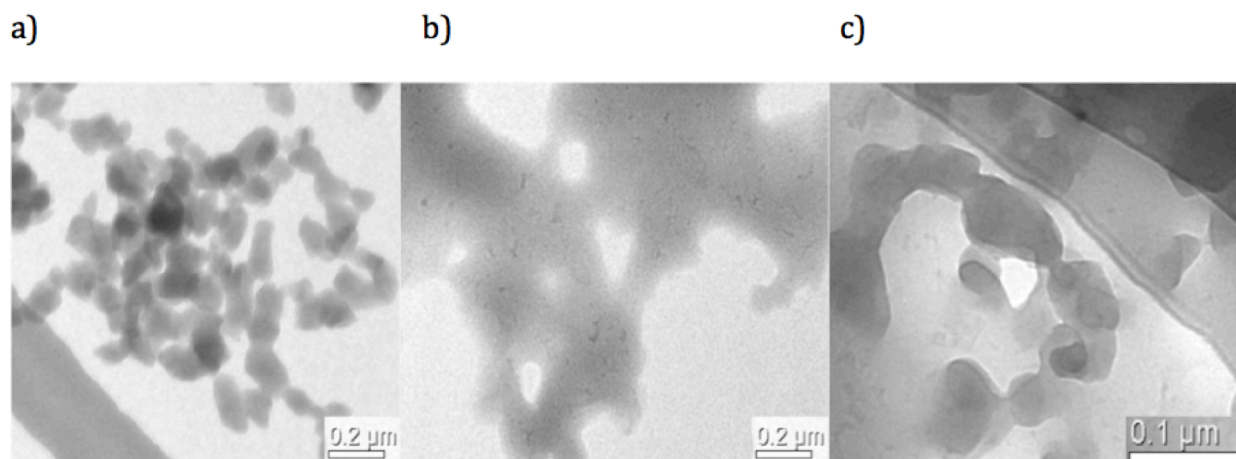


Figure 4.4. Cryo-TEM images using using the toluene-methanol (1/1 (v/v)) of a) **PF8** aggregates, b) **PSi-S** aggregates, and c) **PF8** and **PSi-S** hetero-aggregates.

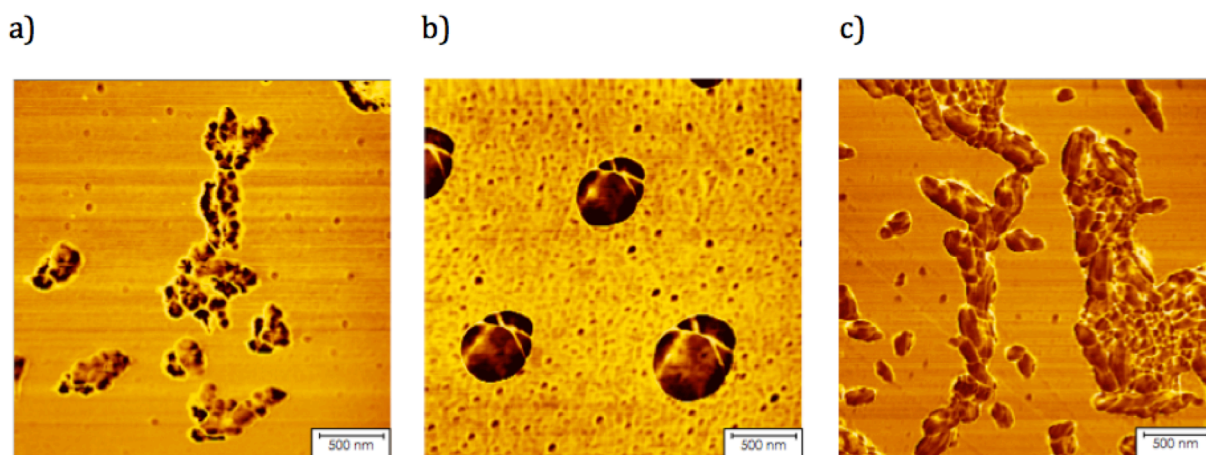


Figure 4.5. Tapping-mode AFM images on HOPG using the toluene-methanol (1/1 (v/v)) for the a) **PSi-S** aggregates, b) **PF8** aggregates and c) **PF8** and **PSi-S** hetero-aggregates (ratio of 2:1).

**PSi-S from  $10^{-5}$  M  $\text{CHCl}_3$  solution**

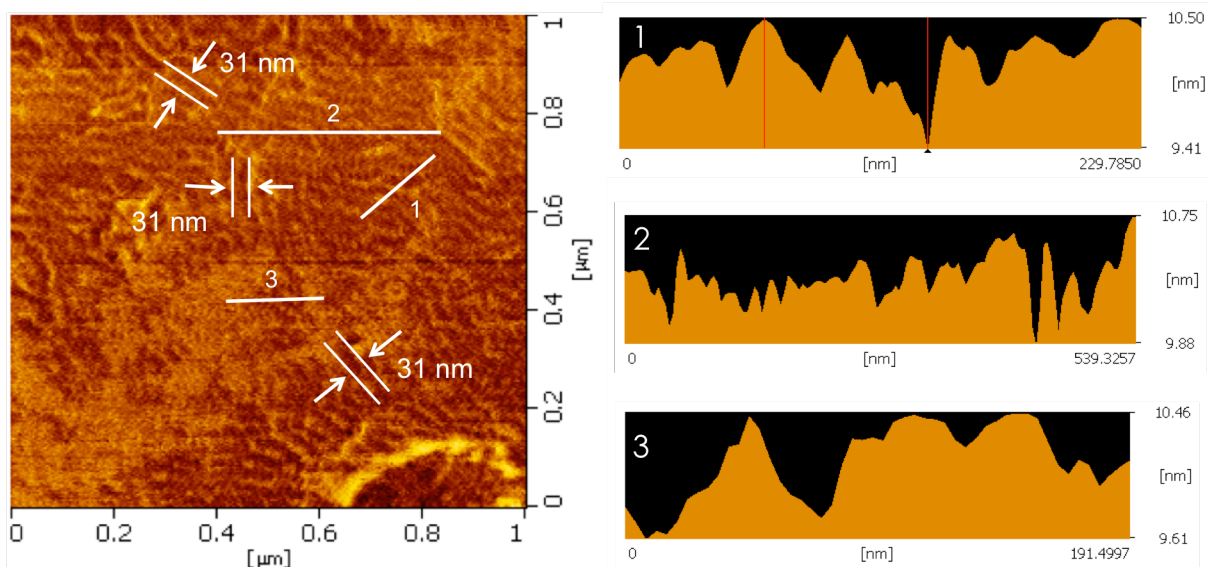


Figure 4.6. DFM-AFM image and height profile with SI-DF20S (coated with Al,  $f = 129$  KHZ,  $R = 2-5$  nm,  $D = 12.5$   $\mu\text{m}$ ,  $C = 12$   $\text{N m}^{-1}$ ) on HOPG casting from  $1 \times 10^{-5}$  M chloroform solution of **PSi-S** ( $M_n = 75,800$ ).

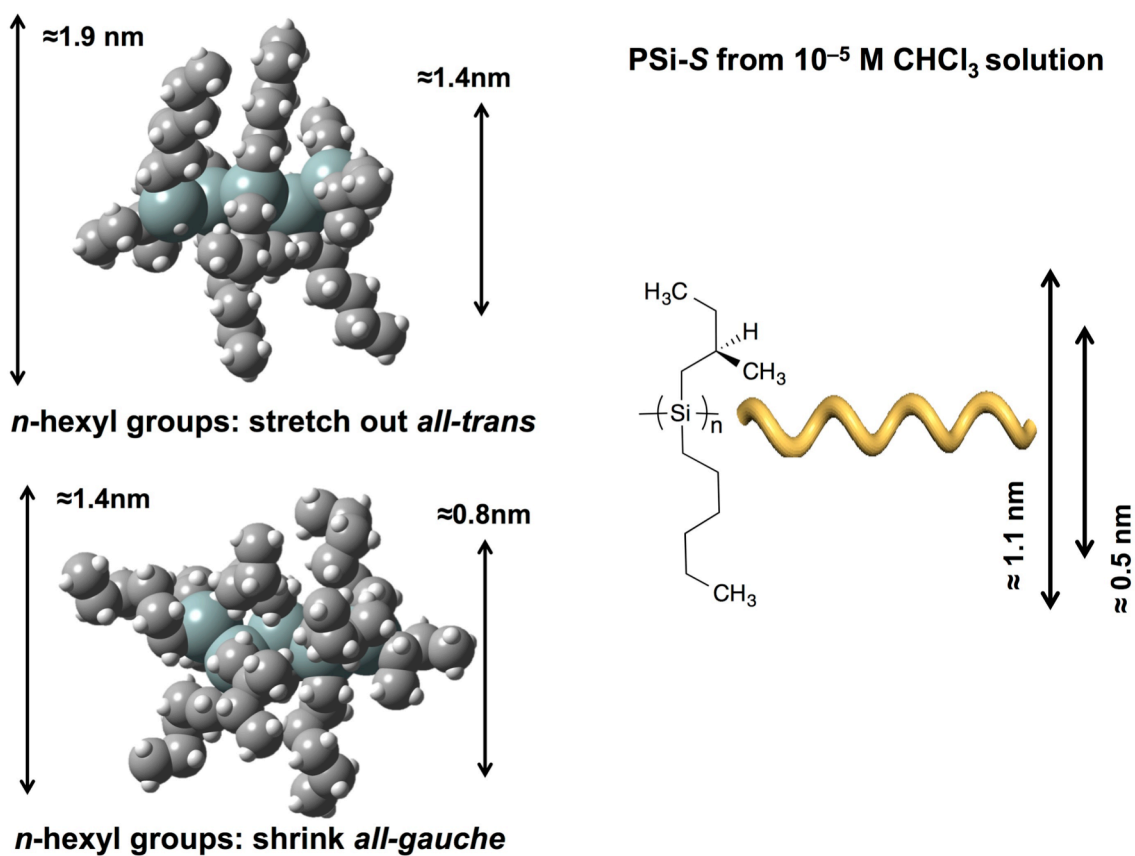


Figure 4.7. Two representative models of *n*-hexyl structures with stretch out (*all-trans*) and shrink (*all-gauche*) forms.

**PSi-S from  $10^{-5}$  M solution of 5% methanol and 95%  $\text{CHCl}_3$**

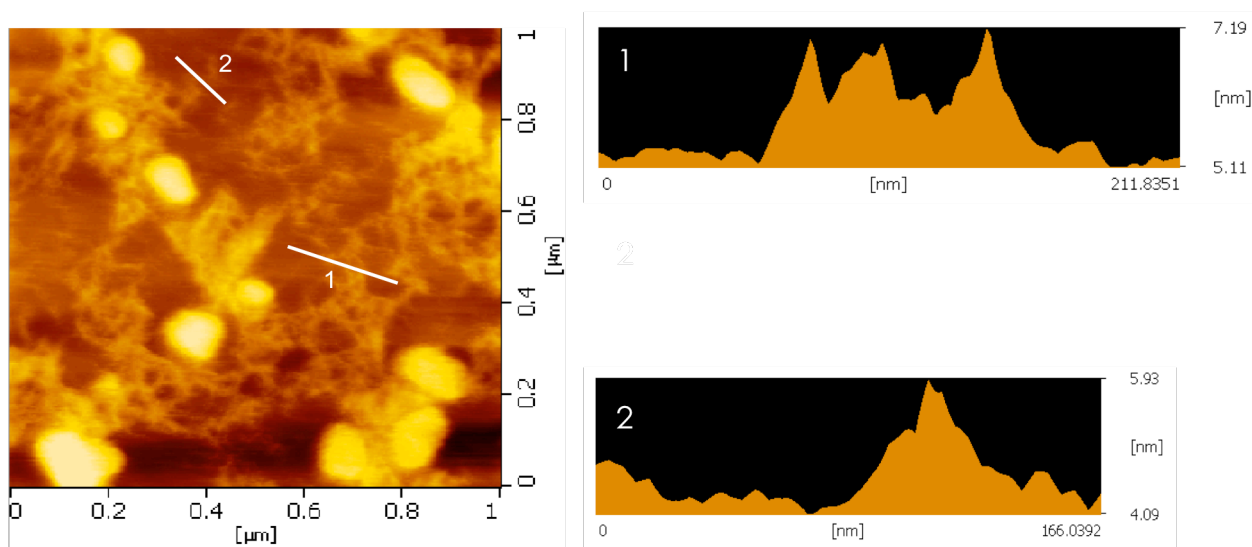


Figure 4.8. DFM-AFM image and height profiles with SI-DF20S (coated with Al,  $f = 129$  KHz,  $R = 2-5$  nm,  $D = 12.5$   $\mu\text{m}$ ,  $C = 12$   $\text{N m}^{-1}$ ) on HOPG casting from  $5 \times 10^{-6}$  M chloroform solution of **PF8** ( $M_n = 78,400$ ).

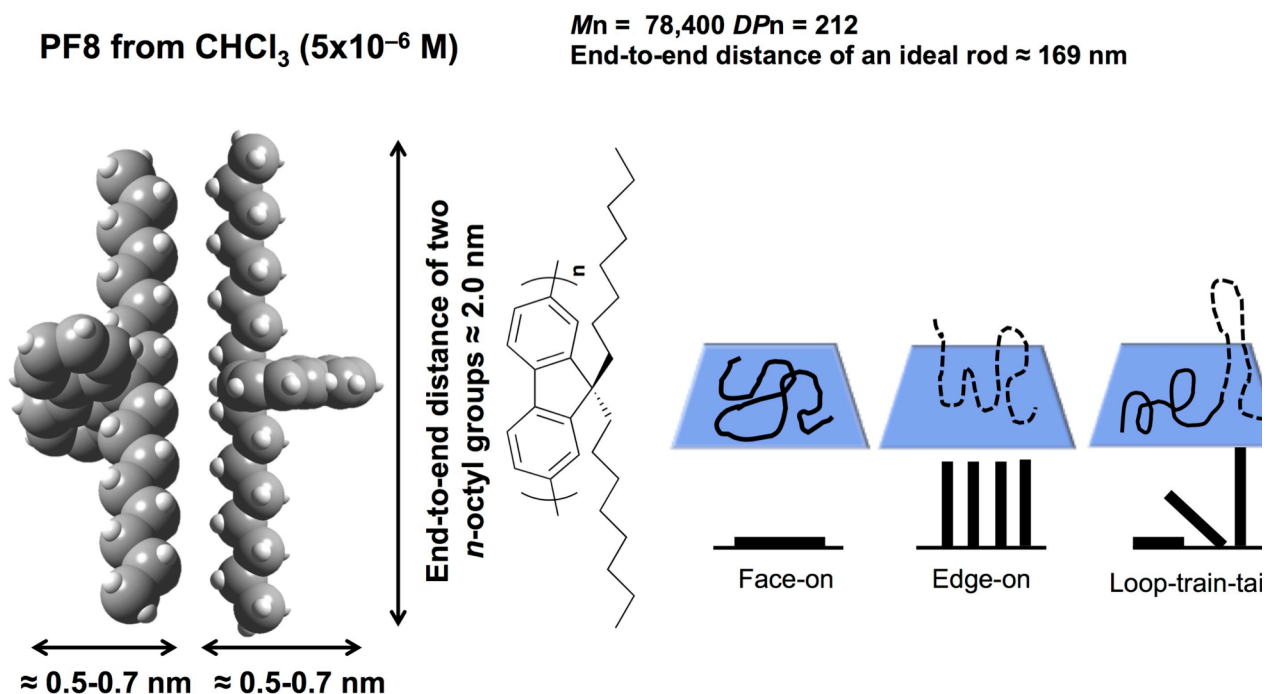


Figure 4.9. A representative model of two  $n$ -octyl groups with stretch out form and several orientations of **PF8** at HOPG.

## Poly(*n*-hexyl-(S)-2 methylbutylsilane) (PSi-S)

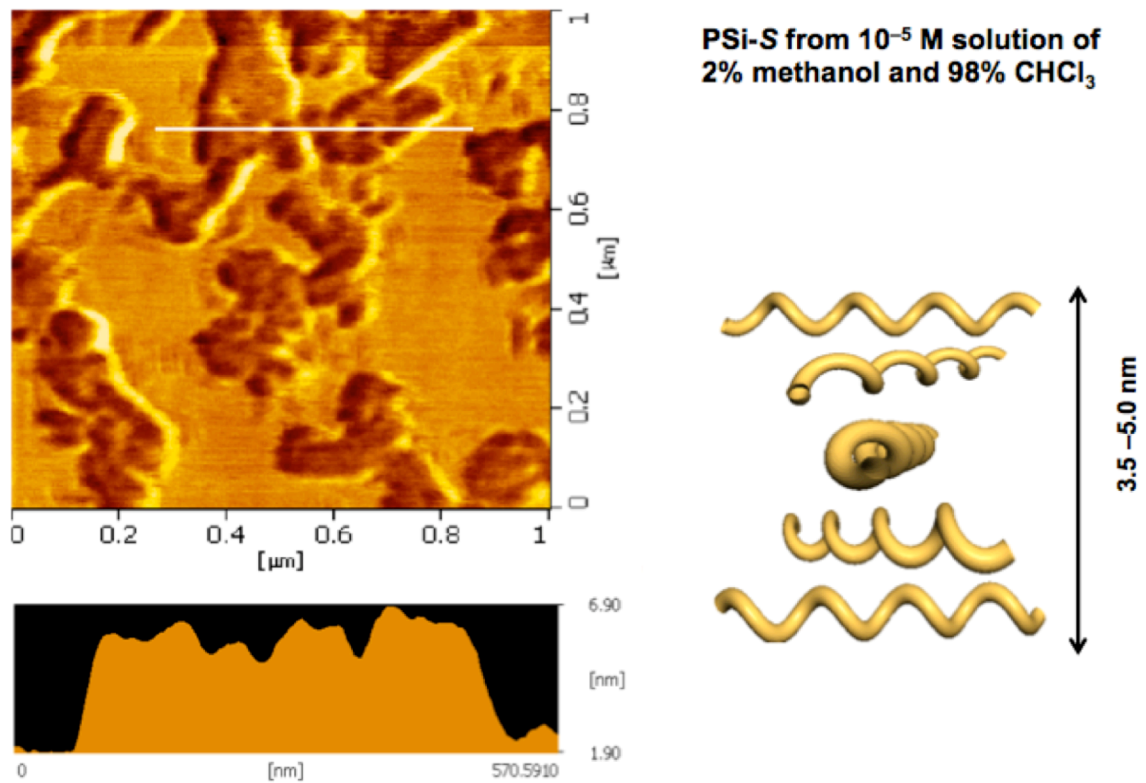


Figure 4.10. (Left) DFM AFM image and height profile with SI-DF20S (coated with Al,  $f = 129$  KHz,  $R = 2-5$  nm,  $D = 12.5$  mm,  $C = 12$  N m $^{-1}$ ) on HOPG casting from  $1 \times 10^{-5}$  M in 2% methanol and 98 % chloroform solution of **PSi-S** ( $M_n = 75,800$ ). (Right) Schematic model of  $7_3$ -helical **PSi-S**.

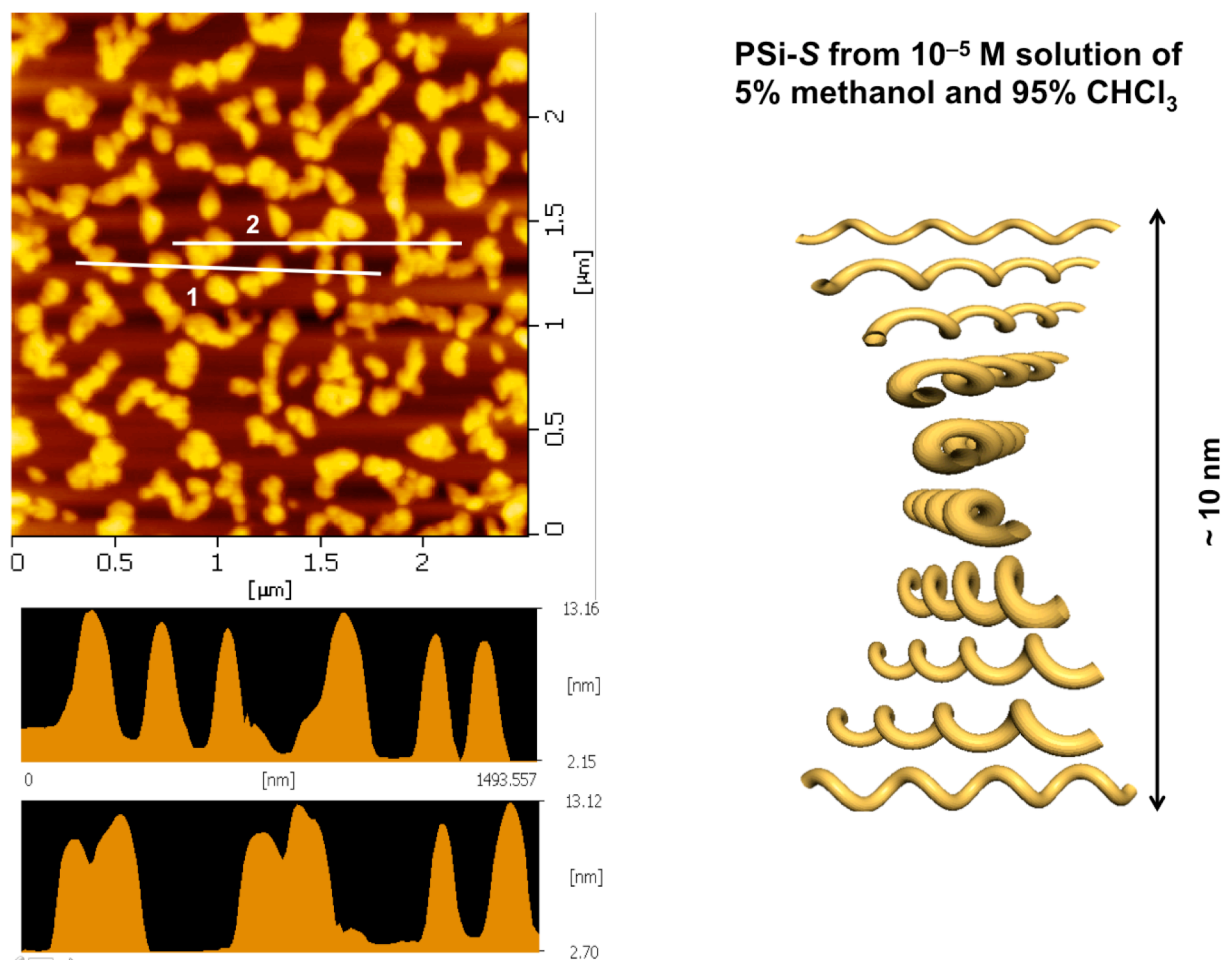


Figure 4.11. (Left) DFM AFM image and height profile with SI-DF20S (coated with Al,  $f = 129$  KHz,  $R = 2-5$  nm,  $D = 12.5$   $\mu\text{m}$ ,  $C = 12$   $\text{Nm}^{-1}$ ) on HOPG casting from 5% methanol and 95 % chloroform solution ( $1 \times 10^{-5}$  M) of **PSi-S** ( $M_n = 75,800$ ). (Right) A schematic model of  $7_3$ -helical **PSi-S** aggregate on HOPG.

Figure 4.8 indicates the diameter of individual **PF8** chain. Figure 4.9 shows the elongated structure of two *n*-octyl groups with *all-trans* conformation. Similarly, a **PSi-S-PF8** hetero-aggregate (at a nominal ratio of 2:1) was cast from a dilute solution ( $\approx 10^{-5}$  M) of 5 % methanol and 95 % chloroform (Figure 4.11) and 10 % methanol and 90 % chloroform (Figure 4.11). The use of volatile chloroform yielded better AFM images than less-volatile toluene.

The height value of 1.1 nm is nearly identical to the  $d$ -spacing (12.2 and 12.4 Å) of the **PSi-S** solid (Figure 4.2 and 4.3). The WAXD and AFM images suggested that  $n$ -hexyl groups adopt a contracted geometry on HOPG. The averaged end-to-end distance of **PSi-S** arrays on HOPG is  $\approx$  31 nm. This value corresponds to  $\approx$  170 Si-repeating units but is one-third of  $DP_n$  (= 458) evaluated by GPC analysis. However, we could not obtain a clear helical molecular image of **PSi-S** on HOPG, probably because of the AFM tip broadening effect, as the current AFM tip size (2–5 nm) was comparable with the  $7_3$ -helical pitch (1.3–1.5 nm) of **PSi-S**.

In the presence of methanol in chloroform, the cross-section values of **PSi-S** sharply increased. The cross-section obtained from 5 % methanol and 95 % chloroform was in the range of  $\approx$  3.5 nm and  $\approx$  5.0 nm, equivalent to a 5–7 molecule thickness of **PSi-S**. The cross-section after removal of 10 % methanol and 90 % chloroform was in the range of 8 nm to 11 nm, yielding an 11–15 molecule thickness of **PSi-S**. These AFM images clearly indicated that **PSi-S** spontaneously formed aggregates with the help of methanol as an aggregation-inducing solvent. The aggregate size and height of **PSi-S** largely depended on the initial volume fraction of methanol.

Height profiles of **PF8** obtained in chloroform ranged from  $\approx$  0.5 nm to  $\approx$  2 nm. Assuming an elongated structure of two  $n$ -octyl groups with *all-trans* conformation, the estimated end-to-end distance of two side groups was  $\approx$  2.0 nm, and the thickness of the **PF8** rings was  $\approx$  0.5–0.7 nm. Because of their semi-flexible nature, **PF8** chains can relax into an ill-defined, highly entangled arrangement on HOPG, including face-one, edge-on and loop-train-tail structures positioned as outlined in Figure 4.9.

From **PSi-S** ( $1 \times 10^{-5}$  M) and **PF8** ( $0.5 \times 10^{-5}$  M) solution of 5% methanol and 95%  $\text{CHCl}_3$

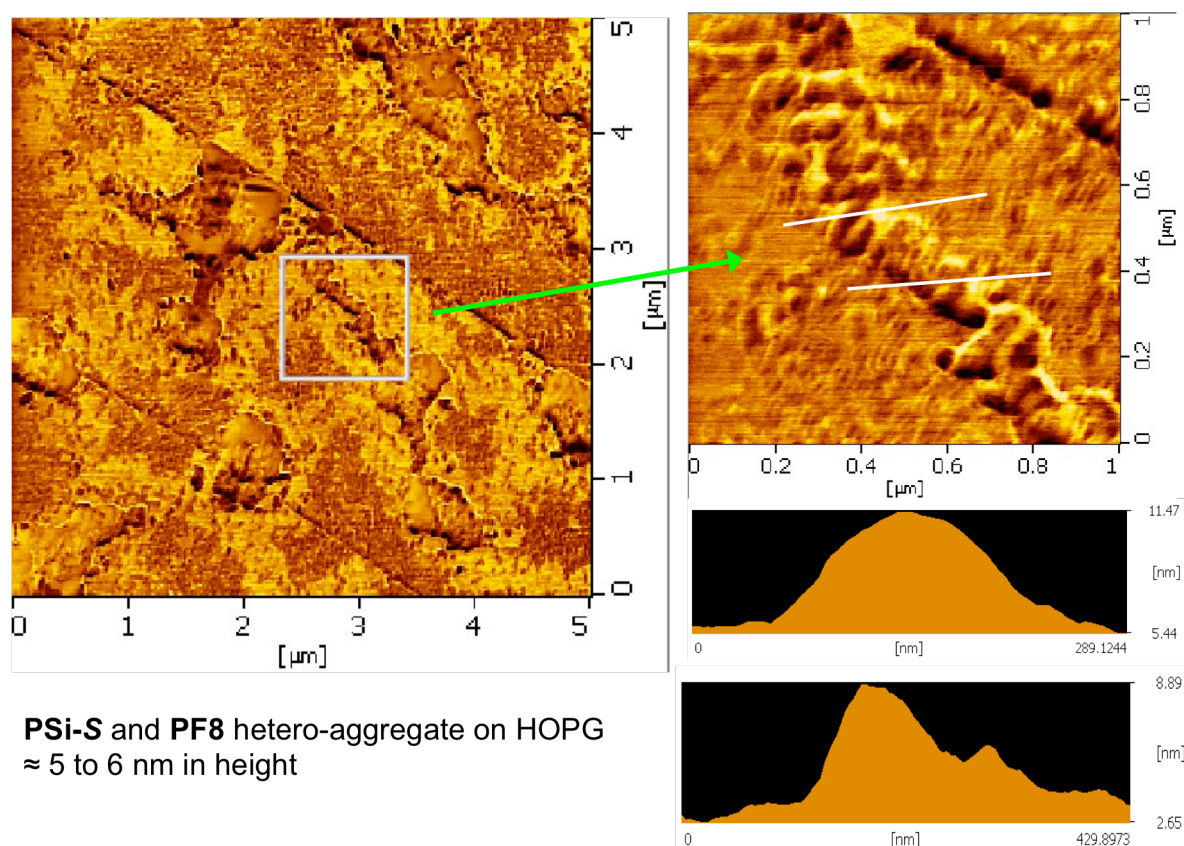


Figure 4.12. DFM AFM images and height profiles with SI-DF20S (coated with Al,  $f = 129$  KHz,  $R = 2-5$  nm,  $D = 12.5$  mm,  $C = 12$  N m $^{-1}$ ) on HOPG casting from **PF8** ( $0.5 \times 10^{-5}$  M) and **PSi-S** ( $1.0 \times 10^{-5}$  M) (2:1 ratio) from solution of 5% methanol and 95%  $\text{CHCl}_3$ .

Finally, height profiles of **PSi-S** and **PF8** aggregates obtained with 5 % methanol and 95 % chloroform indicate that the aggregates had an almost uniform cross-sectional height ranging from 5.5 to 6.1 nm (Figure 4.12). These images suggest that **PSi** chains and **PF8** chains spontaneously co-aggregated at a 2-to-1 ratio on HOPG during co-evaporation of chloroform and methanol. The AFM images do not show segregated structures of **PSi** and **PF8**. The height of  $\approx 6$  nm corresponds to two **PSi** chains interacting with two *n*-octyl groups of two **PF8** chains, as illustrated in Figure 4.13.

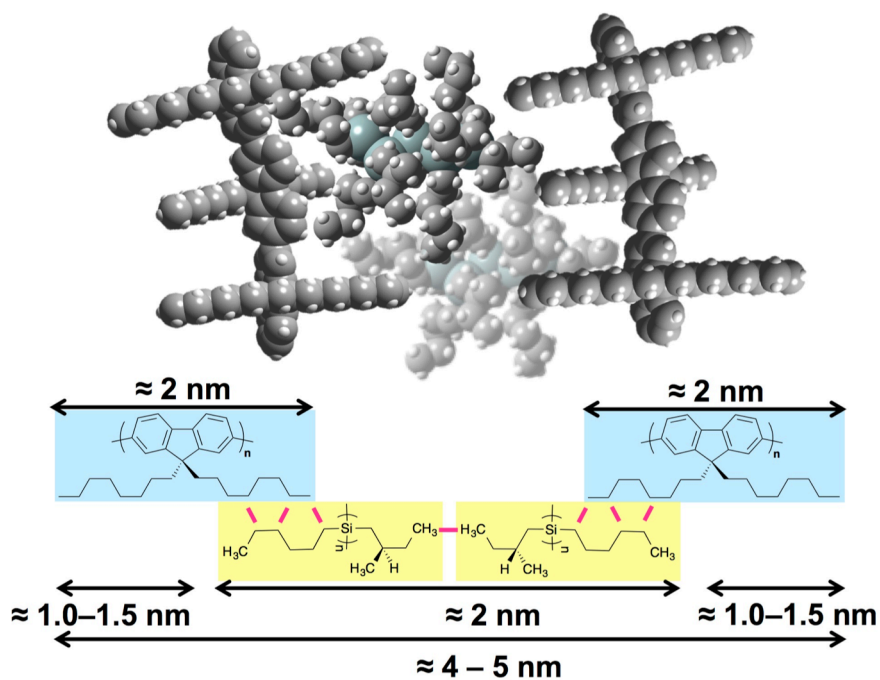


Figure 4.13. Speculated cross-section and computer generated models of **PSi-S-PF8** (= 2:1 ratio) hetero-aggregate to explain height profile (diameter of the aggregate) in Fig. S23. Red lines are possible attractive C-H/H-C interactions, causing an interdigitation between several alkyl side chains of **PSi-S** and **PF8**.

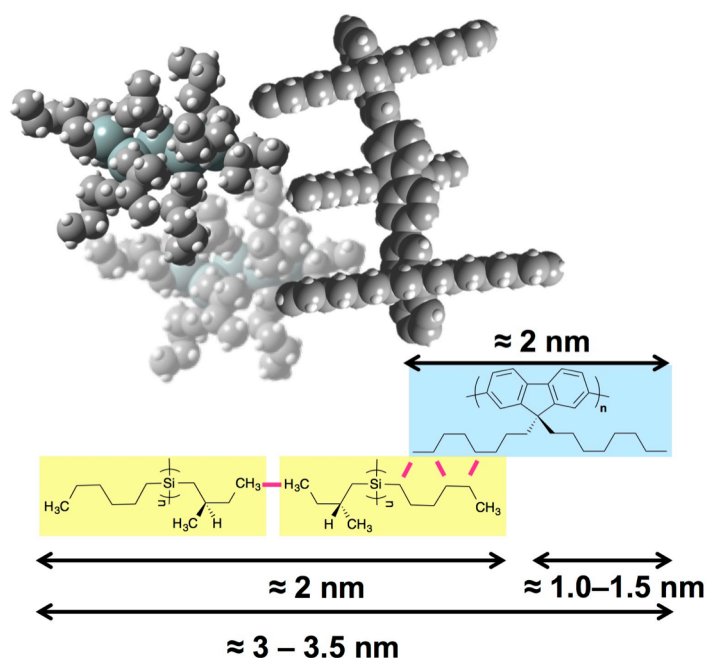


Figure 4.14. Height of  $\approx 5$  nm comes from two **PSi-S** chains with shrink *n*-hexyl groups and one **PF8** chain with stretch-out *n*-octyl groups.

Additionally, we viewed two heights of  $\approx 1.5$  nm and  $\approx 3$  nm, depending on the position of the AFM tip. These heights are ascribed to two **PSi** chains and two **PSi** chains with one side of one **PF8** chain, respectively (Figure 4.14). Although we did not obtain a clear helical AFM image of the hetero-aggregates, several alkyl side chains between **PSi** and **PF8** are assumed to be interdigitated and coagulated. In this case, we postulate that two helical **PSi-S** chains form a double strand by loose wrapping of one **PF8** chain. The double-strand **PSi-S** is responsible for the intense exciton couplet CD signals at 310–320 nm<sup>2,3</sup> (Figure 3.1). From the AFM images, the twisted but more planar **PF8** aggregate suspension in the cosolvents might be responsible for the CD-/CPL-active  $\beta$ -phase at 434 nm<sup>4,5</sup> (Figure 3.2).

### 4.3 Possible interactions between non-charged P*Si* and PF8

Two unanswered questions still remained: (i) Do the CPL and CD activities of the P*Si*-selective photobleached PF8 aggregates arise from intermolecular covalent bonds with a photodecomposed moiety of P*Si* or from non-covalent interactions alone? Additionally, (ii) what types of intermolecular interactions between PF8 and P*Si* are responsible for the scaffolding capability?

To address the first question, we measured the CD and UV-Vis spectra of a homogeneous chloroform solution containing photobleached aggregates of P*Si*-S-PF8 (=2:1). Figure 4.15(a) and 4.15(b) show the CD and UV-Vis spectra of the photobleached aggregates (313 nm, 60 s) by adding chloroform; for comparison, the spectra of the corresponding original and photobleached aggregates in toluene-methanol cosolvent (1.5/1.5 (v/v)) before and after 313 nm irradiation for 60 s are also shown. The CD and UV-Vis bands of the  $\alpha$ -phase ( $\approx 350$  and  $\approx 400$  nm) and  $\beta$ -phase ( $\approx 433$  nm) of PF8 completely disappeared in chloroform. Intermolecular crosslinking reactions did not occur in the aggregate during the photoscissoring process. The predicted silyl radical species<sup>7</sup> did not contribute to the maintenance of the CD and CPL activities in the P*Si*-S-PF8 aggregate.

Regarding the second question, we assume that H/H interactions (termed dihydrogen bonds) exist in the dimer of the saturated hydrocarbons as an extension of CH/ $\pi$  and London dispersion interactions.<sup>8</sup> This proposal is based on rigorous calculations at the second-order Møller-Plesset (MP2) level with the 6-311++G(3df, 3pd) basis set. In methane dimers, the stabilization energy arises from the weakly charged C<sup>-</sup>-H<sup>+</sup>/H<sup>-</sup>-C<sup>+</sup> pair in the valance bond; in particular, the positioning of the neighborhoods is critical. Staggered and eclipsed triple H/H contacts of the CH<sub>3</sub>/H<sub>3</sub>C pair had a dissociation energy of 1.6–1.8 kJ mol<sup>-1</sup>, and the staggered and

eclipsed double H/H contacts of the CH<sub>2</sub>/H<sub>2</sub>C pair had a dissociation energy of 1.0–1.4 kJ mol<sup>-1</sup>.<sup>8-11</sup>

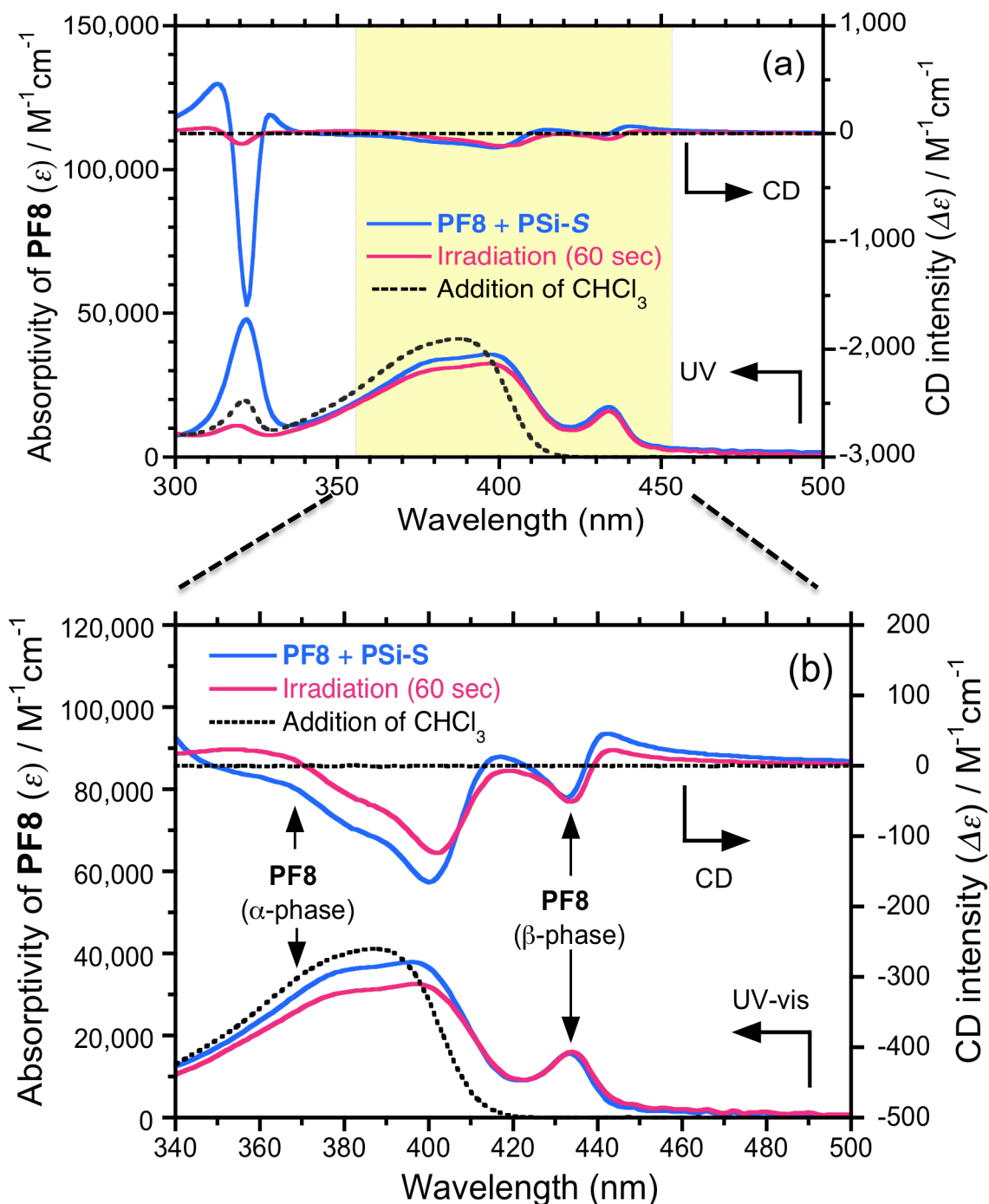


Figure 4.15. (a) CD and UV-Vis spectra and (b) magnified spectra of the photobleached aggregates of **PF8** ( $2.5 \times 10^{-5}$  M) and **PSi-S** ( $5.0 \times 10^{-5}$  M) dissolved in a homogeneous chloroform solution as well as the original and photobleached aggregate suspension for comparison in a toluene-methanol cosolvent (1.5/1.5 (v/v)) before and after irradiation at 313 nm ( $14 \text{ mW cm}^{-2}$ ) for 60 s.

However, in *n*-alkane dimers, a staggered supramolecule with 3:3 and 1:1 contacts asymptotically stabilized as the methylene number increases. The dissociation energy plateaued at six methylenes, reaching 1.56 and 2.40 kJ mol<sup>-1</sup>, respectively.<sup>9-11</sup>

Recently, Hariharan *et al.* demonstrated experimentally and computationally that, in crystals of pyrenes substituted with acetyl and anthracene groups, the attractive H/H interactions between sp<sup>2</sup> C–H of pyrene and sp<sup>3</sup> C–H of methyl (from of acetyl) and between sp<sup>2</sup> C–H of pyrene and sp<sup>2</sup> C–H of anthracene with the help of CH/π interaction facilitate the generation of specific patterns, such as herringbone, brickwork and columnar structures.<sup>12,13</sup>

These fascinating outcomes lead us to propose that the minimal carbon number in the *n*-alkane dimer is six. Therefore, multiple attractive C–H/H–C interactions between the two *n*-octyl groups (**PF8**) and the *n*-hexyl group (**PSi-S** and **-R**) are sufficiently strong for scaffolding capability, irrespective of the absence of electrostatic, hydrogen-bonding, dipole-dipole, CH/π, CH/N, CH/O and π/π interactions. Our preliminary study indicated that an optimal *n*-alkyl side-chain length pair between **PF8** and **PSi** exists, enabling an enhanced scaffolding capability with high *g*<sub>CD</sub> values.

The <sup>13</sup>C-NMR measurements for solid-state **PF8**, *n*-hexyl-group **PSi-S** and a **PSi-S-PF8** combination of 2:1 ratio are shown in Figures 4.16 and 4.17. Previous characterization of weak forces of CH-...π interactions was first recognize using the 1D carbon MAS NMR in Tris-(*o*-phenylenedioxy)spirocyclotriposphazene and polyethylene (TPP/PE) system.<sup>14</sup> It was determine that distance between the two nearest observed units through CH-...π is 3.0 Å and it is slightly longer than the CH-CH interactions with 2.16 Å.<sup>12,16</sup>

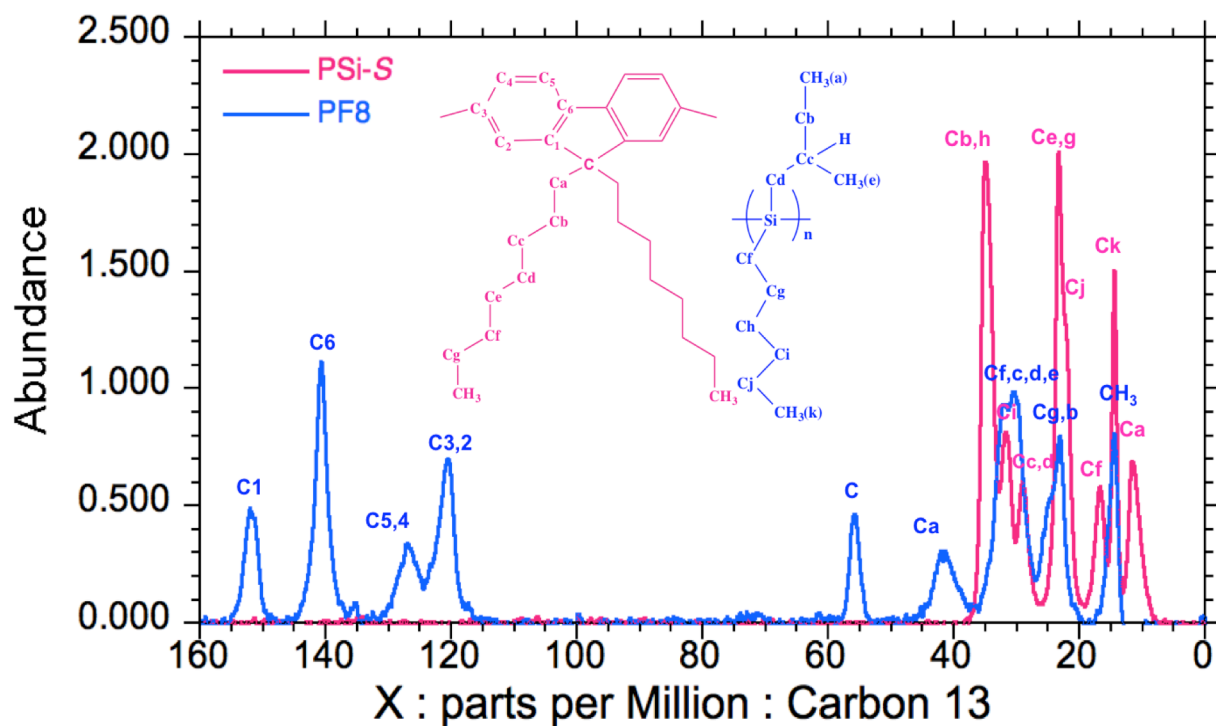


Figure 4.16. CP MASS  $^{13}\text{C}$ -NMR spectra of **PF8** and **PSi-S**.

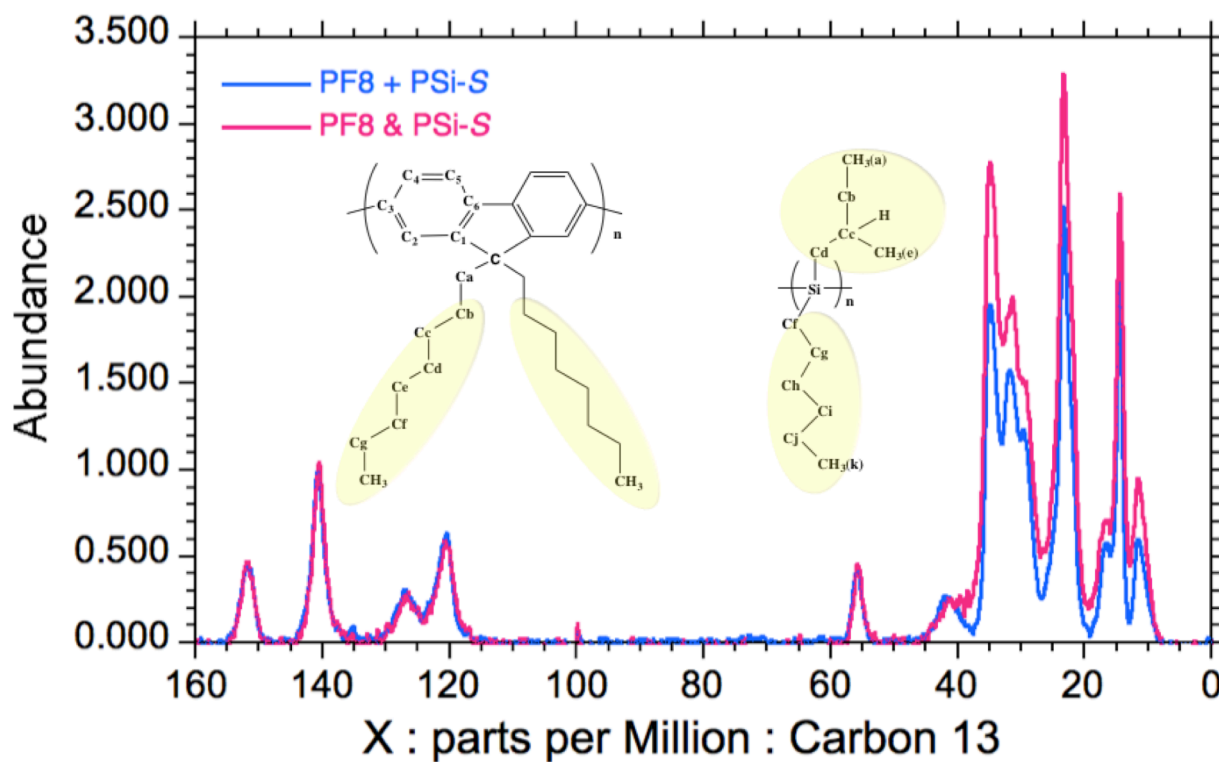


Figure 4.17. CH-CH interaction of alkyl-side chain between **PF8-PSi-S**.

After normalization at the fluorene benzene group, a higher peak was observed at the CH-CH alkyl side-chain group, which provides experimental evidence that attractive C-H/H-C interactions do occur during the polymer association, as indicated by the computational calculation and experimental studies of pyrenes, acetyl and anthracene monomer units.

Various supramolecular polymer complexes using single- and dual-components of molecular and oligomeric building blocks hold promise for the design of (chir)optical, semiconducting, and biological functions, as well as well-defined, higher-order fibrous and gel structures.<sup>16-19</sup> Relatively directional, intense hydrogen,  $\pi$ - $\pi$  stacking and electron donor-acceptor interactions are the driving forces for these structures.

As demonstrated in this work, even non-directional weak interactions can contribute to supra-macromolecular complexation comprising non-charged, non-polar  $\pi$ - and  $\sigma$ -conjugated polymers, although the detailed structure of the resultant hetero-aggregate is challenging to characterize. Nevertheless, this approach is beneficial to more freely design (chir)optical and electronic functions.

#### **4.4 Proposal of possible interactions between non-charged P*Si* and P*F8***

Based on the previous experimental results, we propose a possible scenario of emerging CD-/CPL-active **P*F8*** aggregate when non-helix **P*F8*** is employed with **P*Si-S*** as a helix scaffold (Figures 4.18 and 4.19), from stage I to stage IV.

Stage I. In good solvents (toluene and chloroform), semi-flexible **P*F8*** has a rich conformational freedom along C-C single bonds between fluorine rings, whereas **P*Si-S*** adopts a rigid  $7_3$  helical structure due to restricted Si-Si single bonds. Long *n*-hexyl and *n*-octyl side chains

fully interact with solvents to adopt a fairly elongated geometry.

Stage II. By changing from pure good solvent to a poorer cosolvent through the slow addition of methanol, **PSi-S** preferentially self-assembles to a higher-order helical structure, while **PF8** exists as an individual polymer chain even in the poorer cosolvent. The key factor is that **PSi-S** possesses intense self-aggregation ability relative to **PF8**, arising from large differences in main chain rigidity and solubility in the poorer solvent. In this case, *n*-hexyl groups adopt a contracted geometry.

Stage III. When transitioning from the poorer to very poor cosolvents by further addition of methanol, the higher-order **PSi-S** helical motif causes a complexation with **PF8** due to its restricted solubility in the poor solvent. Multiple C-H/H-C interactions between *n*-hexyl groups of **PSi-S** and *n*-octyl groups of **PF8** are responsible for the attractive macromolecular complexation. In this case, the matching of side chain lengths of **PSi-S** and **PF8** is another critical factor. Then, **PSi-S** helicity is efficiently transferred to **PF8** due to a sharp loss of conformational freedom, yielding CD-/CPL-active but metastable  $\beta$ -phase **PF8** hetero-aggregates maintained by rigid **PSi-S** helicity. The metastability was confirmed by the complete loss of the CD signal of **PF8** when chloroform was added to the hetero-aggregate.

Stage IV. **PSi-S** and **PF8** hetero-aggregates transition to CD-/CPL-**PF8** aggregates after the complete removal of **PSi-S** as a helix scaffold by the photoscissoring reaction at the Si $\sigma$ -Si $\sigma^*$  transition. In this case, **PF8** chains transition to the thermodynamically stable chiral  $\beta$ -phase. The chiral  $\beta$ -phase **PF8** structures are stabilized through multiple C-H/H-C interactions between *n*-octyl groups.

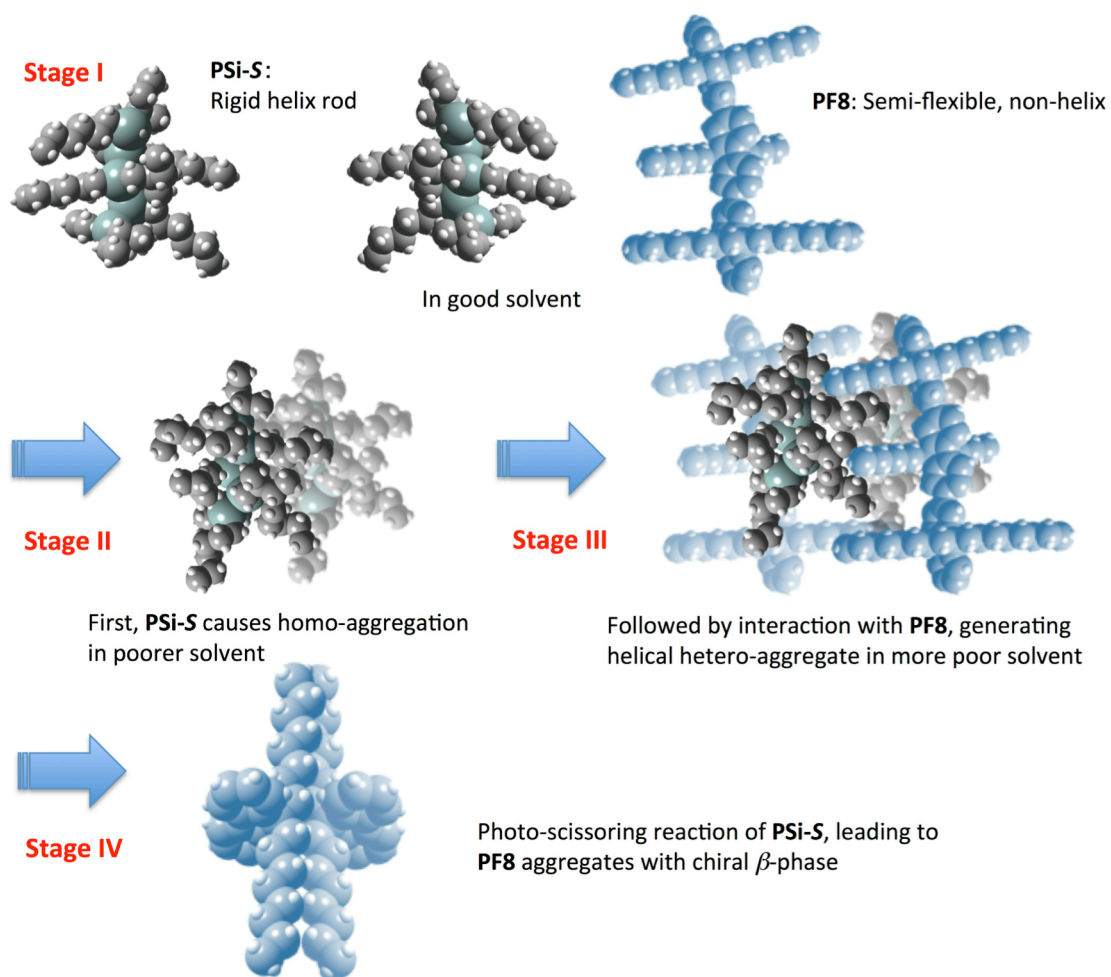


Figure 4.18 Computer generated the scenario of **PSi-S** helicity transfer to helical  $\beta$ -phase **PF8** during hetero-aggregation of **PSi-S** and **PF8**, followed by removal of **PSi-S** scaffold by **PSi-S** selective photoscissoring reaction in poor solvents.

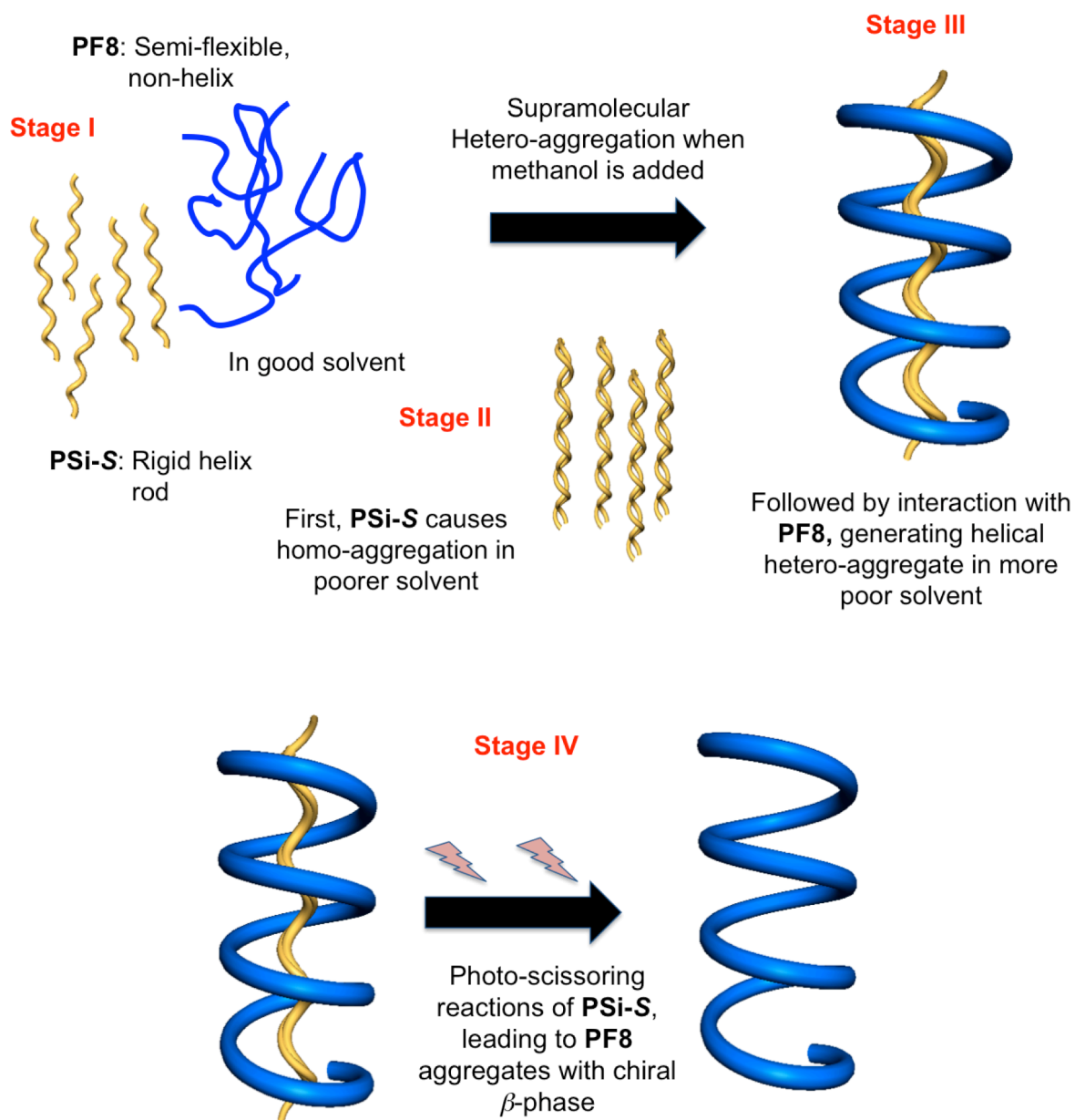


Figure 4.19. Illustrative scenario of **PSi-S** helicity transfer to helical  $\beta$ -phase **PF8** during hetero-aggregation of **PSi-S** and **PF8**, followed by removal of **PSi-S** scaffold by **PSi-S** selective photoscissoring reaction in poor solvents.

## 4.5 References

- (1) Knaapila, M.; Konopkova, Z.; Torkkeli, M.; Haase, D.; Liermann, H. -P.; Guha, S.; Scherf, U. *Phys. Rev. E* **2013**, *87*, 022602
- (2) Nakano, Y.; Ichianagi, F.; Naito, M.; Yang, Y. -G.; Fujiki, M. *Chem. Commun.* **2012**, *48*, 6636
- (3) Shiraki, T.; Shindome, S.; Toshimitsu, F.; Fujigaya, T.; Nakashima, N. *Polym. Chem.* **2015**, *6*, 5103.
- (4) Kawagoe, Y.; Fujiki, M.; Nakano, Y. *New J. Chem.* **2010**, *34*, 637.
- (5) Liu, Y.; Murao, T.; Nakano, Y.; Naito, M.; Fujiki, M. *Soft. Matter* **2008**, *4*, 2396.
- (6) Miller, R. D.; Michl, J. *Chem. Rev.* **1989**, *89*, 1359.
- (7) Le Gac, S.; Schwartz, E.; Koeph, M.; Cornelissen, J. J. L. M.; Rowan, A. E.; Nolte, R. J. M. *Chem. Eur. J.* **2010**, *16*, 6176.
- (8) Danovich, D.; Shaik, S.; Neese, F.; Echeverria, J.; Aullon, G.; Alvarez, S. *J. Chem. Theory Comput.* **2013**, *9*, 1977.
- (9) Echeverria, J.; Aullon, G.; Danovich, D.; Shaik, S.; Alvarez, S. *Nat. Chem.* **2011**, *3*, 323
- (10) Michalak, A.; Mitoraj, M.; Ziegler, T. *J. Phys. Chem. A*, **2008**, *112*, 1933.
- (11) Rajagopal, S. K.; Philip, A. M.; Nagarajan, K.; Hariharan, M. *Chem. Commun.* **2014**, *50*, 8644
- (12) Nagarajan, K.; Rajagopal, S. K.; Hariharan, M. *CrystEngComm*, **2014**, *16*, 8946.
- (13) Aida, T.; Meijer, E. W.; Stupp, S. I. *Science* **2012**, *335*, 813.(13)
- (14) De Greef, T. F. A.; Meijer, E. W. *Nature* **2008**, *453*, 171.
- (15) Yang, L.; Tan, X.; Wang, Z.; Zhang, X. *Chem. Rev.* **2015**, *115*, 7196.
- (16) Sozzani, P.; Comotti, A.; Bracco, S.; Simonutti, R. *Chem. Commun.* **2004**, *20*, 768
- (17) Krieg, E.; Bastings, M. M. C.; Besenius, P.; Rybtchinski, B. *Chem. Rev.* **2016**, *116*, 2414.
- (18) Verswyvel, M.; Koeckelberghs, G. *Polym. Chem.* **2012**, *3*, 3203.
- (19) Palmans, A. R. A.; Vekemans, J. A. J. M.; Havinga, E. E.; Meijer, E. W. *Angew. Chem. Int. Ed. Engl.* **1997**, *36*, 2648.

## Chapter 5. Factors affecting the ability of helical scaffolding of PSi to PF8

### 5.1 Optofluidic effect revealed as chiroptical amplification

The cosolvent was optimized by optofluidically tuning  $n_D$  and produced a great enhancement in the  $g_{CD}$  value of the hetero-aggregate at a specific  $n_D$  of  $\approx 1.41$  (Figure 5.1), where the mixture of good and poor solvents (toluene and methanol) was 1/1 (v/v). The **PSi-S** CD spectra are shown in Figure 5.2. The  $g_{CD}$ - $n_D$  relationship shows a broad distribution for chiral **PSi**-induced **PF8** particles. This distribution indicates that the **PSi-S** and **PF8** aggregates adopt a stable shape over a wide range of poor to good cosolvents.<sup>1-4</sup>

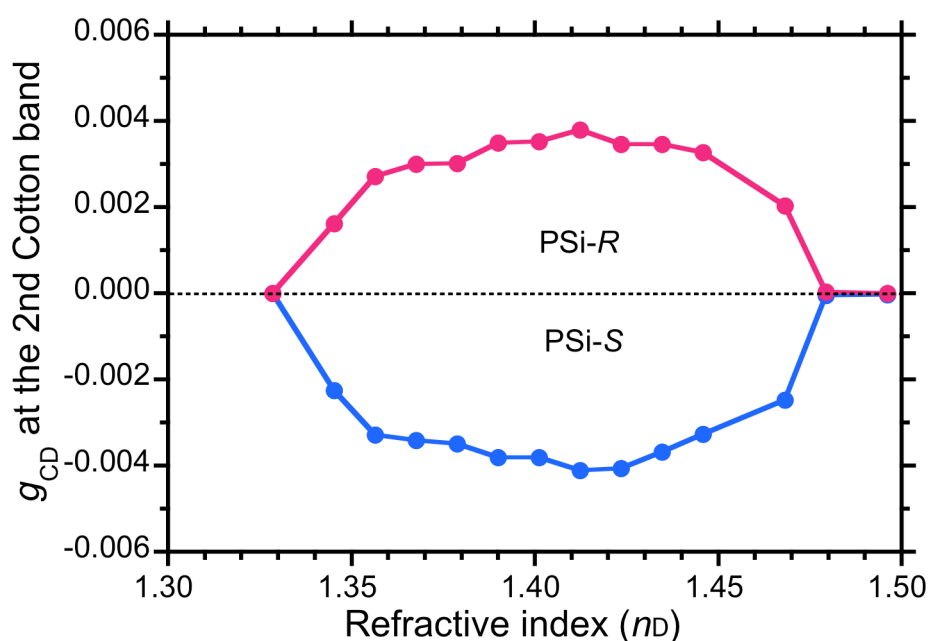


Figure 5.1. The  $g_{CD}$  value of **PF8** at 401 nm in toluene-MeOH cosolvents as a function of the refractive index ( $n_D$ ) in the hetero-aggregate of the **PSi** and **PF8** molar ratio is  $= 5.0 \times 10^{-5}$  M and  $2.5 \times 10^{-5}$  M. The  $M_n$  values of **PSi-S**, **PSi-R** and **PF8** are 75,800, 73,900 and 78,800, respectively.

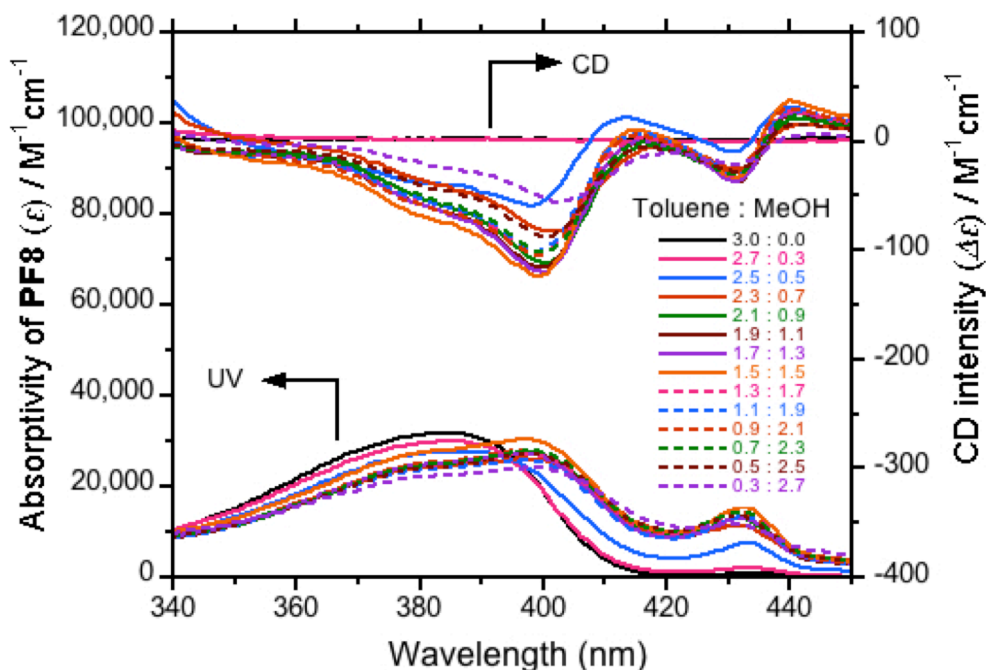


Figure 5.2. CD and UV-Vis spectra of hetero-aggregates of **PSi-S** and **PF8** with various amount toluene-methanol cosolvent (v/v) with  $[\mathbf{PF8}] = 2.5 \times 10^{-5} \text{ M}$  and  $[\mathbf{PSi-S}] = 5.0 \times 10^{-5} \text{ M}$  as their repeating units. The  $M_n$  values of **PSi-S** and **PF8** were 75,800 and 78,800, respectively.

However, improper ratios of good and poor solvents in the optofluidic medium may cause instability of the aggregate structures. A similar effect has been identified in  $\pi$ -conjugated polymers, molecules and supramolecular polymer self-assembled systems experimentally and by computational modeling.<sup>12</sup>

## 5.2 Polymer molar ratio dependence

To gain additional insight into whether intermolecular interactions between **PSi-S** (**PSi-R**) and **PF8** are stoichiometric, a Job's plot<sup>5-7</sup> was constructed for the **PSi-PF8** aggregates; such plots are useful for evaluating supramolecular complexes and are applicable to polymer-polymer supramolecular complexes.<sup>8-13</sup> The  $g_{\text{CD}}$  value at the second Cotton band (401 nm) as a function of

the molar ratio (as a repeating unit) of **PF8**/[**PF8**+**PSi-S**(**PSi-R**)] is shown in Figure 5.3.

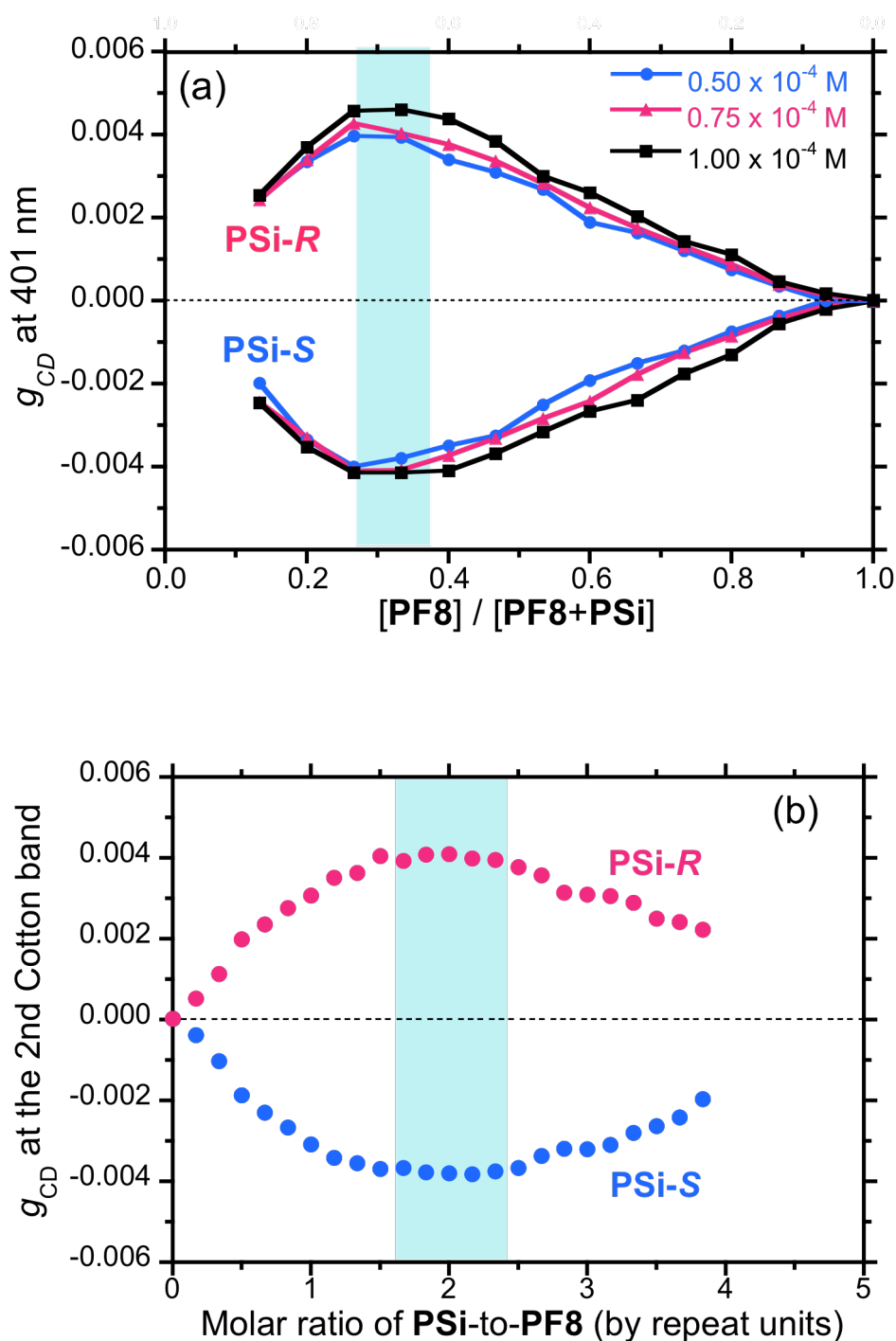


Figure 5.3. a) Job's plot. The  $g_{CD}$  value of **PF8** as a function of the molar ratio of **PF8** in the hetero-aggregate. Three solution concentrations were tested:  $(0.50, 0.75, 1.00) \times 10^{-4}$  M in toluene. b) The  $g_{CD}$  value of **PF8** at 401 nm as a function of the **PSi-to-PF8** molar ratio when  $[\text{PF8}]_0 = 2.5 \times 10^{-5}$  M.

Surprisingly, the **PSi-S**-and-**PF8** (and **PSi-R**-and-**PF8**) hetero-aggregates preferentially adopt a 2-to-1 **PSi-PF8** ratio because the  $g_{CD}$  values reach a maximum at **PF8**/[**PF8+PSi-S**] and **PF8**/[**PF8+PSi-R**] of approximately 0.33. The hetero-aggregates do not obey the sergeant-and-soldier principle that is often observed in  $\pi$ - $\pi$  stacked supramolecules and stiff helical copolymers.<sup>10,14-16</sup> Further analysis of the Job's plot indicates that the **PSi-PF8** hetero-aggregate is a supra-macromolecular complex with a 2-to-1 ratio (by repeating units) when the concentration of **PF8** is fixed at  $2.5 \times 10^{-5}$  M (Figure 5.3b). The 2-to-1 ratio is equivalent to 51:49 (by weight).

Recently, spontaneous generation of a similar supra-macromolecular triplex (so-called "stereocomplex") consisting of *isotactic* (*it*)- and *syndiotactic* (*st*)-poly(methyl methacrylate) (PMMA) with a 2-to-1 ratio was confirmed by HR-AFM and X-ray structural analyses.<sup>10</sup> The stereocomplex on HOPG, however, may exist as a mixture of *left*- and *right*-handed triple helices.

Notably, **PSi-S** and **PSi-R**, in particular, adopt a rigid rod-like helical global conformation. However, **PF8** adopts a semi-flexible CD-silent helical conformation with substantial rotational freedom along the C-C bonds between the fluorene rings in the fluidic toluene solution. The combination of a highly rigid rod-like helix and semi-flexible CD-silent helical conformation may be critical for designing aggregation-induced scaffolding systems.

### 5.3 Molecular weight dependence of helical scaffolding

A well-designed supramolecular architecture can promote well-defined molecular interaction when two bodies adhere. This interaction is expected to be closely related to the process of spontaneous assembly.<sup>17-19</sup> To clarify whether  $M_n$  values of **PF8** and **PSi** values affect the

**PSi-and-PF8** scaffolding capability, we examined the  $g_{CD}$  value of **PSi-and-PF8** with 2-to-1 hetero-aggregates as a function of  $M_n$  values of **PF8** and **PSi-S** in detail. Four **PF8** samples with  $PDI \approx 1.7-2.1$  and six **PSi-S** samples with  $PDI \approx 1.3-1.5$  were isolated by an ordinary fractionation method with IPA, ethanol and methanol as precipitating solvents. The obtained fractionation  $M_n$  is listed in Tables 2.1 and 2.2. For comparison, one **PSi-R** sample with  $PDI \approx 1.3$  was used.

Table 5.1. **PSi-S** and **PSi-R** chain length and monomer unit at different molecular weight.

Chiral centre	$M_n$	$M_w/M_n$	Length of <b>PSi</b> (nm)	$DP_n$
S	80,400	1.4	57	436
S	75,800	1.3	54	411
R	73,900	1.4	53	401
S	40,500	1.5	29	220
S	27,400	1.4	20	149
S	17,100	1.3	12	93
S	9,800	1.5	7	53

Table 5.2. **PF8** main chain length and number average monomer unit at different molecular weights.

Fraction	$M_n$	$M_w/M_n$	Length of <b>PF8</b> (nm)	$DP_n$
1	89,800	2.0	194	230
2	82,800	2.1	179	212
3	78,400	1.8	169	201
4	59,500	1.7	129	152

As concluded from the irradiation time dependence at 313 nm of **PSi-S-PF8** aggregation, the  $g_{CD}$  value of the hetero-aggregates greatly depends on the  $M_n$  value of **PSi-S** when **PF8** with  $M_n$  is fixed at 82,800 (Figure 5.4). It is evident that among six **PSi-S** samples, the  $g_{CD}$  value is maximized when **PSi-S** is  $M_n = 40,500$  before and after the 313 nm irradiation. Thus, the  $g_{CD}$  value does not monotonically increase as the  $M_n$  value of **PSi-S** increases (Figure 5.5).

The scaffolding capability is crucial in providing ideal intermolecular interaction between **PF8** and **PSi-S**. The  $g_{CD}$  value of the **PSi-S-PF8** aggregate monotonically increases and tends to plateau as the  $M_n$  value of **PSi-S** increases from 9,800 and 80,400 (Figure 5.6). The  $g_{CD}$  value of the **PSi-S-PF8** aggregate weakly depends on the  $M_n$  value of **PF8**.

A pair of two different linear polymers with oppositely charged pairs may display enhanced electrostatic interaction as their main-chain lengths increase, due to substantial intermolecular locking.<sup>20,21</sup> However, in the case of pair of non-charged polymers, the semi-flexible **PF8** may gradually lose its wrapping capability toward rod-like **PSi-S** above the critical  $M_n \approx 80,000$ . Rod-like **PSi-S** efficiently acts as an efficient scaffold toward semi-flexible **PF8** regardless of the value of  $M_n$  of **PSi-S** (between 9,800 and 80,400). The scaffolding ability of **PSi-S** is maintained during photochemical scissoring of Si-Si bonds.

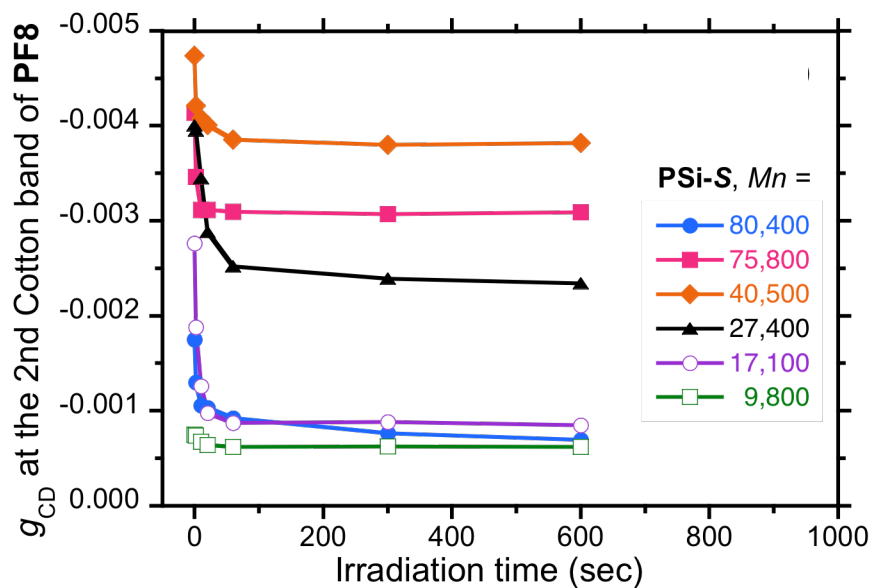


Figure 5.4. The  $g_{CD}$  value of **PF8** at 401 nm using **PSi-S** with different molecular weight and **PF8** ( $M_n = 82,800$ ) hetero-aggregates with a 2-to-1 ratio produced in a toluene-methanol cosolvent (1.5/1.5 (v/v)) with  $[PF8] = 2.5 \times 10^{-5}$  M and  $[PSi-S] = 5.0 \times 10^{-5}$  M as the repeating units and as a function of the irradiation time at 313 nm ( $14 \mu W cm^{-2}$ ).

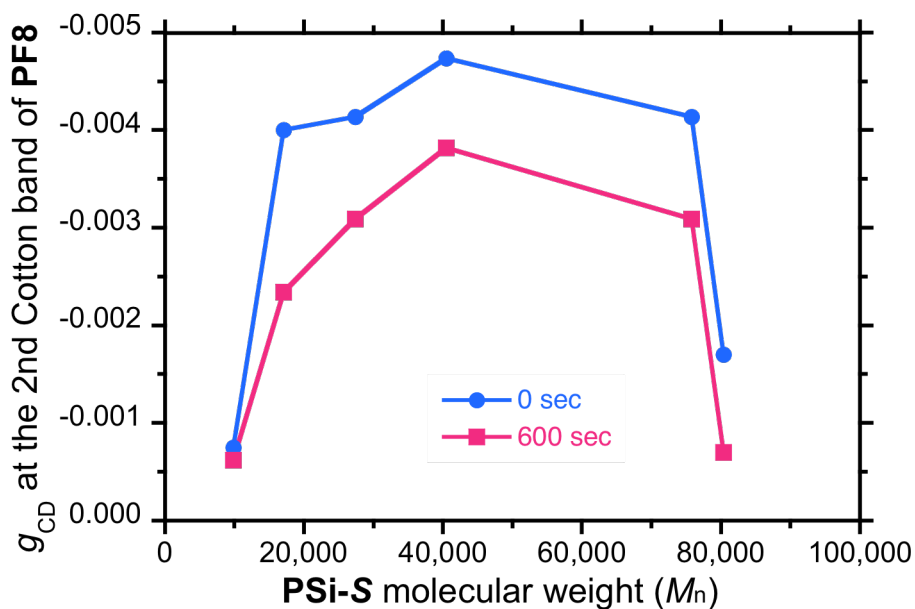


Figure 5.5. The  $g_{CD}$  value at 401 nm of **PSi-S-PF8** aggregate as a function of **PSi-S** before and after irradiation time at 313 nm ( $14 \mu W cm^{-2}$ ) for 600 s

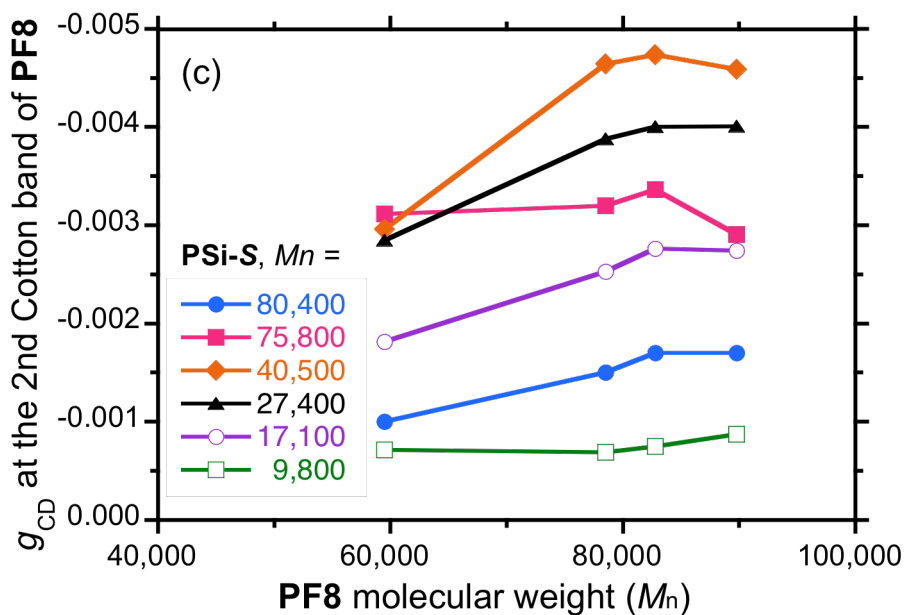


Figure 5.6. The  $g_{CD}$  value at 401 nm of **PSi-S-PF8** hetero-aggregates (2-to-1 ratio produced in a toluene-methanol cosolvent (1.5/1.5 (v/v) with  $[PF8] = 2.5 \times 10^{-5}$  M and  $[PSi-S] = 5.0 \times 10^{-5}$  M as their repeating units) as a function of both  $M_n$  values with **PF8** and **PSi-S**.

To further consider which factor among molecular weight, main-chain length and  $DP_n$  is the critical factor to afford the more favorable scaffolding ability and to explore the reason why the best **PSi-S-PF8** aggregate with the greatest  $g_{CD}$  value corresponds to the 1-to-2 ratio as repeating units, we evaluated main chain lengths and  $DP_n$  values of **PF8**, **PSi-S** and **PSi-R** from the corresponding  $M_n$  values (Tables 5.1 and 5.2).

The stoichiometry of repeating units of **PF8** and **PSi** is a critical factor for the hetero-aggregate, in which **PF8** with  $DP_n \approx 212$  matches **PSi-S** with  $DP_n \approx 220$  in the range of  $DP_n$  between 50 and 436. CD- and UV-vis spectra of the **PSi-S** were photobleached at **PSi-S-PF8** aggregate. Actually, the nearly identical  $DP_n$  values of **PSi-S** and **PF8** afforded the highest  $g_{CD}$  amplitude of  $\approx -0.005$  at 438 nm for **PF8**.

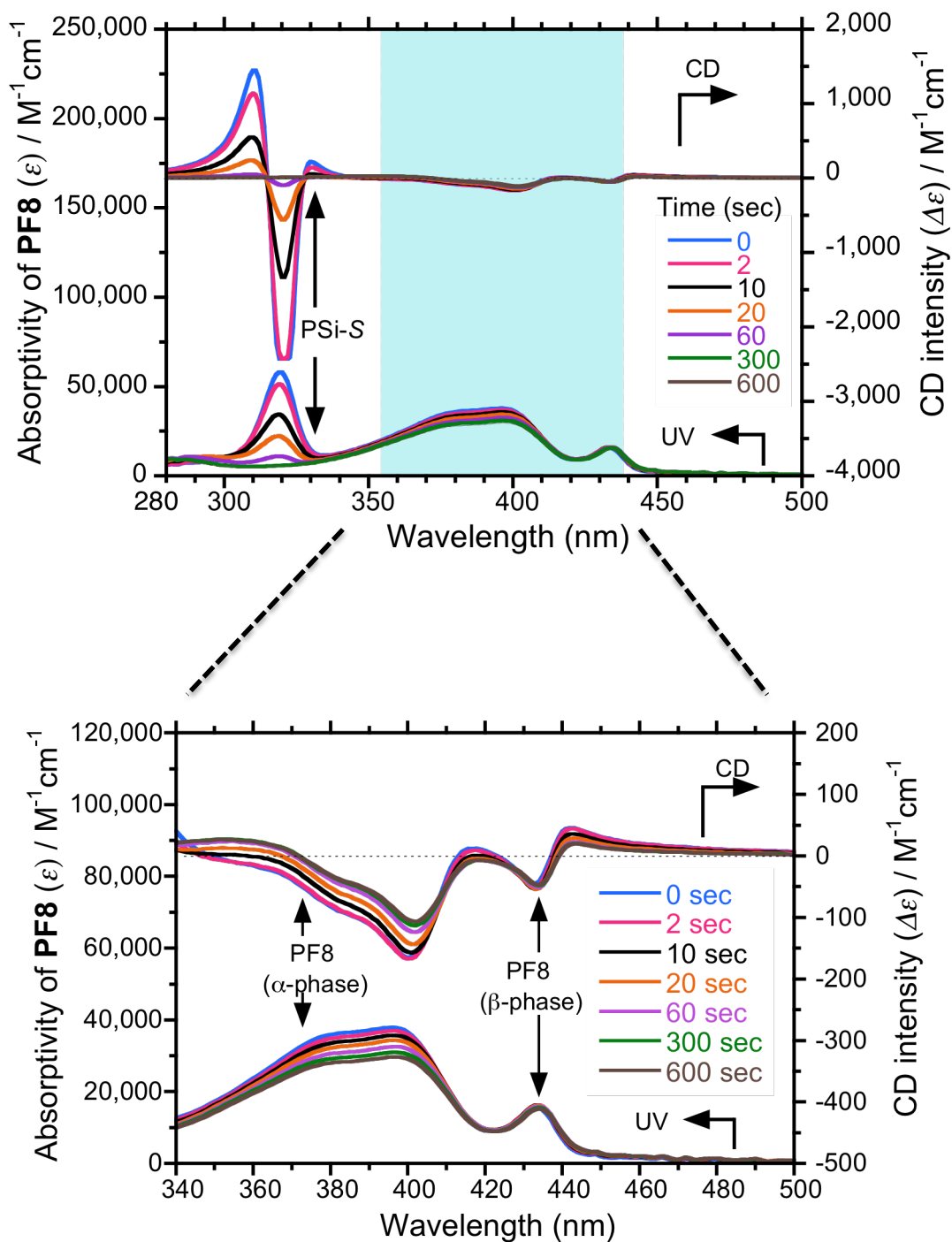


Figure 5.7. CD and UV-Vis spectra of hetero-aggregates under photochemical decomposition of **PSi-S** and **PF8** with a 2-to-1 ratio produced in a toluene-methanol cosolvent (1.5/1.5 (v/v)) with  $[\text{PF8}] = 2.5 \times 10^{-5} \text{ M}$  and  $[\text{PSi-S}] = 5.0 \times 10^{-5} \text{ M}$  as their repeating units. The  $M_w$  values of **PSi-S** and **PF8** were 40,500 and 78,400, respectively.

Harada and Kataoka<sup>20</sup> demonstrated that a precisely controlled main chain length of charged polymers helps to produce a highly ordered supramolecular assembly, resulting in a core-shell structure. In addition to the main chain length, they found that the degree of polymerization (*DP*) plays a key role in constructing the self-assembling structure with the oppositely charged polymers, i.e., a polyion complex. In this case, all the polymers had an extremely narrow *PDI* < 1.1.

Their knowledge and understanding might be applicable to supramolecular complexation between two non-charged **PF8** and **PSi**. The  $DP_n$  values with the best fit between **PF8** and **PSi** are responsible for the supramolecular hetero-aggregation. This idea could be applicable to complexations between two polar polymers and between nonpolar polymers, as well as between the oppositely charged polymers

One remaining question is why the 2-to-1 ratio is the best for the **PSi-S**-and-**PF8** aggregates. Note that each **PF8** repeating unit has two *n*-octyl side chains at the 9,9-position (eight carbons  $\times$  2 = sixteen carbons), whereas each **PSi-S** repeating unit has a single *n*-hexyl side chain (six carbon  $\times$  1). A plausible resolution is that two *n*-octyl side chains of the **PF8** repeating unit interact with two units of **PSi-S** carrying one *n*-hexyl side chain, enabling an efficient interaction of these *n*-alkyl side chains. To build a supramolecular structure, more and longer alkyl side chains of polyfluorene derivatives are needed to efficiently wrap around the rigid rod-like **PSi-S** helical main chains.

#### 5.4 Polymer alkyl side-chain dependency

Despite the weakness of the CH...HC interactions, their accumulation may result in strongly attractive interaction.<sup>22-24</sup> Fokin *et al.* predict that the sticky layer of graphene can exceed

150 kcal mol<sup>-1</sup> of binding energy with 1.1-1.2 kcal mol<sup>-1</sup> per carbon atom by applying both valence bond and molecular orbital-based theory computationally. The CD spectra of **PSi-S-PF8** with varying alkyl side-chain length hetero-aggregates are shown in Figure 5.8. The  $M_n$  fractionation of polyfluorenes and polysilanes used in this study are provided in Tables 5.3 and 5.4. The calculated  $g_{CD}$  value of the hetero-aggregate with a 2-to-1 ratio emphasize that the highest  $g_{CD}$  value of  $\approx -0.012$  at the **PF8**  $\alpha$ -phase cotton side band is preferred when the **PSi-S-PF8** hetero-aggregate alkyl side-chain lengths are both 7 (Figure 5.9). Detailed  $g_{CD}$  values of **PSi-S-PF8** hetero-aggregates of **PF7** and **PSi-S (7)** are shown in Figure 5.10.

The experimental results suggest that sufficient CH...HC interactions are required because weak intermolecular forces are the main domains to hold both polymers intact. The CH...HC interactions become stronger with the branching of alkene as a result of electronic reorganization due to charge transfer from one bond to the other. The organization of staggered conformation within the two CH moieties of alkyl-side chains less than 7 lead to an attractive force at short distances.<sup>24,25</sup>

Computationally, Alvarez *et al.*<sup>22</sup> demonstrated that the valance bond does not change at a 15-25 Å short “infinite” distance, providing relaxation that allows stabilization by 0.74 kcal mol<sup>-1</sup> and explains the binding energy to the CH cluster. Larger alkenes cause difficulties in reorganization of the bonding electron of the two interacting CH bonds via recoupling of these electrons at the H...H and C...C bonds. Correspondingly, this effect results in breakdown of the total dispersion interaction, which leads to an inability to attach the two molecules. This mechanism is related to the Pauli repulsion force.

Moreover, as the alkyl side-chains increase, difficulties in providing a well-aligned

direction for CH...HC interactions are more likely to occur. This effect implies that high thermodynamic potentials are preferred; thus, the slippage arrangement for longer-distance alkyl side-chains may reduce the effectiveness of CH...HC interactions and lead to decreasing  $g_{CD}$  values for **PSi-S** and polyfluorene.

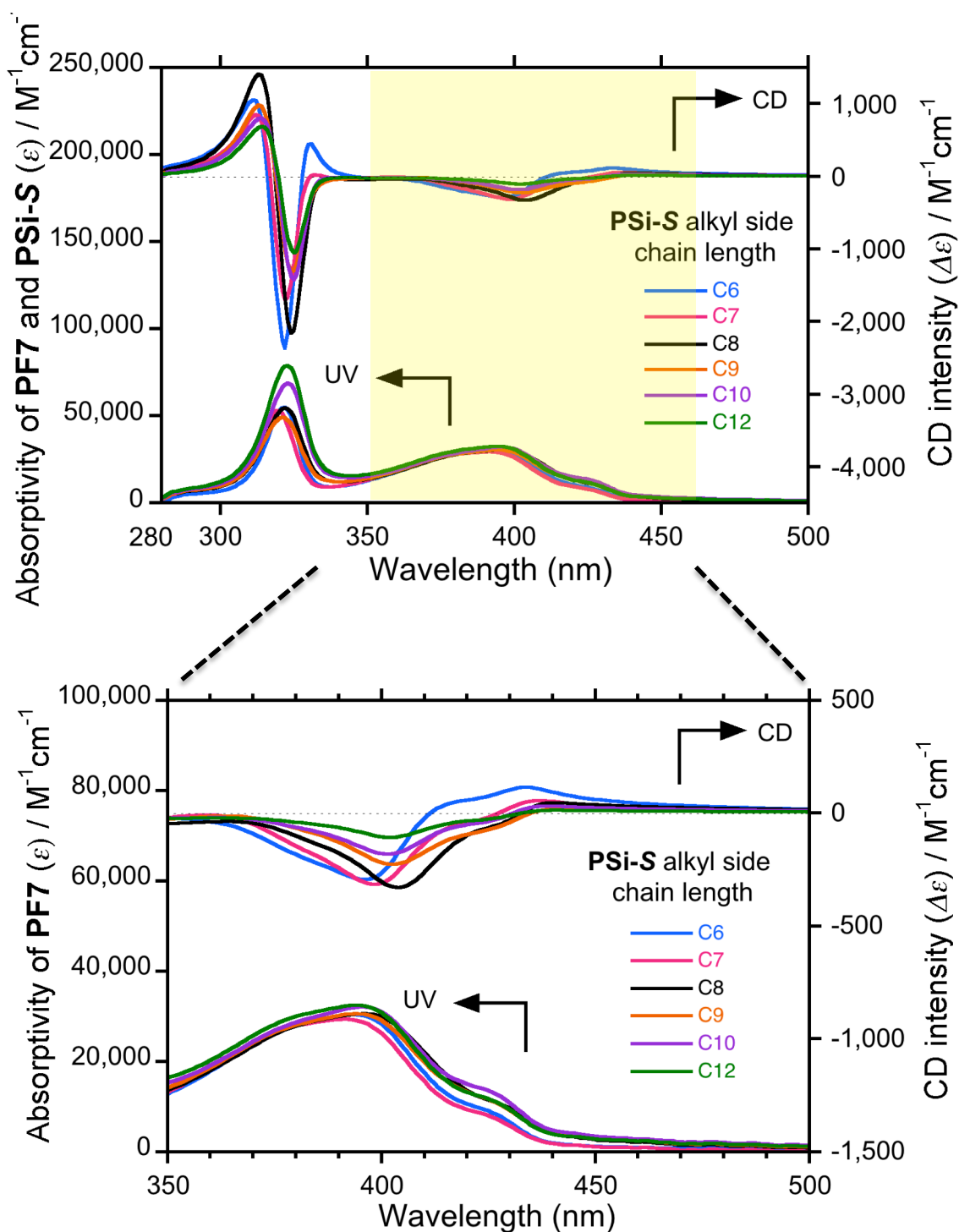


Figure 5.8. CD and UV-Vis spectra of hetero-aggregates of **PSi-S** and **PF7** with a 2-to-1 ratio produced in a toluene-methanol cosolvent (1.5/1.5 (v/v)) with  $[\text{PF7}] = 2.5 \times 10^{-5} \text{ M}$  and  $[\text{PSi-S}] = 5.0 \times 10^{-5} \text{ M}$ .

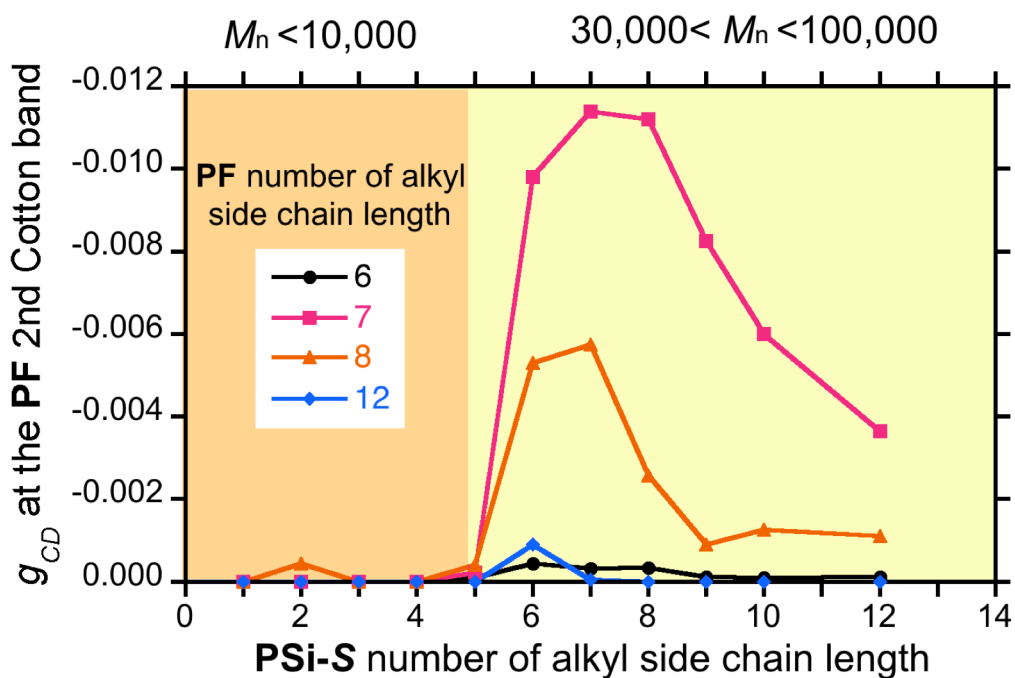


Figure 5.9. The  $g_{CD}$  value **PSi-S-PF8** with different alkyl side-chain length hetero-aggregate with a 2-to-1 ratio produced in a toluene-methanol cosolvent (1.5/1.5 (v/v)) with  $[PF8] = 2.5 \times 10^{-5}$  M and  $[PSi-S] = 5.0 \times 10^{-5}$  M as their repeating units.

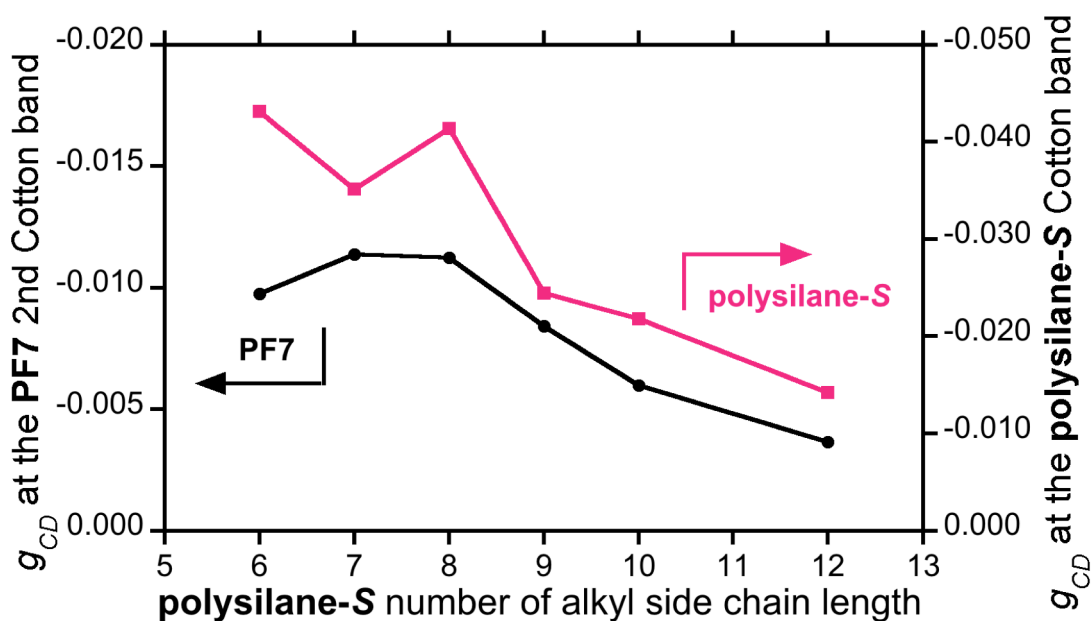


Figure 5.10. The  $g_{CD}$  value at 401 nm of **PSi-S-PF8** aggregate as a function of **PSi-S** before and after irradiation time at 313 nm ( $14 \mu W cm^{-2}$ ) for 600 s

Table 5.3. Various length of **PF8** alkyl side-chain length molecular weights.

Polyfluorene	$M_n$	$M_w/M_n$
<b>PF6</b>	26,800	3.6
<b>PF7</b>	36,200	2.5
<b>PF8</b>	48,400	1.8
<b>PF12</b>	38,000	2.8

Table 5.4. Various length of **PSi-S** alkyl side-chain length molecular weights.

Alkyl side-chain length	$M_n$	$M_w/M_n$
<b>PSi-S (1)</b>	8,600	2.6
<b>PSi-S (2)</b>	7,300	2.4
<b>PSi-S (3)</b>	7,600	3.1
<b>PSi-S (4)</b>	40,500	1.5
<b>PSi-S (5)</b>	27,400	1.4
<b>PSi-S (6)</b>	40,800	1.3
<b>PSi-S (7)</b>	36,500	1.7
<b>PSi-S (8)</b>	87,200	1.5
<b>PSi-S (9)</b>	74,400	3.7
<b>PSi-S(10)</b>	60,100	1.5
<b>PSi-S(12)</b>	41,500	1.8

## 5.5 PSi-S scaffold main-chain helical dependency

To express the main chain inherent helices of chiral polysilane, the type of chiral scaffold can be divided into 2 types of twist sense that correspond to majority-rule polysilane and sergeant-soldier polysilane. The majority-rule polysilane refers to the **PSi-R-*ran*-PSi-S** copolymers with access copolymers of *R* or *S* in a copolymer system. The “sergeant and soldier” polysilane was described as **PSi-R(*S*)-*ran*-PSi-*i*Bu** copolymers when one chiral element imposes its screw sense on a large “platoon” of achiral copolymer fragments.

### 5.5.1 Majority-rule polysilane (PSi-R-*ran*-PSi-S)

The CD and UV-Vis spectra of **PSi-R-*ran*-PSi-S** of the minimally reacted copolymer of *R* and *S* poly[*n*-methyl-2-methylbutylsilane] in hetero-aggregate form are shown in Figure 5.11. The **PSi-R-*ran*-PSi-S**  $M_n$  value percentage (%) is listed in Table 5.5. The CD signal of **PSi-R-*ran*-PSi-S** helicity transfer to **PF8** during hetero-aggregation features different trends of helix amplification, as has been observed in the polyisocyanate system.<sup>26-28</sup> Previously, Gestel<sup>29</sup> proposed a model that can be apply to self-assembled polymers system in aggregates based on the consideration of free-energy penalties of chiral component handedness. The model is consistent with the **PSi-R-*ran*-PSi-S-PF8** hetero-aggregate system, for which it predicts a monotonic increase with increasing helix penalties.

Notably, although the  $g_{CD}$  value ( $\approx 10^{-4}$ ) helix amplification for **PSi-R-*ran*-PSi-S-PF8** hetero-aggregate is small with respect to pure helices of chiral **PSi-PF8** hetero-aggregate (Figure 5.12), it was justified that the helix amplification is strongly tuned by the exciton coupling aggregate helix superstructure of the **PSi** scaffold. The CPL and PL spectra (Figure 5.13) arising from the  $\beta$ -phase **PF8** in the **PSi-R-*ran*-PSi-S-PF8** hetero-aggregate also confirm the formation of

a chiral structure in **PF8**, and the chiral structure nearly disappears after 60 s irradiation time. The data confirm that the behavior of the hetero-aggregate is much different than when it is in solution or the homo-aggregate state.

Table 5.5. **PSi-R-ran-PSi-S** % of **R** and **S**

(%)	$M_n$	$M_w/M_n$
60-and-40	48,800	2.0
53-and-47	57,800	1.8
50-and-50	89,000	2.6
47-and-53	45,500	2.0
40-and-60	74,500	2.5

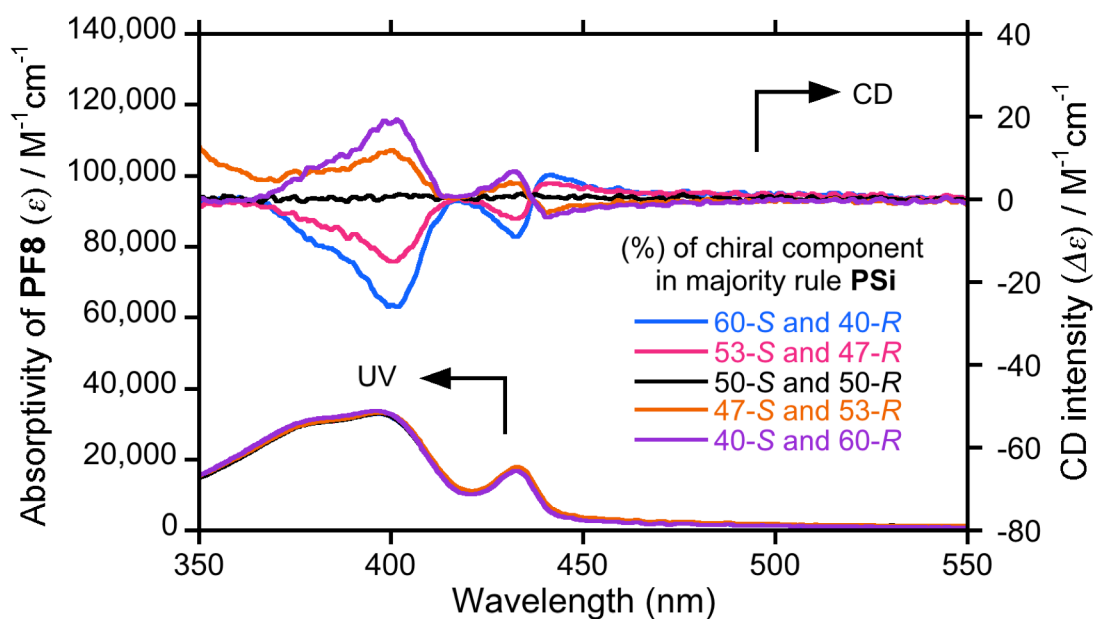


Figure 5.11. The CD and UV-Vis spectra of majority-rule **PSi-R-ran-PSi-S-PF8** hetero-aggregate with **PF8**  $M_n$  were 78,400, respectively.

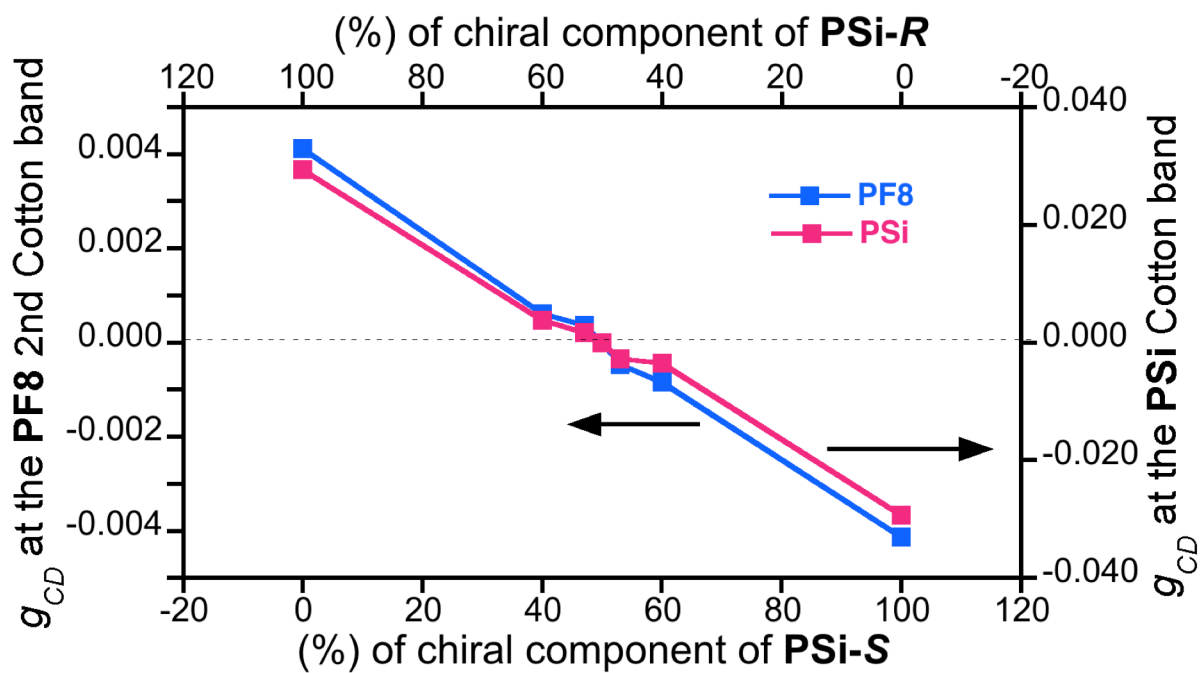


Figure 5.12. The  $g_{CD}$  value of **PF8** and **PSi-R-ran-PSi-S** hetero-aggregate with **PF8**  $M_n$  were 78,400, respectively.

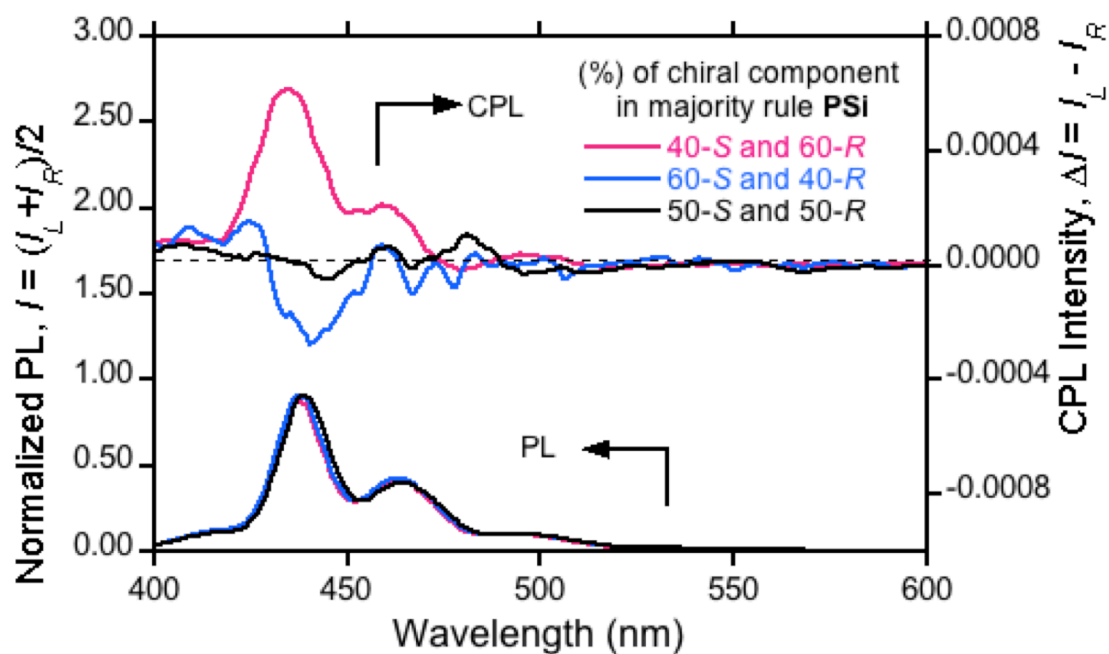


Figure 5.13. The CPL- and PL value from the  $\beta$ -phase **PF8** of **PF8** and **PSi-R-ran-PSi-S** hetero-aggregate with **PF8**  $M_n$  were 78,400, respectively.

### 5.5.2 Sergeant-soldier polysilane (PSi-*R(S)*-*ran*-PSi-*i*Bu)

In Figure 5.14, a rewinding effect or helix inversion in the CD spectra can be observed for both sergeant-soldier polysilane copolymers (PSi-*R(S)*-*ran*-PSi-*i*Bu) and PF8 in hetero-aggregate form. Previously, Fujiki observed similar helical screw sense inversion for the same sergeant-soldier polysilane in isooctane at -5 °C and 80 °C.<sup>30</sup> Recently, the Liu group detected abnormalities in a copolymer gel system of bolaamphiphiles containing L-histidine methyl ester head groups upon changing the molar ratio of both the chiral and achiral units.<sup>31</sup>

Suginome *et al.*<sup>32</sup> also reported an inversion phenomenon in poly(quinoxaline-2,3-diyl) copolymers containing chiral (*S*)-3-octylxymethyl and achiral propoxymethyl side chain units depending on the aromatic solvent. The explanations in terms of chiral conflict are consistent with Sato's claim that both the degree and the direction depend on the structure of the helical neighboring units.<sup>33</sup> The adopted energy preferences ( $\Delta G_h$ ) are based on the assumption that the chiral sergeant unit is either adjacent to another chiral sergeant ( $\Delta G_{h,CC}$ ) or to an achiral soldier unit ( $\Delta G_{h,CA}$ ).<sup>32</sup> This dominance will determine the screw sense of the end structure.

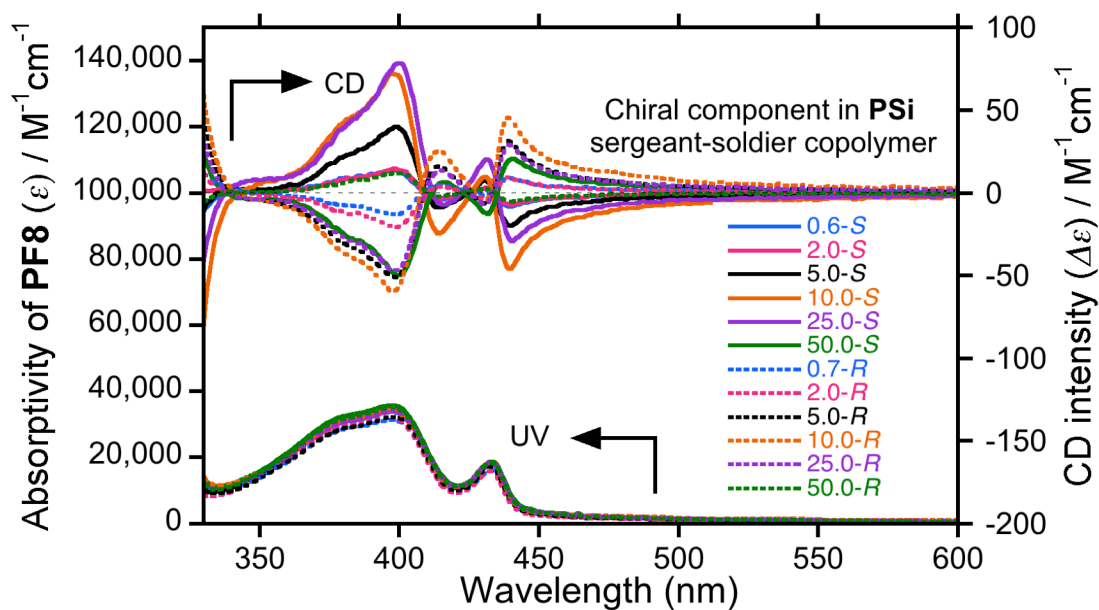


Figure 5.14. The CD- and UV-spectra of **(PSi-*R(S)*-ran-PSi-*i*Bu)-PF8** in hetero-aggregate (2-to-1 ratio).

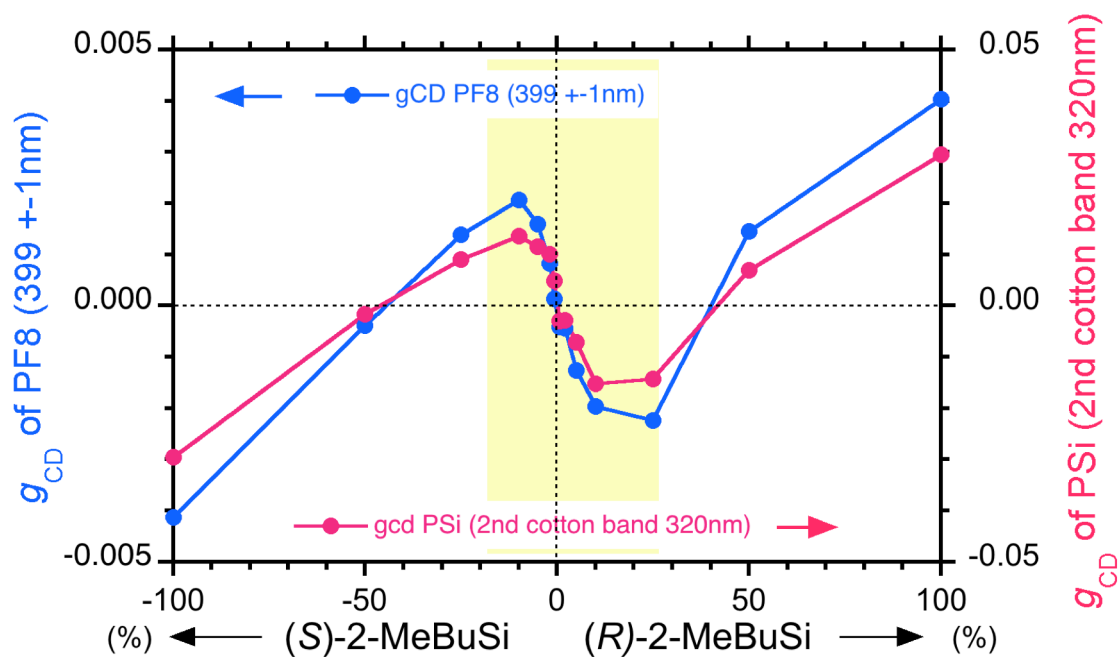


Figure 5.15. The  $g_{CD}$  value of **(PSi-*R(S)*-ran-PSi-*i*Bu)-PF8** in hetero-aggregate with **PF8** at 401 nm and **PSi** at 320 nm of **PSi-PF8** aggregate as a function of *S*- and *R*.

In the **(PSi-*R(S)*-*ran*-PSi-*iBu*)-PF8** hetero-aggregate, the helical switching exhibited an increasing trend in  $g_{CD}$  until **(PSi-*R(S)*-*ran*-PSi-*iBu*)** reached its limit of 10 % chiral units in both **PSi-*R*** and **PSi-*(S)***. Above 10 % chiral units in **(PSi-*R(S)*-*ran*-PSi-*iBu*)**, the helical inversion demonstrated a state of recovery, and the decrease in  $g_{CD}$  indicated the tendency of the **(PSi-*R(S)*-*ran*-PSi-*iBu*)** system to return to its original screw senses. Above 50 % chiral units, the **(PSi-*R(S)*-*ran*-PSi-*iBu*)** shows full recovery; however, the  $g_{CD}$  value is small compared to the pure screw sense in **PSi-*R*** or **PSi-*(S)***, as illustrated in Figure 5.16. In the **(PSi-*R(S)*-*ran*-PSi-*iBu*)-PF8** hetero-aggregate helical transfer, the **PF8** exhibited the same screw senses of the **PSi** scaffold, where were similar to the other **PSi-PF8** hetero-aggregate system. The helices structure was also maintained, as evidenced by the CD and CPL signals after irradiation at 313 nm ( $14 \mu\text{W cm}^{-2}$ ) for 60 s (Figure 5.16).

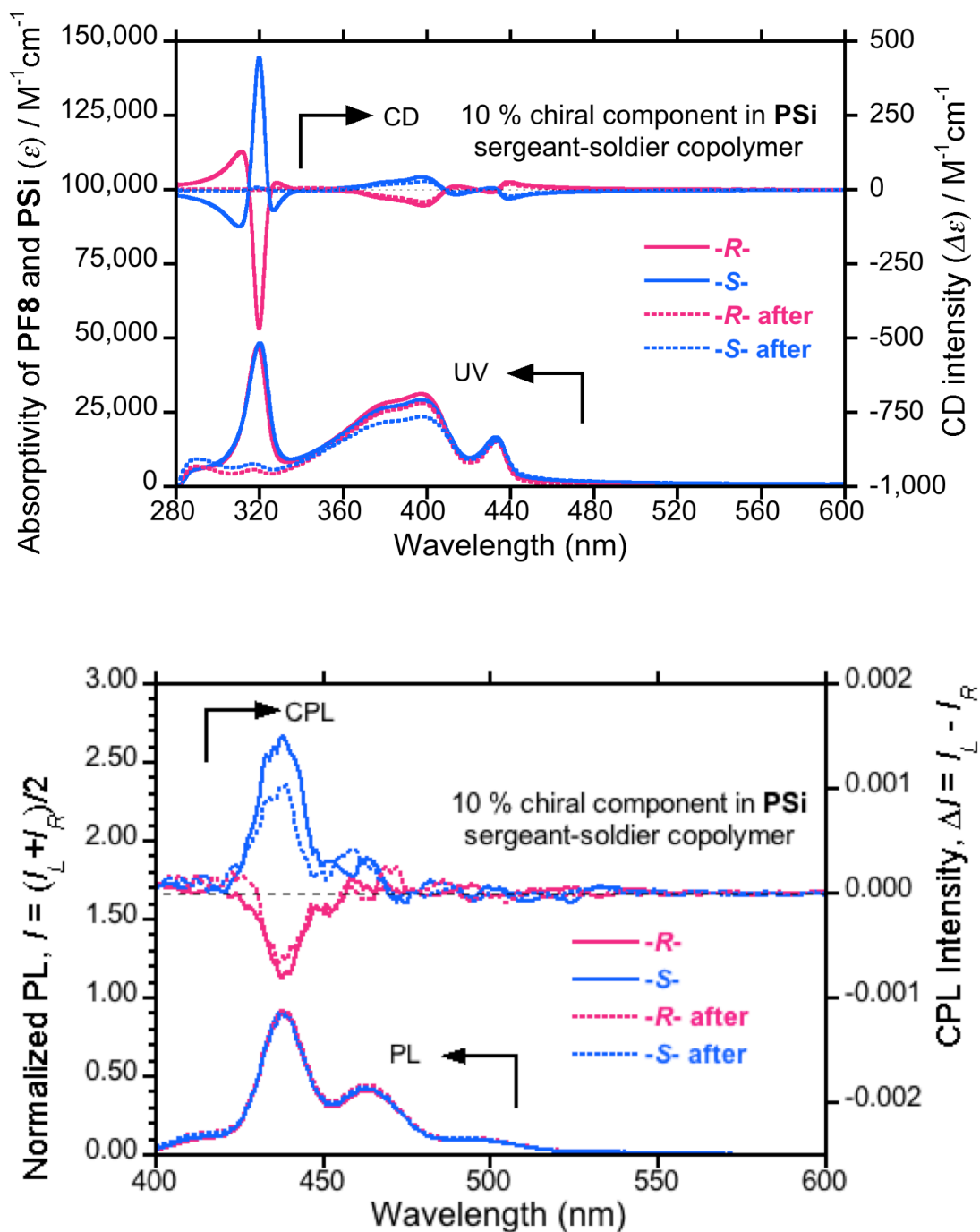


Figure 5.16. The (a) CD- and (b) PL- and CPL spectra of 10% chiral component of (PSi-R(S)-ran-PSi-iBu)-PF8 hetero-aggregate before and after irradiation time at 313 nm ( $14 \mu W cm^{-2}$ ) for 600 s.

## 5.6 PSi-S scaffold interacting with PF8T2

Finally, Figure 5.17 shows that the CD-silent green photoluminescent poly[(9,9-di-*n*-octylfluoren-2,7-diyl)-*alt*-bithiophene] (**PF8T2**) successfully transitions into a CD-active **PF8T2** after hetero-aggregation occurs. This procedure enabled the induction of helical architecture in other  $\pi$ -conjugate polymers using the **PSi** scaffold. Similar to the **PSi-PF8** hetero-aggregate system, the optically active **PF8T2** in the hetero-aggregate of **PSi-PF8** after photochemical decomposition at 313 nm ( $14 \mu\text{W cm}^{-2}$ ) for 60 s remained active with a slight decrease in CD intensity after scaffold removal.

In the excited state, the CPL spectra (Figure 5.18) confirm the results of the CD spectra. It is assumed that sufficiently strong attractive C-H/H-C interactions exist between two *n*-octyl groups of **PF8T2** and that the single *n*-hexyl group of **PSi** is responsible for the scaffolding capability, regardless of the absence of electrostatic, hydrogen-bonding, dipole-dipole, CH/ $\pi$ , CH/N, CH/O and  $\pi/\pi$  interactions.

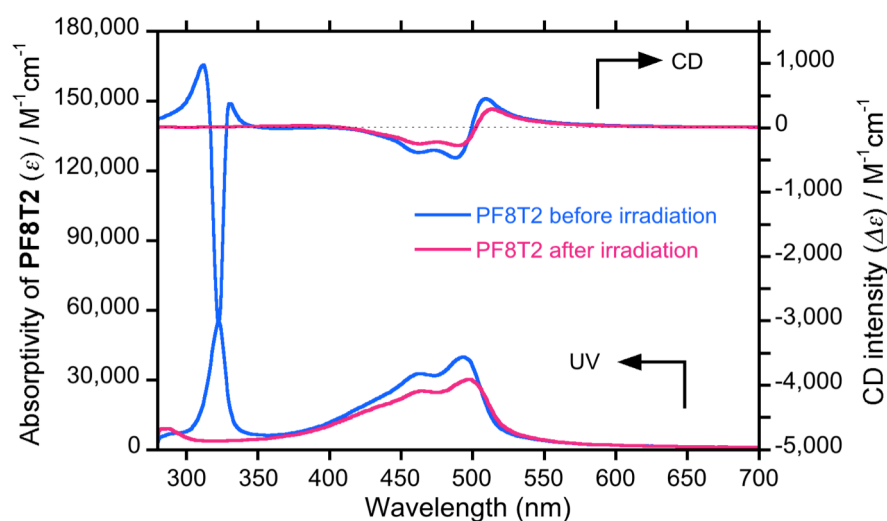


Figure 5.17. CD and UV-Vis spectra of hetero-aggregates under photochemical decomposition of **PSi-S** and **PF8T2** with a 2-to-1 ratio produced in a toluene-methanol cosolvent (1.5/1.5 (v/v)) with  $[\text{PF8T2}] = 2.0 \times 10^{-5} \text{ M}$  and  $[\text{PSi-S}] = 4.0 \times 10^{-5} \text{ M}$  as their repeating units (2-to-1 ratio) before and after irradiation time at 313 nm ( $14 \mu\text{W cm}^{-2}$ ) for 60 s.

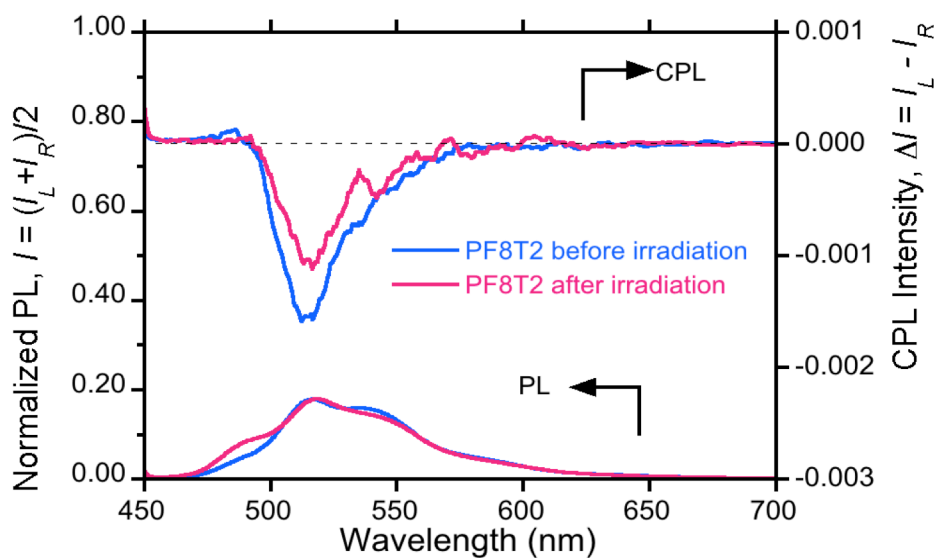


Figure 5.18. CPL- and PL spectra of hetero-aggregates under photochemical decomposition of **PSi-S** and **PF8T2** with a 2-to-1 ratio produced in a toluene-methanol cosolvent (1.5/1.5 (v/v)) with  $[\text{PF8T2}] = 2.0 \times 10^{-5} \text{ M}$  and  $[\text{PSi-S}] = 4.0 \times 10^{-5} \text{ M}$  as their repeating units (2-to-1 ratio) before and after irradiation time at 313 nm ( $14 \mu\text{W cm}^{-2}$ ) for 60 s.

## 5.7 References

- (1) Korevaar, P. A.; Schaefer, C.; De Greef T. F. A.; Meijer, E. W. *J. Am. Chem. Soc.* **2012**, *134*, 13482.
- (2) Marzal, R. M. E.; Nalam, P. C.; Bolisetty, S.; Spencer, N. D. *Soft. Matter* **2013**, *9*, 4045.
- (3) Mei, J.; Leung, N. L. C.; Kwok, R. T. K.; Lam, J. W. Y.; Tang, B. Z. *Chem. Rev.* **2015**, *21*, 11718
- (4) Jonkheijm, P.; Schoot, P. V. D.; Schenning A. P. H. J.; Meijer, E. W. *Science*, **2006**, *313*, 80.
- (5) Steed, J. W.; Atwood, J. L. *Supramolecular Chemistry*, 2nd Ed, Wiley (2013)
- (6) Kawanami, Y. S.; Katsumata, Y.; Mizoguchi, J. - i.; Nishijima, M.; Fukuhara, G.; Yang, C.; Mori, T.; Inoue, Y. *Org. Lett.* **2012**, *14*, 4962.
- (7) Basilio, N.; Pinetro, A.; Silva, J. P. D.; Rio, L. G. *J. Org. Chem.* **2013**, *78*, 9113.
- (8) Shiraki, T.; Shindome, S.; Toshimitsu, F.; Fujigaya, T.; Nakashima, N. *Polym. Chem.* **2015**, *6*, 5103.
- (9) Shiraki, T.; Dawn, A.; Tsuchiya, Y.; Shinkai, S. *J. Am. Chem. Soc.* **2010**, *132*, 13928.
- (10) Kumaki, J.; Kawauchi, T.; Okoshi, K.; Kusanagi, H.; Yashima, E. *Angew. Chem. Int. Ed.* **2007**, *46*, 5348.
- (11) van Gorp, J. J.; Vekemans, J. A. J. M.; Meijer, E. W. *J. Am. Chem. Soc.* **2002**, *124*, 14759.
- (12) Smulders, M. M. J.; Filot, I. A. W.; Meijer, E. W. *J. Am. Chem. Soc.* **2010**, *132*, 611.
- (13) Tabei, J.; Nakamura, R.; Sanda, F.; Masuda, T. *Macromolecules*, **2004**, *37*, 1175.
- (14) Green, M. M. and Reidy, M. P. *J. Am. Chem. Soc.* **1989**, *111*, 6452.
- (15) Pijper, D.; Jongejan, M. G. M.; Meetsma, A.; Feringa, B. L. *J. Am. Chem. Soc.* **2008**, *130*, 4541.
- (16) Kajitani, T.; Onouchi, H.; Sakurai, S. I.; Nagai, K.; Okoshi, K.; Onitsuka, K.; Yashima, E. *J. Am. Chem. Soc.* **2011**, *133*, 9156.
- (17) Lehn, J. M. *Angew. Chem. Int. Ed. Engl.* **1990**, *29*, 1304.
- (18) Ray, C. R.; Moore, J. S. *Adv. Polym. Sci.* **2005**, *177*, 91.
- (19) Nagata, Y.; Yamada, T.; Adachi, T.; Akai, Y.; Yamamoto T.; Suginome, M. *J. Am. Chem. Soc.* **2013**, *135*, 10104.
- (20) Harada, A.; K. Kataoka. *Macromolecules* **1995**, *28*, 5294.
- (21) Harada, A.; K. Kataoka. *Science*, **1999**, *283*, 65.
- (22) Danovich, D.; Shaik, S.; Neese, F.; Echeverria, J.; Aullon, G.; Alvarez, S. *J. Chem. Theory Comput.* **2013**, *9*, 1977.
- (23) Echeverria, J.; Aullon, G.; Danovich, D.; Shaik, S.; Alvarez, S. *Nat. Chem.* **2011**, *3*, 323
- (24) Fokin, A. A.; Gerbig, D.; Schreiner, P. R. *J. Am. Chem. Soc.* **2011**, *133*, 20036.
- (25) Fokin, A. A.; Chernish, L. V.; Gunchenko, P. A.; Tikhonchuk, E. Y.; Hausmann, H.; Serafin,

- M.; Dahl, J. E.; Carson, R. M. K; Schreiner, P. R. *J. Am. Chem. Soc.* **2012**, *134*, 13641.
- (26) Green, M. M.; Garetz, B. A.; Munoz, B.; Chang, H. P. *J. Am. Chem. Soc.* **1995**, *117*, 4181.
- (27) Green, M. M.; Peterson, N. C.; Sato, C.; Teramoto, A.; Cook, R.; Lifson, S. *Science* **1995**, *268*, 1860.
- (28) Green, M. M. and Reidy, M. P. *J. Am. Chem. Soc.* **1989**, *111*, 6452.
- (29) Gestel, J. V. *Macromolecules* **2004**, *37*, 3894.
- (30) Fujiki, M. *The Chemical Record*, **2009**, *9*, 271.
- (31) Liu, Y.; Chen, C.; Wang, T.; Liu, M. *Langmuir* **2016**, *32*, 322
- (32) Nagata, Y.; Nishikawa, T.; Suginome, M. *ACS Macro Lett.* **2016**, *5*, 519
- (33) Sato, T.; Terao, K.; Teramoto, A.; Fujiki, M. *Macromolecules* **2007**, *40*, 5355.

## Chapter 6. Concluding remarks

It has been demonstrated that non-charged artificial helical Si-Si bond polymers (**PSi-S** and **PSi-R**) can induce CPL and CD activity in non-charged, non-helical poly(9,9-di-*n*-octylfluorene) (**PF8**) in the aggregated state. This thesis establishes that **PSi-S** and **PSi-R** are beneficial as versatile scaffolds because they are easily removable by photoscission of the Si-Si bond at 313 nm. This dissertation contains three sections:

The first section (chapter 3) revealed experimental evidence of **PSi** helix scaffolding capability to **PF8** before and after complete removal of **PSi**. The **PF8-PSi-S** hetero-aggregates exhibited several intense CD bands arising from the exciton couplet due to helically assorted **PSi** at approximately 320 nm and the *a*-phase and *b*-phase of the chiral **PF8** at 399 nm and 435 nm. This finding verifies that macromolecular helicity transfer from non-charged **PSi** to non-charged non-helical **PF8** is possible. It was also found that the chirality of **PF8** is retained even after inducing photoscission of Si-Si at 313 nm. **PSi-S** decomposes rapidly within 60 s, which indicates that **PSi** acts efficiently as a photochemically removable scaffold that enables the generation of chiral **PF8** when non-helical **PF8** is employed as a starting material.

In the second section of chapter 4, which addressed the verification of the possible mechanism and the molecular structures, the structures of **PF8**, **PSi-S**, and **PSi-S-and-PF8** hetero-aggregates were revealed by DFM-AFM. From several height profiles of DFM-AFM images, the AFM height of **PSi-S** cast from pure chloroform solution was found to range from  $\approx 0.5$  to  $\approx 1.1$  nm on HOPG. These heights are nearly consistent with the diameters of individual **PSi-S** chains laterally aligned on the HOPG surface. In contrast, **PF8** adopts an ill-defined, highly entangled arrangement on HOPG that includes face-on, edge-on and loop-train-tail structures. Finally, height

profiles of **PSi-S** and **PF8** aggregates obtained with 5 % methanol and 95 % chloroform indicated that the aggregates had an almost uniform cross-sectional height that ranged from 5.5 to 6.1 nm.

In the chapter 5, on determining factors affecting the chirality amplifications, the cosolvent displayed a great enhancement in the  $g_{CD}$  value of the hetero-aggregate at a specific  $n_D$  of  $\approx 1.41$  when the mixture of good and poor solvents (toluene and methanol) was 1/1 (v/v). Surprisingly, **PSi-and-PF8** hetero-aggregates preferentially adopt a 2-to-1 stoichiometric ratio. Additionally, the molecular weight of the polymers plays a crucial role in providing sufficient chirality transfer. Nearly identical  $DP_n$  values of **PSi-S** and **PF8** afforded the highest  $g_{CD}$  amplitude of  $\approx -0.005$  at 438 nm of **PF8**. Moreover, *n*-alkyl side-chain length of 7 carbons for both **PSi-S** and **PF8** produced the highest  $g_{CD}$  value of  $\approx -0.012$  at 438 nm for **PF7**. However, with further increases in the side-chain lengths of both polymers, the  $g_{CD}$  amplitude decreased. Thus, the amplification of  $g_{CD}$  is highly dependent on the main-chain helicity of the scaffolding ability.

Also in chapter 5, the author investigated whether sergent-soldier and majority-rules models are applicable to the current **PSi** scaffolding systems. When **PSi-R-ran-PSi-S** copolymers are employed, **PSi-R-ran-PSi-S-and-PF8** hetero-aggregates exhibit a majority rule effect and behave differently from polyisocyanate copolymers. However, when **PSi-R(S)-ran-PSi-tBu** copolymers are employed, a rewinding effect is observed in the copolymer system of the hetero-aggregates below 50 % chiral content. Finally, the author verified that **PSi** is transferable to non-helical **PF8T2** as an aggregate form, as proven by the CD and CPL spectra.

These outcomes led the author to propose that multiple attractive C-H/H-C interactions between the two *n*-octyl groups (**PF8**) and the *n*-hexyl group (**PSi-S** and **-R**) are sufficiently strong for scaffolding capability, irrespective of the absence of electrostatic, hydrogen-bonding,

dipole-dipole, CH/ $\pi$ , CH/N, CH/O and  $\pi/\pi$  interactions.

## List of publications and conferences

### Academic journals

- 1) Nor Azura Abdul Rahim and Michiya Fujiki (**First author**)  
“Aggregation-induced scaffolding: Photoscissable helical polysilane generates circularly polarized luminescent polyfluorene”  
*Polymer Chemistry* (RSC), **7**, 4618-4629 (2016).
- 2) M. Fujiki, K. Yoshida, N. Suzuki, N. A. A. Rahim and J. A. Jalil  
“Tempo-spatial chirogenesis. Limonene-induced mirror symmetry breaking of Si–Si bond polymers during aggregation in chiral fluidic media”  
*Journal of Photochemistry and Photobiology A: Chemistry* (Elsevier), **331**, 120-129 (2016).
- 3) Y. Zhao, N. A. A. Rahim, Y. Xia, M. Fujiki, B. Song, Z. Zhang, W. Zhang, and X. Zhu  
“Supramolecular chirality in achiral polyfluorene: Chiral gelation, memory of chirality and chiral sensing property”  
*Macromolecules* (ACS), **49**, 3214–3221 (2016).
- 4) T. Amako, K. Nakabayashi, N. Suzuki, S. Guo, N. A. A. Rahim, T. Harada, M. Fujiki and Y. Imai  
“Pyrene magic: Chiroptical enciphering and deciphering 1,3-Dioxolane bearing two wirepullings to drive two remote pyrenes”  
*Chemical Communications* (RSC), **51**, 8237-8240 (2015).
- 5) L. Wang, N. Suzuki, J. Liu, T. Matsuda, N. A. A. Rahim, W. Zhang, M. Fujiki, Z. Zhang, N. Zhou and X. Zhu  
“Limonene induced chiroptical generation and inversion during aggregation of achiral polyfluorene analogs: Structure-dependency and mechanism”  
*Polymer Chemistry* (RSC), **5**, 5920-5927 (2014).

## International conferences

- 1) N. A. A. Rahim, S. Guo, N. Suzuki and M. Fujiki.

“Chirality transfer efficiency of  $\sigma$ -conjugated polysilane bearing alkyl (*S*)-side chain length dependency to  $\pi$ -conjugates poly(9,9-dioctyl-2,7-fluorene). 15-20 December 2015, International Chemical Congress of Pacific Basin Societies (PACIFICHEM 2015). Honolulu Hawaii, USA. Oral presentation.

- 2) N. A. A. Rahim and M. Fujiki.

“Emerging optically active luminescent poly(dioctyl-fluorene) aggregates through helical amplification from *n*-hexyl-(*S*)-dialkyl-polysilane. 9-11 September 2015, International Symposium on Organic Chemistry (ISOC 2015), Kuala Lumpur, Malaysia. Oral presentation.

- 3) N. A. A. Rahim and M. Fujiki.

“Limonene chirality transfer to poly(9,9-di-*n*-octyl-2,7-fluorene): Effects of good solvents and limonene purification”. 7-11 December 2014, International Polymer Conference (IPC 2014), Tsukuba, Japan. Poster presentation.

## Acknowledgements

First and above all, I praise Allah the almighty for providing me with this opportunity and granting me the capability to proceed successfully. This thesis appears in its current form due to the assistance and guidance of several people.

I would like to express my deep sincere appreciation and gratitude to my supervisor, Prof. Michiya Fujiki, for his guidance, suggestions, encouragement, and patience throughout my PhD enrollment. His deep knowledge in the field of aggregation and spectroscopy has helped me enormously in designing my research from beginning to end of my entire PhD journey. This work would not have been possible without his generous and helpful attitude.

I also gratefully acknowledge the other faculty advisers at the Nara Institute of Science and Technology (NAIST). I extend my gratitude to Prof. Hiroshi Daimon, who constantly offered valuable advice on the direction of the research. I am also thankful to Prof. Hiroko Yamada for his kind suggestion that was not limited to the obstacle that I was confronting but also noted a potential future problem that I would encounter after solving the experimental issue. I extend my gratitude also to Prof. Jun-ichi Kikichi, who kindly responded when I had difficulty in formulating a research direction at the beginning of my work. His valuable comments over time have strengthened my research theme.

I am also thankful to the highly talented technical staff at NAIST, especially Mrs. Sakiko Fujita, who assisted me with the cyro-TEM observations. In addition, her suggestions and advice in terms of sample preparation have been very useful, as polysilanes are very delicate samples under high charging conditions. I am also thankful to Mr. Fumio Asanoma, who helped me with the CP MASS  $^{13}\text{C}$ -NMR measurements. Mr. Kazuhiro Miyake assisted in operating the

AFM-DFM tool. He is a cheerful and approachable person who made the tutorial session very interesting and informative. Mr. Yasuo Okajima assisted with the fluorescence lifetime (PL) measurement. Mrs. Yoshiko Nishikawa assisted in operating the dynamic light scattering (DLS) tool. Mr. Shohei Katao assisted with the XRD measurement, and Mr. Masahiro Fujihara kindly provided a DSC and TGA tutorial session.

I gratefully acknowledge PhD funding through the Skim Latihan Akademik IPTA (SLAI) fellowship from Universiti Malaysia Perlis and Kementerian pengajian Tinggi. Without this funding, I doubt it would have been possible to pursue a doctoral degree in the first place.

I am also thankful to the laboratory members in the Advanced Polymer Science Laboratory, including students who have already graduated from NAIST, not just for our laboratory discussions but also for the enjoyable time we spent outside the laboratory.

My biggest thanks goes to my father, Abdul Rahim Bin Taib, who has taken good care of me and my sister since my mother passed away when I was 9 years old. His sacrifices to ensure that I received a good education will always be remembered. Finally, I thank my husband, Mohammad Mujahidin Bin Suhaimi. I will always admire your patience and willingness to take care of our children, Hariz Hazim, Hana Hadhira, Hana Hafiya and Hana Harumi, while I was completing my PhD.

October 2016

Nor Azura Binti Abdul Rahim